STATE OF CALIFORNIA DEPARTMENT OF TRANSPORTATION

TECHNICAL REPORT DOCUMENTATION PAGE

TR0003 (REV. 10/98)

1. REPORT NUMBER	2. GOVERNMENT ASSOCIATION NUMBER	3. RECIPIENT'S CATALOG NUMBER
CA/UCD-SESM-08-01		

4. TITLE AND SUBTITLE	5. REPORT DATE
Development of Guidelines for Incorporation of Vertical Ground Motion Effects in Seismic Design of Highway BRIDGES	May 2008
	6. PERFORMING ORGANIZATION CODE CA/UCD-SESM-08-01
7. AUTHOR(S) Sashi Kunnath, Norman Abrahamson, Y.H. Chai, Emrah Erduran and Zeynep Yilmaz	8. PERFORMING ORGANIZATION REPORT NO. CA/UCD-SESM-08-01
9. PERFORMING ORGANIZATION NAME AND ADDRESS California Department of Transportation Division of Research and Innovation, MS-83 1227 O Street Sacramento CA 95814	10. WORK UNIT NUMBER 11. CONTRACT OR GRANT NUMBER 59A0434
12. SPONSORING AGENCY AND ADDRESS California Department of Transportation Sacramento, CA 95819	13. TYPE OF REPORT AND PERIOD COVERED Final Technical Report (2004 – 2007) 14. SPONSORING AGENCY CODE

15. SUPPLEMENTAL NOTES

16. ABSTRACT

This study was undertaken with the objective of assessing the current provisions in SDC-2006 for incorporating vertical effects of ground motions in seismic evaluation and design of ordinary highway bridges. A comprehensive series of simulations was carried out on a range of typical bridge configurations to isolate the effects of vertical motions. Results of these analyses reveal that vertical ground motions can have a significant effect on (i) the axial force demand in columns; (ii) moment demands at the face of the bent cap, and (iii) moment demands at the middle of the span. The first two issues are found to be less of a concern in the present study since the axial capacity of the columns and the moment capacity of the girders at the face of the bent cap are generally adequate to resist the increase in the respective demands due to vertical effects. On the other hand, the amplification of negative moments in the mid-span section is identified as the primary issue that should be addressed in the context of existing seismic guidelines in SDC-2006. In particular, the current requirement that vertical ground motions be considered only for sites where the expected peak rock acceleration is at least 0.6g is not an adequate basis to assess the significance of vertical effects. A second SDC criterion that is in need of reexamination is the design specification for the consideration of vertical effects by means of a static load equivalent to 25% of the dead load applied in the upward and downward directions. The reinforcement resulting from this requirement is found to be inadequate for a significant number of cases examined in this study. It is also shown that an elastic response spectrum analysis is an effective tool to determine the effects of vertical ground motions on the bridge superstructures. A set of vertical design spectra and a simplified design procedure that uses the proposed elastic spectra were developed.

17. KEY WORDS	18. DISTRIBUTION STATEMENT	
Vertical acceleration, near-fault ground motions, ordinary highway bridges, nonlinear analysis, seismic design	No restrictions. This document is available to the public through the National Technical Information Service, Springfield, VA 22161	
19. SECURITY CLASSIFICATION (of this report) Unclassified	20. NUMBER OF PAGES ~ 120	21. PRICE

DEVELOPMENT OF GUIDELINES FOR INCORPORATION OF VERTICAL GROUND MOTION EFFECTS IN SEISMIC DESIGN OF HIGHWAY BRIDGES

A Technical Report Submitted to the California Department of Transportation under Contract 59A0434

Sashi K. Kunnath
Norman Abrahamson
Y.H. Chai
Emrah Erduran
Zeynep Yilmaz

May 2008

Department of Civil and Environmental Engineering
Structural Engineering and Structural Mechanics
University of California at Davis

Disclaimer

The results, recommendations and opinions presented in this report are those of the authors and do not necessarily reflect the viewpoints of the California Department of Transportation or the State of California.

Acknowledgements

Funding for this study provided by the California Department of Transportation (Caltrans) under Contract No.59A0434 is gratefully acknowledged. Input and comments from Li-Hong Sheng, Mark Yashinsky, Mark Mahan, Don Lee and Mike Van De Pol are sincerely appreciated.

Abstract

This study was undertaken with the objective of assessing the current provisions in SDC-2006 for incorporating vertical effects of ground motions in seismic evaluation and design of ordinary highway bridges. A comprehensive series of simulations was carried out on a range of typical bridge configurations to isolate the effects of vertical motions. Results of these analyses reveal that vertical ground motions can have a significant effect on (i) the axial force demand in columns; (ii) moment demands at the face of the bent cap, and (iii) moment demands at the middle of the span. The first two issues are found to be less of a concern in the present study since the axial capacity of the columns and the moment capacity of the girders at the face of the bent cap are generally adequate to resist the increase in the respective demands due to vertical effects. On the other hand, the amplification of negative moments in the mid-span section is identified as the primary issue that should be addressed in the context of existing seismic guidelines in SDC-2006. In particular, the current requirement that vertical ground motions be considered only for sites where the expected peak rock acceleration is at least 0.6g is not an adequate basis to assess the significance of vertical effects. A second SDC criterion that is in need of reexamination is the design specification for the consideration of vertical effects by means of a static load equivalent to 25% of the dead load applied in the upward and downward directions. The reinforcement resulting from this requirement is found to be inadequate for a significant number of cases examined in this study. It is also shown that an elastic response spectrum analysis is an effective tool to determine the effects of vertical ground motions on the bridge superstructures. A set of vertical design spectra and a simplified design procedure that uses the proposed elastic spectra were developed.

TABLE OF CONTENTS

LIST OF FIGURES

LIST OF TABLES

1 INTRODUCTION

"Ordinary Standard Bridge" is a term used by California Department of Transportation (Caltrans) to identify bridges which can be designed using the direct and basic approach outlined in Seismic Design Criteria, SDC-2006 (Caltrans 2006). For a bridge to be considered as an Ordinary Standard Bridge, SDC-2006 sets forth the following basic requirements: (1) the span length should be less than 90m, (2) the bridge should be constructed with normal weight concrete, (3) foundations must be supported on spread footings, pile caps with piles or pile shafts, and (4) the soil is not susceptible to liquefaction, lateral spreading or scour. For ordinary standard bridges constructed on sites where the peak rock acceleration is expected to be more than 0.6g, SDC-2006 requires consideration of vertical effects but does not require analysis of the structure under combined horizontal and vertical components of the ground motion. Instead, it stipulates the check of the nominal capacity of the structure designed considering horizontal effects only under an equivalent vertical load with a magnitude of 25% of the dead load (DL) of the structure applied separately in the upward and downward directions to account for vertical effects.

One of the early studies on the effect of vertical accelerations was conducted by Saadeghvaziri and Foutch (1991) who reported that the variation of axial forces due to vertical excitations reduced the energy-dissipating capacity of bridge columns and also influenced the shear capacity of the section. Broekhuizen (1996) and Yu et al. (1997) both investigated the response of several overpasses on the SR 14/15 interchange following the 1994 Northridge earthquake. The former study showed that the vertical accelerations could significantly increase tensile stresses in the deck while the latter research found significant increases (about 20%) in axial force and only a marginal change in the longitudinal moment when vertical motions were considered in the evaluation. The evaluation of 60 prestressed box-girder bridges by Gloyd (1997) indicated that the dynamic response from vertical acceleration was larger than dead load effects. Papazoglou and Elnashai (1996) reported analytical and field evidence of

the damaging effect of vertical ground motions on both building and highway bridge structures. The authors contend that strong vertical motions induced significant fluctuations in axial forces in vertical elements leading to a reduction of the column shear capacity. In certain cases, compression failure of columns was also reported to be likely. These observations were also confirmed through numerical simulations. Later Elnashai and Papazoglou (1997) and Collier and Elnashai (2001) worked on simplified procedures to combine vertical and horizontal ground motions. Both papers focus on near-fault ground motions that have been recorded within 15 km of the causative fault since these ground motions were observed to possess significant vertical components. Moreover, it was suggested to limit the damping ratio of elements susceptible to vertical effects to 2%. This is because firstly, vertical ground motions are associated with higher frequency oscillations and hence lower damping. Secondly, there are limited hysteretic energy dissipation mechanisms for vertical inelastic response than in the case of transverse response. Button et al. (2002) examined several parameters including ground motion and structural system characteristics. However, most of their studies were limited to linear response spectrum and linear dynamic analyses. More recently, Veletzos et. al. (2006) carried out a combined experimental-analytical investigation on the seismic response of precast segmental bridge superstructures. Among other issues, they also examined the effects of vertical ground motions. Their numerical analyses indicated that the prestressing tendons above the piers of one of the bridge structures yielded under positive bending. The median positive bending rotations were found to increase by as much as 400% due to vertical ground motions.

On the subject of ground motion characteristics of vertical excitations, Bozorgnia and Niazi (1993) studied the variation in the ratio of vertical to horizontal spectral accelerations and found that the ratios were smaller for longer periods than for short periods. Silva (1997) showed that the vertical motion histories show a pattern in which short-period vertical motion arrived before the main horizontal motions, while the longer-period motions arrived at about the same time as the other horizontal components. Recently, Bozorgnia and Campbell (2004) examined the characteristics of

response spectra of free-field vertical motions recorded during the 1994 Northridge earthquake and found the vertical to horizontal (V/H) response spectral ratios to be strongly dependent on period and site-to-source distance. They also concluded that the commonly assumed V/H ratio of 2/3 is exceeded for short periods but may be conservative for longer periods.

This research was undertaken in light of recent renewed interest in near-field motions and the realization that the ratio of vertical to horizontal peak ground acceleration can be larger in near-fault records than far-fault records. The study aims in particular to evaluate the simplified procedure employed by Caltrans in SDC 2006 to account for the effect of vertical component of ground motions in the design of ordinary highway bridges. A systematic evaluation was carried out on two classes of ordinary bridges: overcrossings and short multi-span bridges. Of these two bridge types, over-crossings were selected as the main focus of this study for two reasons: First, these are generally smaller span structures that have reinforced concrete superstructures that are expected to be more vulnerable to the effects of vertical ground motions than prestressed concrete girders since the presence of prestressing tendons increase the safety margin of the superstructure to gravitational effects. Secondly, the vertical period of over-crossings tend to fall in the range of the peak spectral demand of vertical ground motions.

The evaluation in this study is based on a comprehensive set of nonlinear response history analyses using a suite of near-fault ground motions. The simulations were performed in two stages: at first only the two horizontal components of the record were applied to the model; this was followed by simultaneous application of both horizontal and vertical components. Several response parameters were monitored in order to identify critical parameters that are most susceptible to vertical effects.

A parallel study examined both the characteristics of vertical ground motions and effects of these motions on the response of the selected bridge configurations. The objective of this phase of study was to address the conditions leading to the vertical component having a significant effect on the response of bridge columns. The key

question of when the vertical component should be incorporated in design is best evaluated by a probabilistic seismic hazard assessment study incorporating probabilistic seismic demand models and ground motion models. In the context of this research, a vector valued probabilistic seismic hazard assessment study is conducted using available resources. Structural demand hazard curves are generated for selected engineering demand parameters for a typical bridge configuration and the probability of exceeding the available capacity is assessed.

Finally, a set of vertical spectra are developed and a simplified design procedure to incorporate vertical effects in the seismic design of ordinary standard bridges is proposed.

2 SELECTION AND MODELING OF THE BRIDGE SYSTEMS

Two types of bridges have been considered in this study: single bent, two span overpasses and multi-span single frame bridges. For the overpass systems, a segment of the Camino Del Norte Bridge was selected as the prototype system whereas the Amador Creek Bridge was used as the prototype bridge for multi-span bridges. Several configurations of each bridge were generated from the base configuration of each system without violating the specifications in SDC-2006 on allowed dimensional and balanced stiffness requirements to cover a wide range of fundamental periods. Overpasses were selected to represent the short-span reinforced concrete systems whereas single frame, multi-span bridges represent the prestressed bridges. Modeling of both systems and selection and details of the configurations will be summarized comprehensively in this chapter.

2.1 MODELING OF A TYPICAL OVER-CROSSING

A portion of the widening project of Camino Del Norte Bridge was used as a typical ordinary standard bridge and representative of a reinforced concrete over-crossing designed according to post-Northridge Caltrans specifications. It is a single bent reinforced concrete bridge with two spans of 101.5 and 100.0 feet in length. The single bent is composed of two octagonal columns with spiral reinforcement. Figure 2-1 shows the elevation view of the Camino Del Norte Bridge along with the column reinforcement details.

The highway over-crossings considered in the study are modeled as nonlinear columns resting on an elastic soil-foundation system supporting an elastic superstructure. For the particular case of evaluating superstructure deformation demands, the box girder is also modeled as an equivalent nonlinear I-section. Figure 2-2a presents the simulation model of a typical two-column over-crossing used in this study. The approximation of the longitudinal box girder as a line element was verified independently using a full 3D representation of the deck with shell elements as shown in Figure 2b.

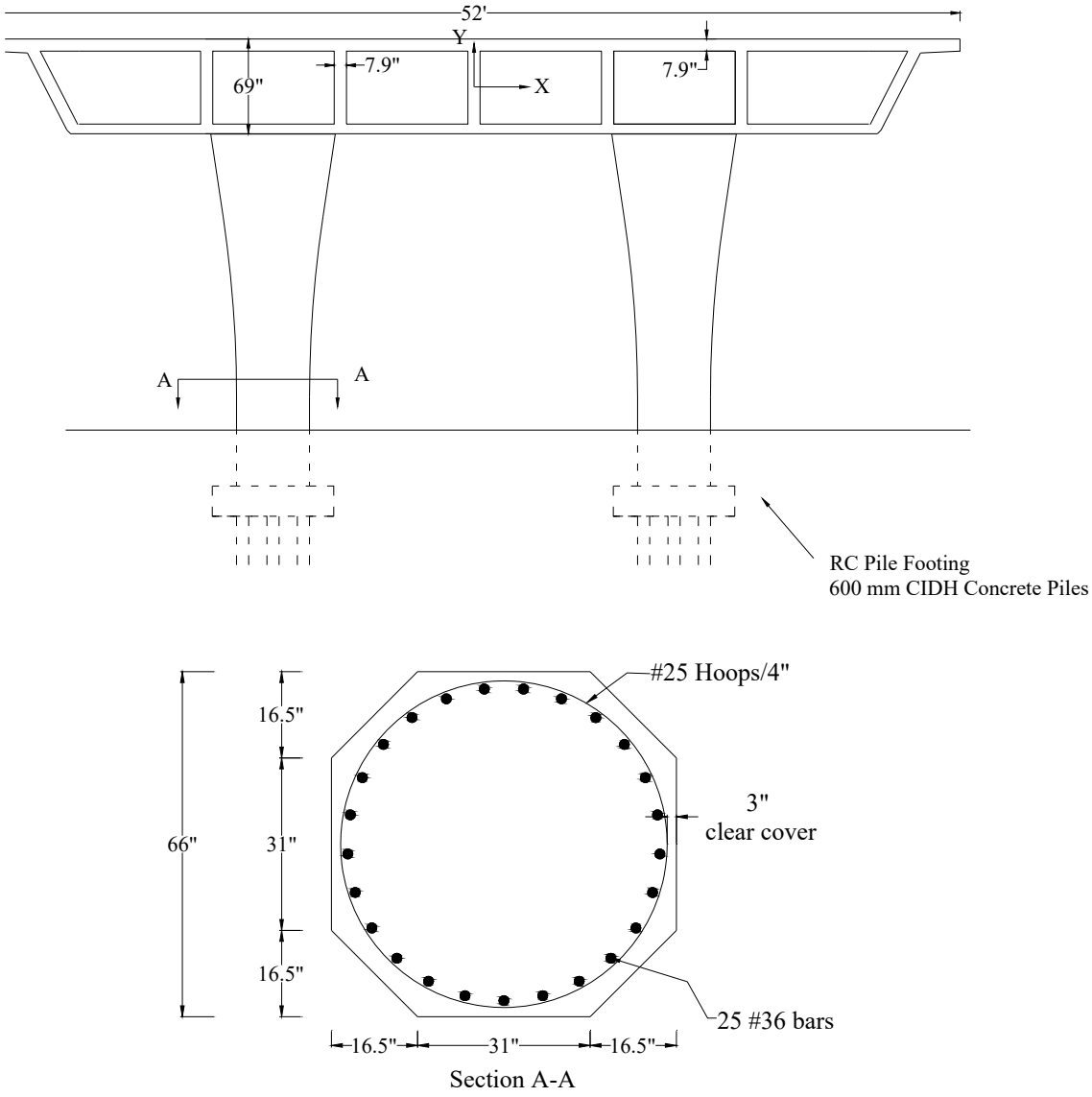

Figure 2-1 - Elevation and sectional details of the Camino Del Norte Bridge

Figure 2-3 presents the variation of (a) axial force in the column and (b) vertical displacement at the middle of the bent as a function of time under a sample ground motion obtained from both the line and shell models. The curves obtained from the two models are indistinguishable for both parameters indicating that the assumption of modeling the deck using line elements has no significant effect on the results of the numerical simulations for two-column bent over-crossings.

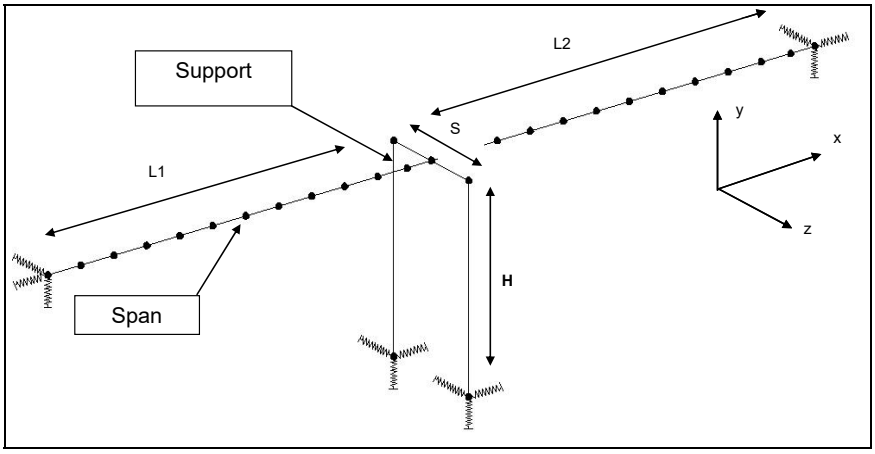

(a)

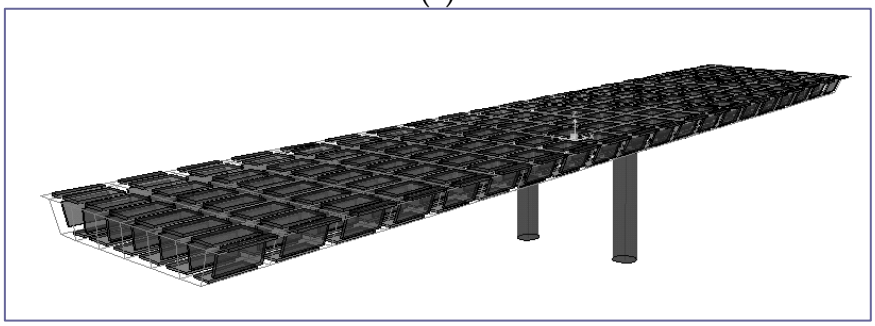

(b)

Figure 2-2 - Modeling of a typical over-crossing: (a) Simplified model used in simulations; (b) Detailed deck model used in verification study

The nonlinear simulations were performed using the open-source software, OpenSEES (2007). Each pier is modeled using a force-based nonlinear beam column element with fixed hinge lengths at element ends. The inelastic behavior of the hinge region is simulated with a discretized fiber section model. Using a fiber section is of critical importance in the present evaluation since it enables the consideration of the variations in the column moment capacity due to changes in the axial force in the columns as a result of vertical ground motions. In order to determine the effective hinge length, a sensitivity study was carried out using previously tested bridge columns. The study concluded that the plastic hinge length expression recommended in SDC-2006 is an effective approach to modeling the nonlinear force-deformation response of bridge columns.

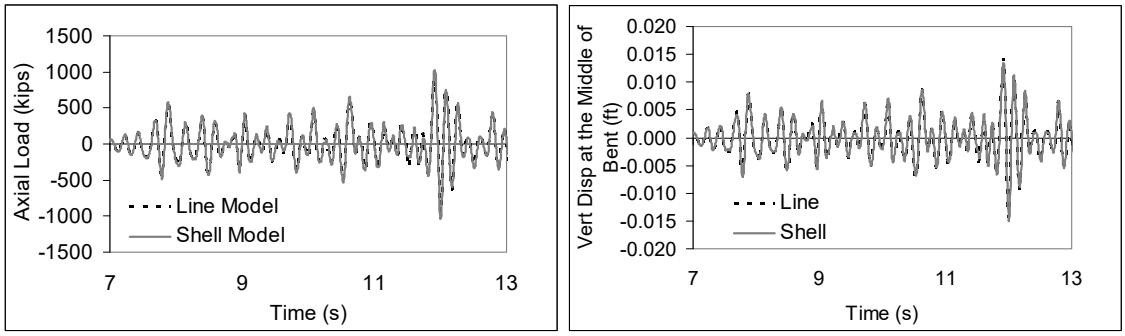

(a) (b)

Figure 2-3 - Time history of (a) axial force in the column and (b) vertical displacement at the middle of the bent obtained from shell and line models

An additional assumption used in the study is also derived from the SDC-2006 guideline which employs a capacity design approach that seeks to limit inelastic behavior to the column elements. In other words, the superstructure is designed to remain elastic under seismic action for the design event. Based on this assumption, the girders were modeled using elastic elements. Table 2-1 summarizes the computed elastic properties of the box girder.

Table 2-1 – Elastic properties of the box girder of Camino Del Norte Bridge

Parameter	***Value***
Area, A	78.8 ft^2
I_x	406.4 ft^4
I_y	16442.7 ft^4
J	173.66.7 ft^4

In the design drawings, the characteristic strength of unconfined concrete (f_c') was specified to be 4 ksi with an ultimate strain of 0.006, while the yield strength of both longitudinal and spiral reinforcement was specified as 60 ksi. The characteristic strength and ultimate strain of confined concrete were computed to be 6.0 ksi and 0.0169 using the model proposed by Mander et al. (1988). The Kent-Scott-Park model was used to model both confined and unconfined concrete, as displayed in Figure 2-4. A bilinear model with a post-yield stiffness of 5% of the initial stiffness was used to model the reinforcing steel.

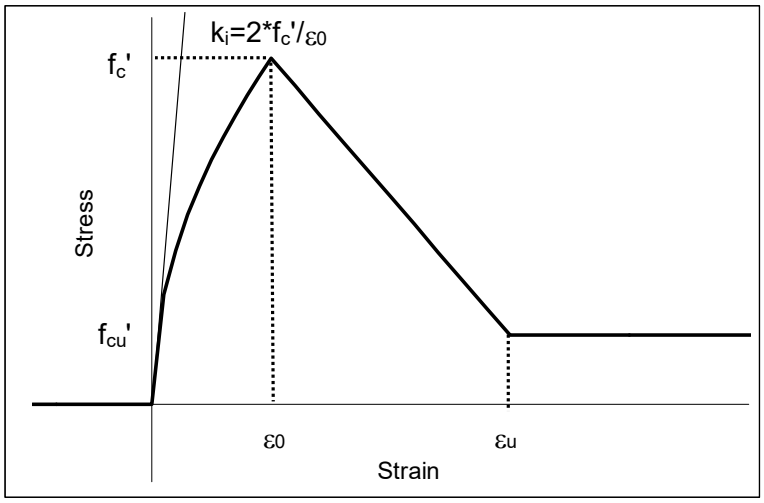

Figure 2-4 - Concrete material model used in simulation study

The columns of the bent are connected to the pile cap with hinge connections using shear keys. Diaphragm type abutments were used at both ends of the bridge. The end conditions both at the abutments and at the bottom of the columns were modeled using spring elements to simulate the flexibility of the soil-pile-foundation system.

Determination of the properties of the springs representing the pile-soil foundation and the abutment systems is one of the challenging tasks in the modeling of bridge systems. SDC-2006 (Caltrans 2006) provides certain guidelines to determine these spring constants. The abutment stiffness in the longitudinal direction was computed as: $K = (K_i\, w\, h)/5.5$, where K_i is the initial stiffness of the abutment and is taken to be equal to 20.0 kip/inch per ft, w and h are the width and height of the diaphragm abutment. For the abutment stiffness in the transverse direction and foundation stiffness in both translational directions, an empirical value equal to 40 kips/inch per pile is used. To check the validity of these assumptions, the observed response of the Painter Street Bridge, which has a very similar layout as Camino Del Norte, was evaluated. The Painter Street Bridge is an instrumented structure and recordings at 17 stations on the bridge during the Petrolia Earthquake (25 April 1992, M_w=7.0) are available. Figure 2-5 shows the plan view of the Painter Street Bridge and the location and configuration of the instrumentation. Several researchers have previously investigated the response of the bridge to the Petrolia

Earthquake (McCallen and Romstad 1994, Zhang and Makris 2002, Goel and Chopra 1997, Price and Eberhard 2005). The purpose of the analysis in the context of this study is only to evaluate the validity of the SDC guidelines to model the springs representing the abutments and pile foundations. Consequently, a nonlinear dynamic analysis under recorded free-field ground motions (channels 12, 13 and 14) during the Petrolia Earthquake was carried out. Results obtained from the nonlinear response history analysis are compared with observed response in Figure 2-6 in the transverse and vertical directions at selected locations. Although the actual response of the bridge could not be reproduced with considerable accuracy, the results are quite satisfactory in the sense that the fundamental period of the bridge could be captured reasonably in all primary orthogonal directions. Some of the discrepancy in the computed response magnitude can be attributed to the fact that the same free field motions were applied at both abutments and pile foundations in the analytical simulations whereas the actual input motions at these locations may have been different. Based on this independent set of analyses of the Painter Street over-crossing, it can be stated that the approximate expressions given in SDC-2006 for the spring coefficients representing the abutments and pile foundations are adequate for this class of highway bridges.

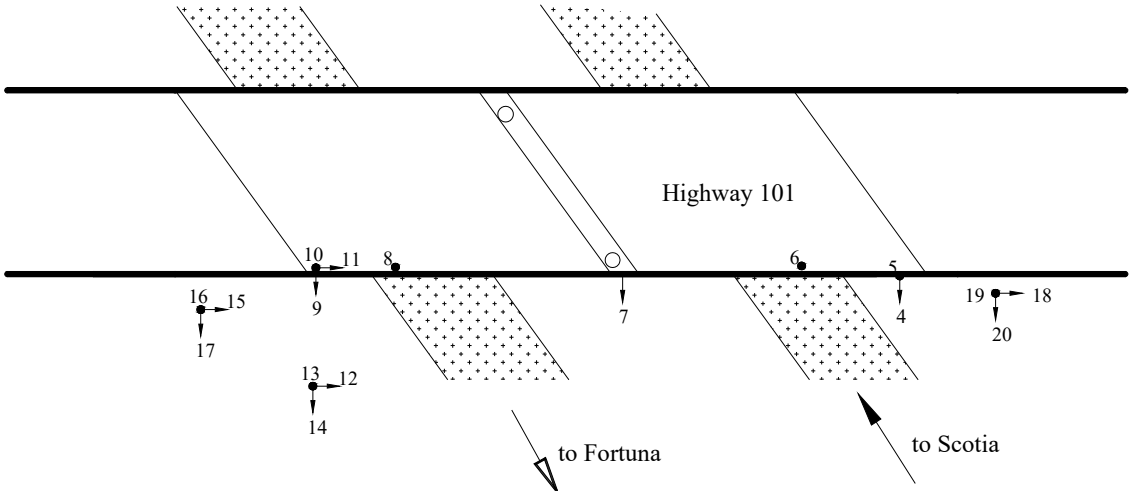

Figure 2-5 - Plan view of the Painter Street Bridge and the position of the accelerometers

Following the validation study, a free vibration analysis was carried out on the base configuration of the Camino Del Norte Bridge and the fundamental periods

were determined to be 0.55, 0.32 and 0.19 seconds in the transverse, longitudinal and vertical directions, respectively. In order to cover a certain range of fundamental periods, particularly in the vertical direction, the original geometry of the bridge was modified. In developing the additional bridge configurations, care was taken not to violate the limits imposed by SDC-2006 on the geometry and dimensional restrictions for Ordinary Standard Bridges. Accordingly, only the span lengths of the bridge, L1 and L2, were modified from the original values, which in turn alter the mass of the bridge, and correspondingly the fundamental period of the bridge in all three directions. The final set of bridge configurations utilized in the evaluation and the periods of these structures are summarized in Table 2-2.

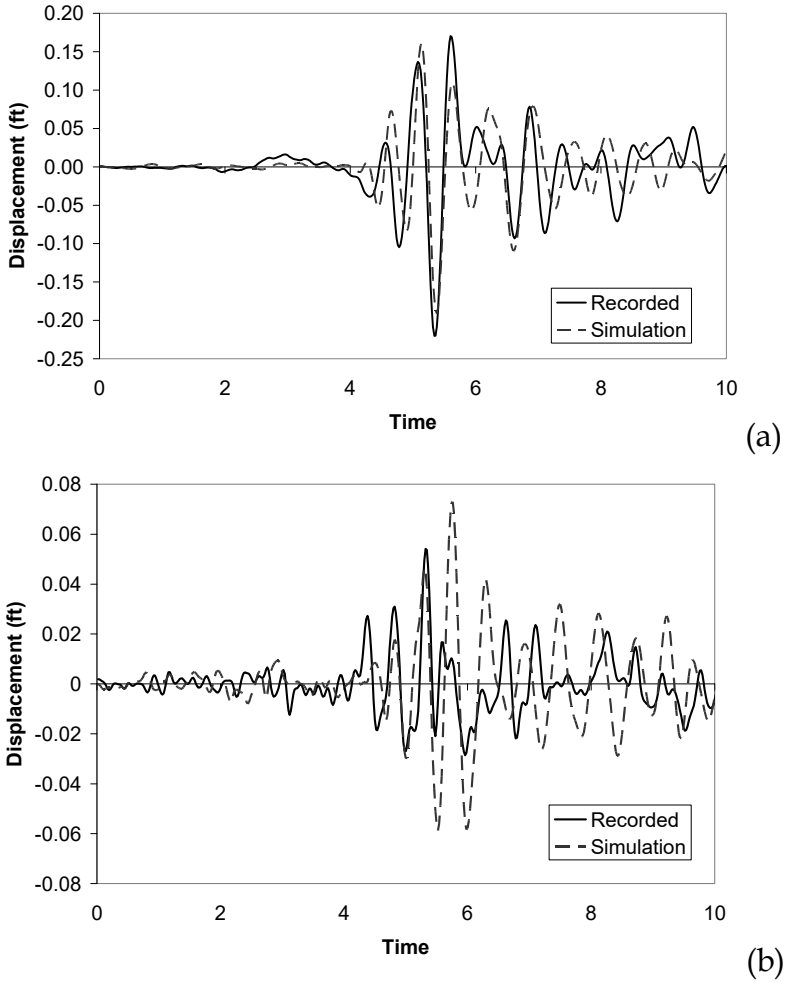

Figure 2-6 - Recorded displacement time history response of Painter Street Bridge together with the results of the response history analysis in (a) transverse direction at column bent (b) vertical direction at the middle of left span

Table 2-2 – Properties and periods of highway over-crossings

Configuration	*L1 (ft)*	*L2 (ft)*	T_L *(s)*	T_T *(s)*	T_V *(s)*
Original	101.5	100.1	0.32	0.55	0.19
Config 1	68.7	67.3	0.27	0.46	0.12
Config 2	134.4	132.9	0.43	0.64	0.30
Config 3	150.8	149.3	0.53	0.68	0.37
Config 4	167.2	165.7	0.62	0.75	0.45
Config 5	118.0	116.5	0.35	0.59	0.24

2.1 MODELING OF MULTI-SPAN SINGLE FRAME BRIDGES

Amador Creek Bridge was selected as the prototype bridge to represent typical multi-span, single frame prestressed concrete bridges built by CalTrans according to post-Northridge design practice. It is a three-bent, four span reinforced concrete bridge with a total length of 685 ft. The bents of the bridge consist of single double-spiral columns. Figure 2-7 presents the elevation view and cross-sectional details of the columns of the Amador Creek Bridge.

As in the case of highway over-crossings, multi-span single frame bridges were also modeled as an elastic superstructure sitting on nonlinear columns on elastic foundation systems. The assumption of elastic superstructure was based on the capacity design approach employed by Caltrans via SDC-2006 (Caltrans 2006). The elastic properties of the Amador Creek Bridge superstructure are presented in Table 2-3.

Table 2-3 – Elastic properties of Amador Creek Bridge superstructure

Parameter	*Value*
Area, A	72.4 ft^2
I_x	527.9 ft^4
I_y	8538.6 ft^4
J	3535.9 ft^4

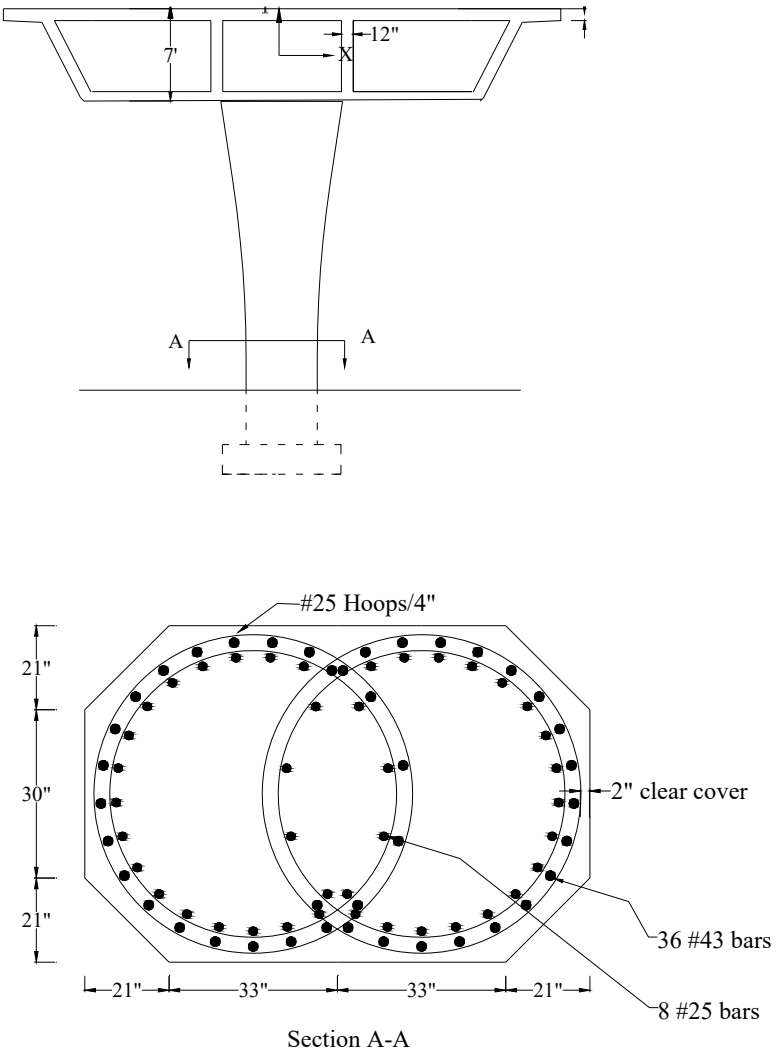

Figure 2-7 - Elevation view and column details of Amador Creek Bridge

An overview of the OpenSEES model of the Amador Creek Bridge is depicted in Figure 2-8 (a). The span lengths of the original bridge are 133 ft (L1) and 177.1 ft (L2), while the heights of the columns are 64.8 ft (H1), 91.9 ft (H2) and 83.7ft (H3). Since the bridge considered is a single column bent bridge, the superstructure is expected to be more vulnerable to torsional effects (rotation about X axis) then multi-column bent bridges. To ensure the proper modeling of torsional properties of the deck, a three dimensional (3D) shell model of the bridge was created in SAP-2000, as depicted in Figure 2-8 (b). A series of elastic modal analyses were carried out on both systems to calibrate the inertial properties of the superstructure of the line model.

Figure 2-9 presents the fundamental elastic mode shapes in longitudinal, transverse, vertical and torsional directions along with the corresponding periods for both shell and line models.

Figure 2-9 clearly shows that the line model created in OpenSEES is capable of capturing the fundamental modes and the corresponding periods of the Amador Creek Bridge in all directions.

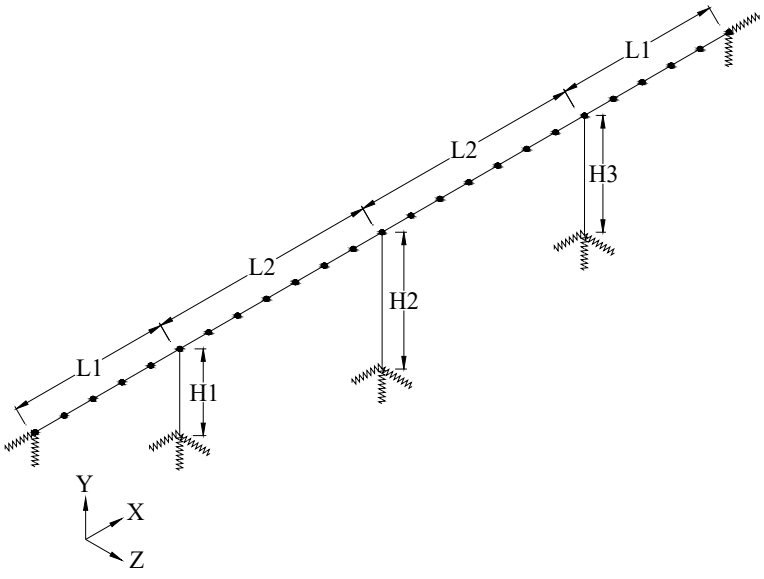

(a)

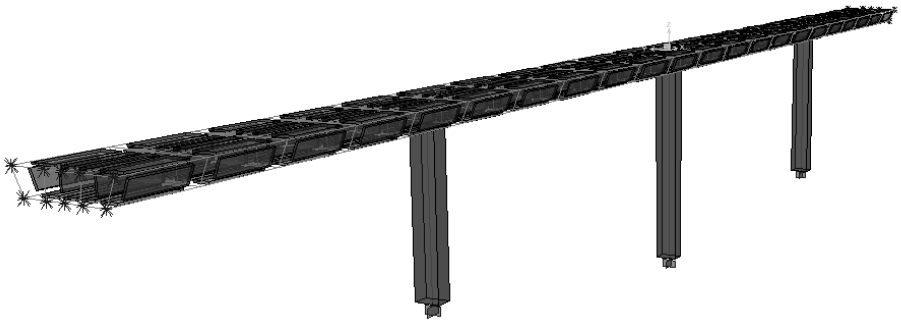

(b)

Figure 2-8 - (a) Line model of the Amador Creek Bridge in OpenSEES, and (b) 3D shell model in SAP-2000

The compressive strength of unconfined concrete and the yield strength of longitudinal reinforcement were specified to be 4 ksi and 60 ksi, respectively in the design drawings. The compressive strength and ultimate strain of confined concrete were computed as 5.83 kips and 0.0157 using Mander's model (1988). Figure 2-4 presents the concrete model used for both confined and unconfined concrete of

multi-span single frame bridges. As indicated previously, a bilinear model with a post-yield stiffness of 5% of the initial stiffness was used to model reinforcing steel.

The columns of the Amador Creek Bridge rest on shallow foundations. Six elastic springs in 3 translational and 3 rotational directions were used to model the soil-foundation system. The approximate expressions proposed in FEMA-356 (FEMA 2000) were used to compute properties of the corresponding springs. Table 2-4 lists the values of the springs representing the foundation system resting on a soil with a shear wave velocity of 1181 ft/s.

Table 2-4 – Elastic properties of springs used to model footings

Spring Direction	*Value*
Translation, x	3.55×10^5 kips/ft
Translation, y	4.12×10^5 kips/ft
Translation, z	3.42×10^5 kips/ft
Rotation, x	7.75×10^7 kips.ft/rad
Rotation, y	8.56×10^7 kips.ft/rad
Rotation, z	3.91×10^7 kips.ft/rad

Seat type abutments were used at both ends of the bridge. Spring systems were used to model the dynamic stiffness of the abutments. In the transverse direction, shear keys are designed to break off during a strong ground motion. Hence, seat type abutments do not possess any stiffness in the transverse direction. In the vertical direction, the movement of the bridge is prevented at the abutments in both upward and downward directions. Thus, the abutments were modeled as restrained supports in the vertical direction. In the longitudinal direction, the bridge is free to move in the opposite direction of the abutment at each end.

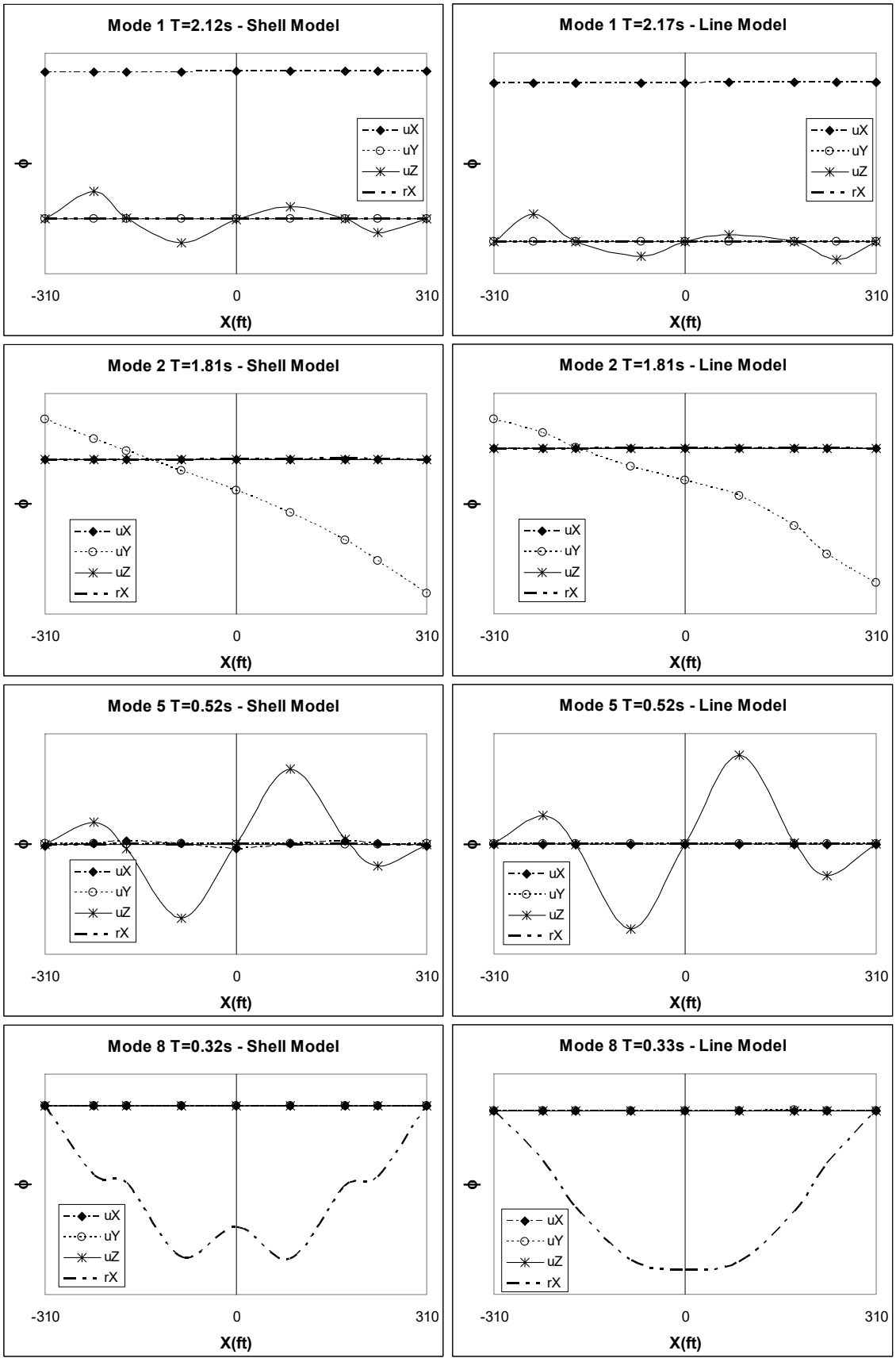

Figure 2-9 - Elastic mode shapes obtained from shell and line models

Towards the abutment there is a certain amount of gap before the deck makes contact with the abutment. When the deck and the abutment are in contact, the stiffness of the abutment is computed as: $K = (K_i\ w\ h)/5.5$, where K_i is the initial stiffness of the abutment and is taken to be equal to 20.0 kips/inch per ft, w and h are the width and height of the abutment. Accordingly, a spring which has no stiffness in tension and elastic in compression with an initial stiffness of 6785 kips/ft and with a 4" gap was used to model the abutment behavior in the longitudinal direction

As in the case of highway over-crossings, different configurations of single frame multi-column bridge systems were developed to be able to consider a range of fundamental parameters. The column heights of the original Amador Creek Bridge are 64.8 ft, 91.9 ft and 83.7 ft for H1, H2, and H3, respectively. With these column heights, Amador Creek Bridge does not conform to the specifications of SDC-2006 (Caltrans 2006) which requires the stiffness ratio of two adjacent bents to be higher than 0.75. Since the main scope of this study considers ordinary standard bridges conforming to the SDC-2006 document, the column heights of the bridge was modified to be equal to 82.0 ft for all configurations.

Table 2-5 summarizes the different configurations obtained for multi-span bridges via altering the span lengths and the fundamental periods of these configurations in 3 directions.

Table 2-5 - Properties and periods of single frame multi-span bridges

Configuration	***L1 (ft)***	***L2 (ft)***	T_L ***(s)***	T_T ***(s)***	T_V ***(s)***
Config 1	132.9	177.2	2.54	1.85	0.53
Config 2	114.8	147.6	2.33	1.69	0.38
Config 3	82.0	114.8	2.04	1.44	0.23

3 GROUND MOTIONS

It is necessary to examine both the characteristics of vertical ground motions and effects of these motions on the response of engineering structures. The key question on this matter is - in what conditions or when does the vertical component need to be considered in structural design. Therefore, the objective of this study is mainly to address the conditions leading to the vertical component having a significant effect on the response of bridge columns. Findings from the overall study are expected to provide a basis for developing revised guidelines to address vertical ground motion effects in the seismic design of highway bridges.

In the near-source region of large earthquakes, the characteristics of strong ground motions change in stable and predictable ways: durations become significantly shorter (Chang et al., 1996; Abrahamson and Silva, 1997), velocity and displacement time histories can increase significantly in amplitude and become more pulse like (depending upon rupture directivity effects), long period fault normal motions show a stable increase over fault parallel motions (Somerville et al., 1997), and short period vertical motions can exceed horizontal motions (Niazi and Bozorgnia, 1991; Bozorgnia et al., 1995) at both rock and soil sites (EPRI, 1993).

Therefore, a preliminary subset of recordings taken from a distance less than 30 km to the fault rupture from earthquakes greater than magnitude 6.0 was considered. The database consists of 794 horizontal and 397 vertical component of recordings from 50 earthquakes worldwide (gathered from PEER_NGA database). Figure 3-1 shows the distribution of data with magnitude and distance; and Figure 3-2 shows the local site conditions of the ground motion stations according to NERHP and Geomatrix soil classification methods. Both figures shows that the records in the dataset are well distributed in magnitude, distance, and site conditions; and the consequent equations obtained using this database will be representative of the entire data space. Initially 56 recordings

having strongest horizontal components (peak ground acceleration of the horizontal component is greater than or equal to 0.5 g) were selected from this dataset, (named as Set 1) and used in non-linear bridge simulations (Table 3-1). Figure 3-3 to Figure 3-5 show the individual and mean response spectra for three components of the selected ground motions.

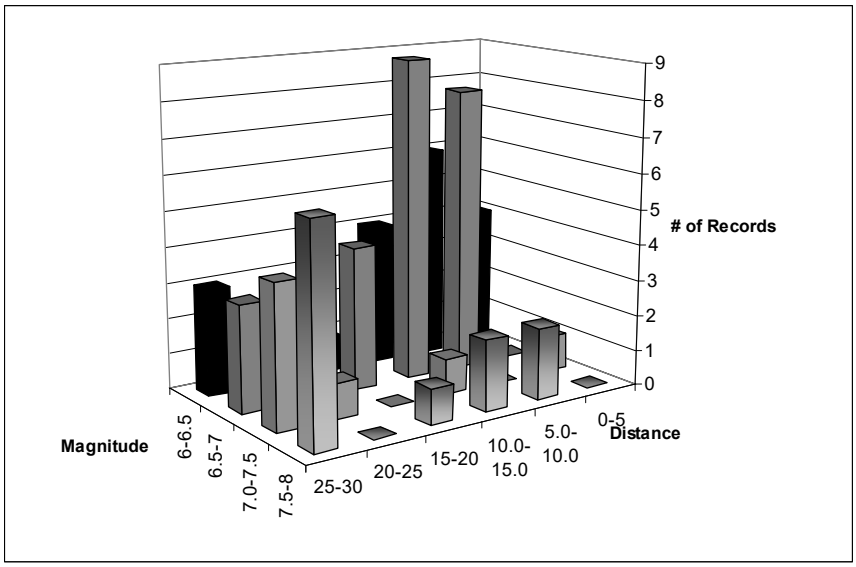

Figure 3-1 - Distribution of Strong Ground Motion Records with Magnitude and Distance

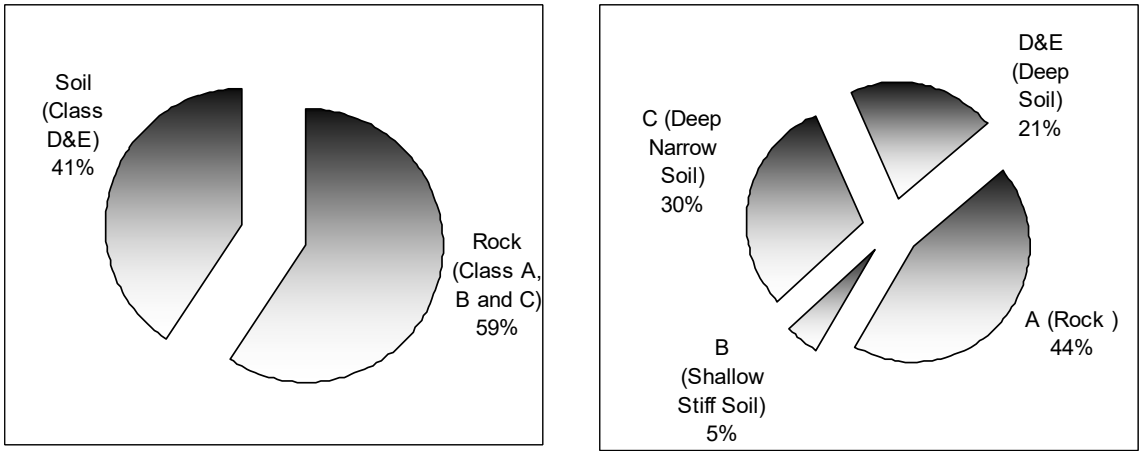

(a) (b)

Figure 3-2 - Distribution of Earthquake Records with respect to NEHRP and Geomatrix Soil Classification

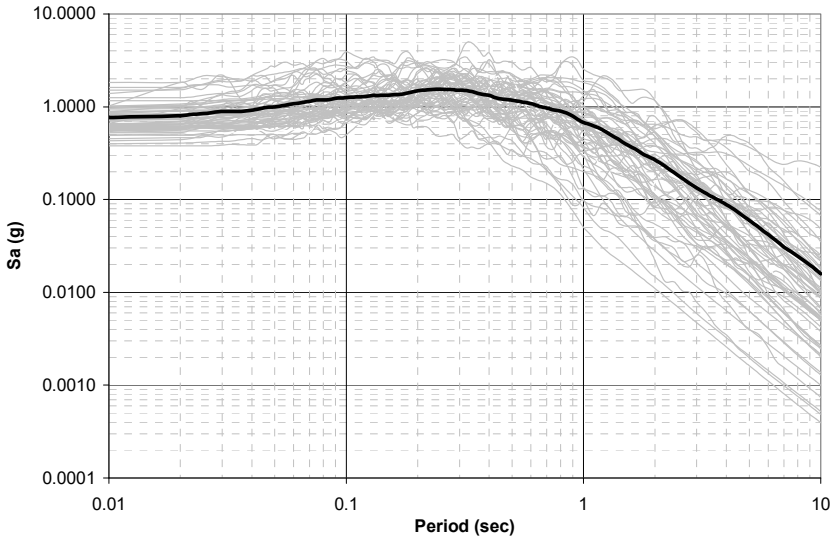

Figure 3-3 - Horizontal Response Spectra for the First Set (First Horizontal Component) (Gray lines show the individual spectrum and the solid black line show the mean)

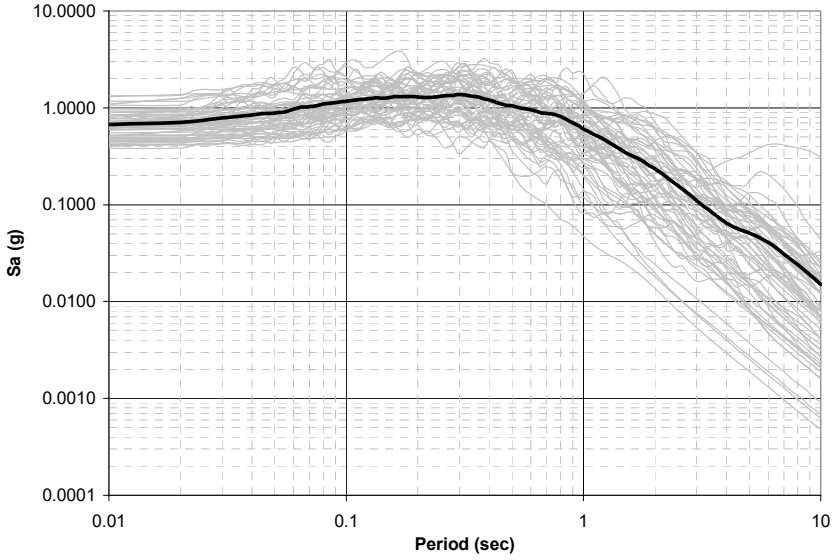

Figure 3-4 - Horizontal Response Spectra for the First Set (Second Horizontal Component) (Gray lines show the individual spectrum and the solid black line show the mean)

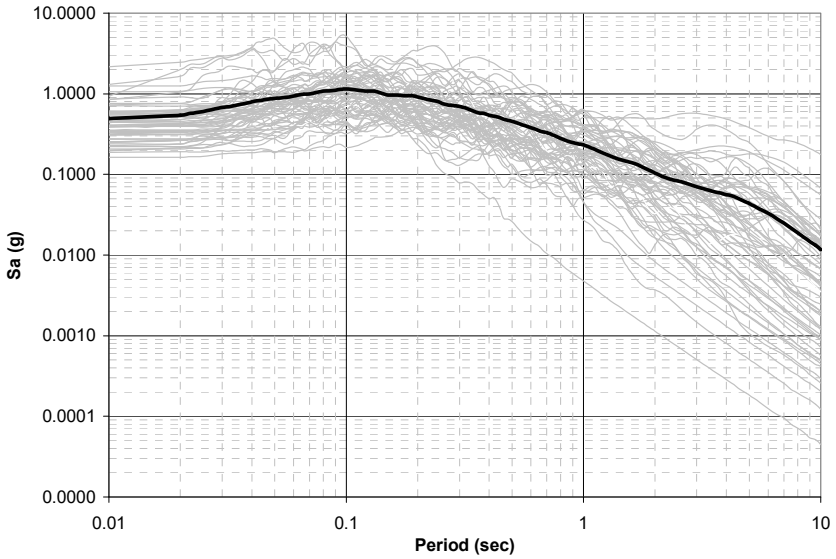

Figure 3-5 - Vertical Response Spectra for the First Set (Vertical Component) (Gray lines show the individual spectrum and the solid black line show the mean)

The characteristics of vertical ground motion have been examined by a number of researchers. Bureau [1981] and Campbell [1982] recognized that the ratio of V/H in the near-source region of large earthquakes was significantly different than that predicted at smaller magnitudes and larger distances. Based on these studies, Campbell [1985] suggested that the standard engineering rule-of-thumb of assuming V/H =2/3 when estimating vertical ground motion for design should be re-evaluated. Niazi and Bozorgnia examined the effects of magnitude and distance on the vertical to horizontal ratio (V/H) for strong ground response spectra in their series of papers from 1989 to 1992. Silva [1997] showed that the magnitude, distance, local site conditions and tectonic environment affect the shapes of horizontal and vertical components of acceleration response spectra. These previous studies in the literature are mainly focused on modeling the horizontal and vertical ground motions and the dependency of vertical to horizontal ratio of proposed ground motion parameters on magnitude, distance and site effects. In any of these studies, neither the proposed ground models were validated by consecutive structural

simulations, nor relationship between proposed models and structural response are investigated.

Inspired by the findings of the previous studies, the sensitivity of ratio of vertical to horizontal ground motion parameters to earthquake properties were examined. Figures 3.6 and 3.9 show the change in the ratio of vertical to horizontal peak ground accelerations with respect to magnitude, distance, horizontal spectral acceleration at T=0.2 second and horizontal spectral acceleration at T=1 second, respectively. Similarly, in Figures 3.7 and 3.8 the change in the ratio of vertical to horizontal peak ground velocity and displacement with respect to magnitude and distance are plotted.

In none of these figures, a significant correlation between the ratios of vertical to horizontal ground motion parameters to earthquake properties could be determined. The cases for which the vertical component had a significant effect on the horizontal response cannot be predetermined from simple characteristics of the ground motions such as the ratio of response spectral values or peak ground motion values (PGA, PGV, and PGD). A closer examination of differences in the vertical and horizontal time histories will provide additional information, since the relative phasing between these components may lead to different structural analyses and design decisions. More complex and detailed analyses are necessary to identify the features of ground motions that create a significant vertical effect.

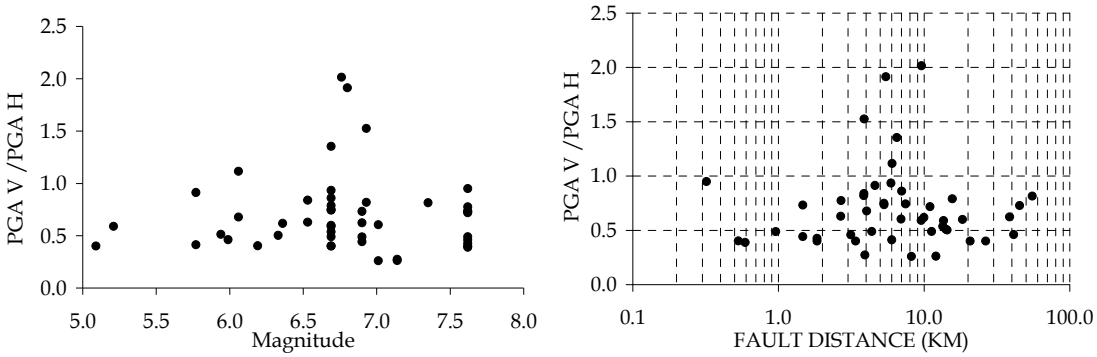

(a) (b)

Figure 3-6 - Ratio of vertical to horizontal peak ground acceleration (a) with respect to magnitude and (b) with respect to distance.

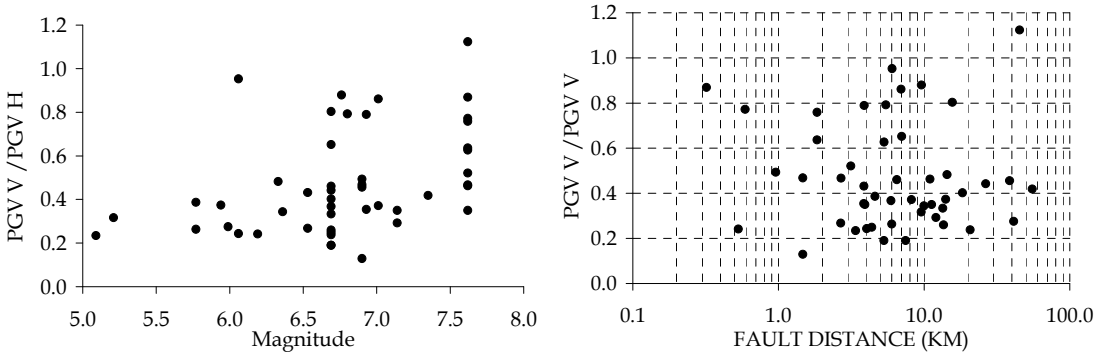

(a) (b)

Figure 3-7 - Ratio of vertical to horizontal peak ground velocity (a) with respect to magnitude and (b) with respect to distance

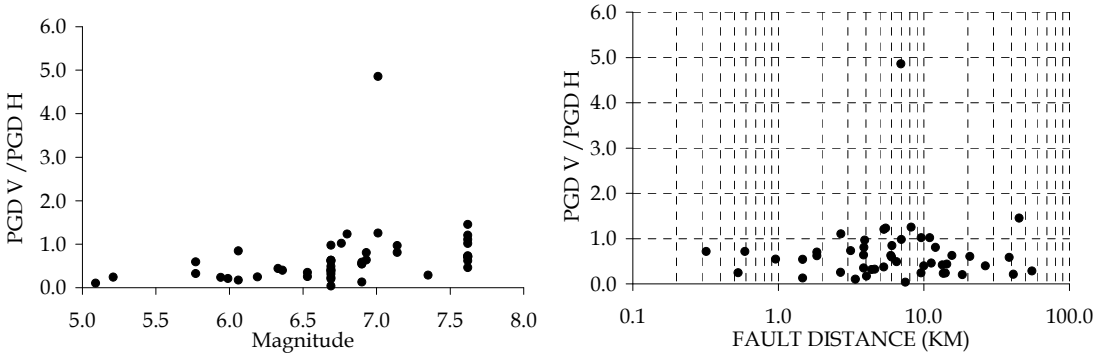

(a) (b)

Figure 3-8 - Ratio of vertical to horizontal peak ground displacement (a) with respect to magnitude and (b) with respect to distance

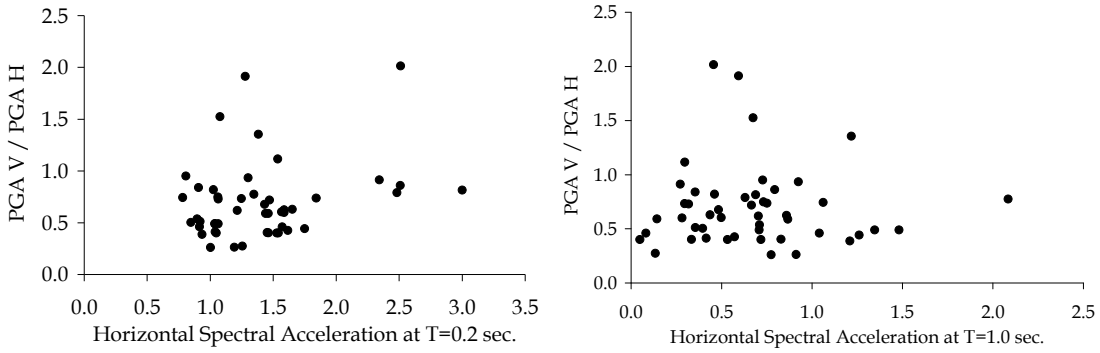

(a) (b)

Figure 3-9 - Ratio of vertical to horizontal peak ground accelerations

(a) with respect to horizontal spectral acceleration at T=0.2 sec. and (b) with respect to horizontal spectral acceleration at T=1 sec.

Table 3-1 - List of first set of ground motions used in nonlinear simulations (Set 1)

Earthquake Name	Station Name	PGA (g)	PGV (inch/sec)	PGD (inch)	Earthquake Magnitude	Closest Distance (miles)
Baja California	Cerro Prieto	1.26	21.96	3.83	5.50	2.29
Big Bear-01	Big Bear Lake - Civic Center	0.51	12.26	1.59	6.46	6.31
Cape Mendocino	Cape Mendocino	1.30	34.81	10.62	7.01	4.32
Cape Mendocino	Petrolia	0.62	27.41	10.13	7.01	5.08
Chi-Chi, Taiwan	CHY028	0.79	28.50	7.13	7.62	1.95
Chi-Chi, Taiwan	CHY080	0.82	34.33	11.02	7.62	1.67
Chi-Chi, Taiwan	TCU065	0.68	39.19	32.19	7.62	0.37
Chi-Chi, Taiwan	TCU068	0.54	81.12	132.41	7.62	0.20
Chi-Chi, Taiwan	TCU071	0.62	23.89	15.20	7.62	3.30
Chi-Chi, Taiwan	TCU079	0.53	20.38	4.93	7.62	6.82
Chi-Chi, Taiwan	TCU084	0.79	36.48	11.33	7.62	6.98
Chi-Chi, Taiwan	TCU088	0.53	7.60	5.51	7.62	11.28
Chi-Chi, Taiwan	TCU095	0.52	21.97	14.14	7.62	28.07
Chi-Chi, Taiwan	TCU129	0.79	18.64	15.25	7.62	1.14
Chi-Chi, Taiwan	WNT	0.75	21.70	9.81	7.62	1.14
Chi-Chi, Taiwan-03	TCU129	0.61	10.43	1.89	6.20	7.97
Chi-Chi, Taiwan-06	TCU079	0.63	14.80	2.13	6.30	6.24
Chi-Chi, Taiwan-06	TCU080	0.58	11.18	1.91	6.30	6.34
Coalinga-02	Oil City	0.58	7.52	0.41	5.09	2.86
Coalinga-05	Transmitter Hill	0.72	13.45	1.50	5.77	3.72
Coalinga-07	Coalinga-14th & Elm	0.58	12.33	1.40	5.21	5.95
Coalinga-01	Pleasant Valley P.P. - yard	0.57	17.75	2.71	6.36	5.23
Erzincan, Turkey	Erzincan	0.49	28.72	9.76	6.69	2.72
Kobe, Japan	KJMA	0.68	30.38	7.39	6.90	0.60
Kobe, Japan	Takatori	0.65	46.77	13.13	6.90	0.91
Duzce, Turkey	Bolu	0.78	23.27	6.96	7.14	7.48
Duzce, Turkey	Lamont 375	0.74	11.09	2.41	7.14	2.44
Gazli, USSR	Karakyr	0.65	24.43	8.41	6.80	3.39
Imperial Valley-06	Bonds Corner	0.68	21.15	5.05	6.53	1.67
Imperial Valley-06	El Centro Array #8	0.54	22.36	12.99	6.53	2.40
Kobe, Japan	Nishi-Akashi	0.49	14.25	4.23	6.90	4.40
Kobe, Japan	Takarazuka	0.71	29.87	9.11	6.90	0.17
Landers	Lucerne	0.73	42.83	74.94	7.28	1.36
Loma Prieta	Corralitos	0.52	16.35	4.17	6.93	2.39
Loma Prieta	LGPC	0.78	30.37	16.80	6.93	2.41
Mammoth Lakes-06	Long Valley Dam Upr L Abut	0.65	13.64	2.14	5.94	8.72
Manjil, Iran	Abbar	0.50	16.98	6.93	7.37	7.80
Morgan Hill	Coyote Lake Dam (SW Abut)	0.94	24.85	4.75	6.19	0.33
N. Palm Springs	North Palm Springs	0.62	19.80	3.12	6.06	2.51
N. Palm Springs	Whitewater Trout Farm	0.55	12.97	2.14	6.06	3.75
Nahanni, Canada	Site 1	1.05	17.46	4.26	6.76	5.97

Earthquake Name	Station Name	PGA (g)	PGV (inch/sec)	PGD (inch)	Earthquake Magnitude	Closest Distance (miles)
Northridge-01	Beverly Hills - 12520 Mulhol	0.51	12.92	2.63	6.69	11.41
Northridge-01	Castaic - Old Ridge Route	0.49	18.31	5.35	6.69	12.87
Northridge-01	Newhall - Fire Sta	0.70	33.40	10.74	6.69	3.68
Northridge-01	Pacoima Dam (upper left)	1.40	31.11	5.55	6.69	4.36
Northridge-01	Pardee - SCE	0.51	22.94	5.23	6.69	4.64
Northridge-01	Rinaldi Receiving Sta	0.63	43.01	11.13	6.69	4.04
Northridge-01	Santa Monica City Hall	0.59	12.31	4.16	6.69	16.44
Northridge-01	Simi Valley - Katherine Rd	0.75	15.43	2.03	6.69	8.34
Northridge-01	Sylmar - Olive View Med FF	0.71	38.35	8.83	6.69	3.29
Northridge-01	Tarzana - Cedar Hill A	1.67	37.68	13.50	6.69	9.69
Northridge-06	Rinaldi Receiving Sta	0.54	10.61	0.78	5.28	3.44
San Fernando	Pacoima Dam upper left abut	1.23	34.62	10.15	6.61	1.12
San Salvador	Geotech Investig Center	0.65	18.65	4.75	5.80	3.91
Victoria, Mexico	Cerro Prieto	0.63	9.83	4.30	6.33	8.93
Whittier Narrows-01	Tarzana - Cedar Hill	0.60	7.95	0.57	5.99	25.61
Explanations:* indicates that the epicentral distance is used instead of closest distance.						

4 RESULTS OF NUMERICAL SIMULATIONS

Based on preliminary studies and extensive literature survey, the main parameters that are affected by the vertical components of ground motions were determined to be the axial force demand in the columns, the moment demand at the face of the bent cap (to be referred to as support moment from hereon and not to be confused with the moment at the abutment support) and the moment demand at the mid-span. All results presented in the following sections were normalized by the corresponding response under dead load only (DL), unless stated otherwise. The benefit of this normalization is two fold: first, it offers a more reasonable basis for comparison of the different bridge configurations, and secondly, SDC-2006 design guidelines treat the vertical acceleration as an equivalent static load expressed as a function of the dead load. Hence this normalization enables direct comparison of the demands with SDC guidelines. It should also be noted that all the dynamic simulations, with or without vertical effects, were carried out after a static gravity analysis.

4.1 NUMERICAL SIMULATIONS ON HIGHWAY OVERCROSSINGS

4.1.1 Nonlinear Time History Analysis

A series of nonlinear dynamic analyses were carried out on the selected highway overpass systems to investigate the effect of vertical acceleration on the behavior of these systems. Although these analyses were carried out for all the ground motions listed in chapter 3 of this report, results will be presented for only a representative set of 30 ground motions.

Figure 4-1 presents the variation of axial force demand in the column, the moment demand at the mid-span and at the face of the bent cap of a typical highway overcrossing as a function of time, with and without vertical effects, for a typical record. Shown also in Figure 4-1 is the moment capacity of the girder at the mid-span and at the face of the bent cap computed from a sectional analysis in both positive and negative bending. These plots show that all the parameters considered in this study are

significantly amplified by the vertical component of the near-fault motions. Moreover, Figure 4-1 shows that the mid-span moment and support moment capacity are both adequate to meet the demands in both directions when vertical effects are neglected. However, once the vertical motions are incorporated in the analysis, both the mid-span moment demand and the support moment demand can exceed the moment capacity of the girder. The inelastic excursions occur often enough to suggest yielding of the longitudinal reinforcement and the development of a potential plastic hinge region. The extent of reinforcement yielding is discussed later.

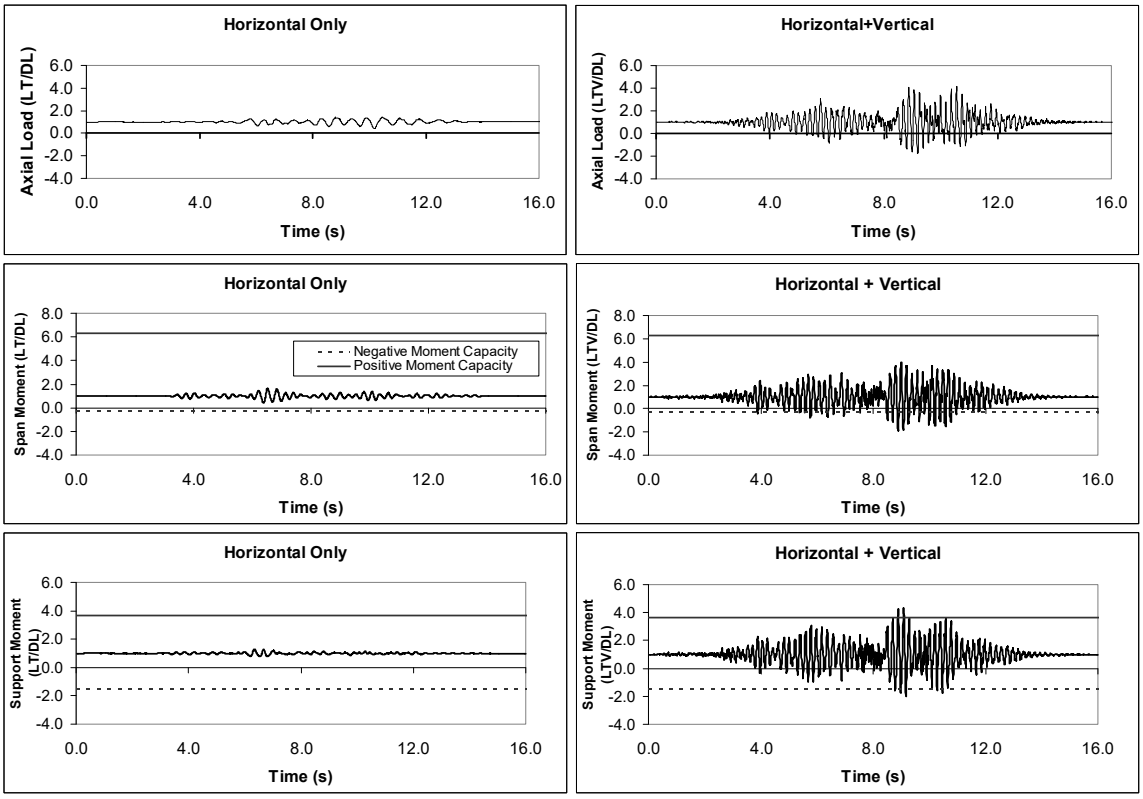

Figure 4-1 - Time history response of axial force demand in the column, moment demand at the mid-span and moment demand at the face of the bent cap with and without vertical effects

First, a set of nonlinear dynamic analyses were carried out using the unscaled ground motions to be able to evaluate the influence of vertical component of ground motions in their original, unscaled form. Presented in Figure 4-2 are the maxima of normalized axial force demands for each ground motion at each vertical period along

with the extreme and mean values obtained under horizontal ground motions only. The data points shown in black represent the increase in the compressive forces whereas the data pints plotted in grey represent a decrease in the column axial force demand. Values less than zero indicate tension. It is evident that the vertical components of ground motions significantly alter the column axial force demands. This effect is more pronounced for systems with shorter periods and tends to decrease with an increase in the vertical period. It is well-known that vertical ground motions are high-frequency motions. The increase in axial force demands with a decrease in vertical period (increase in frequency) is in accordance with the high-frequency characteristic of vertical ground motions.

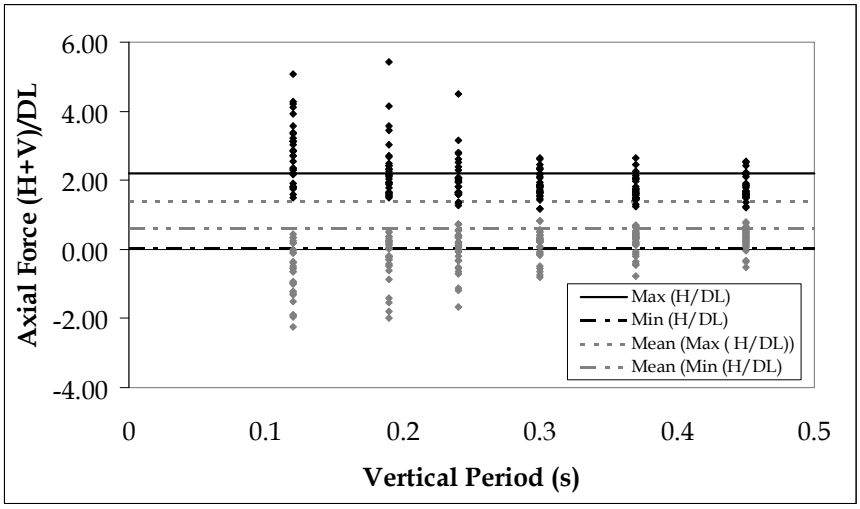

Figure 4-2 – Variation of column axial force demands with vertical period for unscaled ground motions

An immediate effect of the changes in axial force demand in the columns is the variation of flexural and shear capacities of columns. The effect of axial force variation due to vertical effects on the flexural capacity of columns is shown in Figure 4-3. The columns of ordinary standard bridges are designed as ductile members and allowed to plastify under strong shaking. Hence, a decrease in the flexural capacity of the column is not expected to significantly alter the behavior of the system once the increase in the ductility demand leads to lower flexural capacity. However, the increase in the flexural

capacity of the column may significantly alter the behavior of the bridge. Capacity design approach is employed by SDC-2006 (Caltrans 2006) to ensure the plastification is limited to the ends of the columns and the superstructure remains elastic throughout the strong shaking. For this purpose, the flexural capacity of the girder is required to be 20% higher than that of the column. Figure 4-3 reveals that the flexural capacity of the column can be increased by as much as 60% due to variations in the axial force demand as a result of vertical ground motions. This increase in the flexural capacity of columns may jeopardize the capacity design approach of SDC-2006 and shift the plastification zone to the ends of the girders from the column ends. However, the flexural capacity of the girder of the Camino Del Norte Bridge considered in this study is much higher than the observed increase in flexural capacity of the columns. As a result, the increase in the flexural capacity of the columns does not result in the voiding of the capacity design approach.

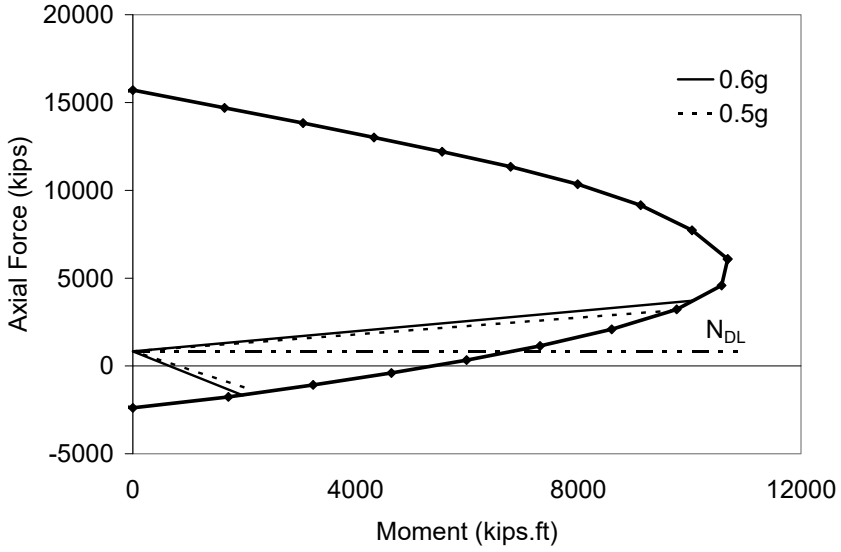

Figure 4-3 – Effect of axial force variations due to vertical ground motions on flexural capacity of columns

Another significant influence of fluctuations in the axial force demand of the columns can be the variation in the shear capacity of the columns. It is well known that the shear capacity of concrete depends on the axial force demand. An increase in the axial force demand in the column such as the one imposed by the vertical components

of near-fault ground motions results in an increase in the shear capacity of the column which is beneficial to the seismic behavior of the column. However, a decrease in the axial force demand on the column results in a decrease in the shear capacity of the column. A decrease on the order of 50% compared to the shear capacity under dead loads was observed in the numerical analyses in cases where the column experiences significant levels of tension, where the concrete contribution to the shear capacity diminishes. To be able to evaluate the effects of the decrease in the shear capacity due to vertical effects, the shear force demand-capacity ratio (DCR) was computed for each case and is plotted in Figure 4-4. In computing the demand capacity ratio, the maximum shear force demand in the column recorded was taken and divided by the shear capacity computed under the minimum axial force demand. Figure 4-4 (a) shows that, despite the decrease in shear capacity of the column due to vertical effects, this reduction due to the variations in the axial force demand is not a significant cause for concern for the bridge configurations considered. It must be recognized though that bridge columns with smaller shear-span ratios may be more susceptible to shear failure. Therefore, a separate set of analysis was carried out by fixing the base of the piers and reducing the height to achieve a shear span of 1.5. The results of the new simulations are shown in Figure 4-4 (b) where there is evidence of demand exceeding capacity in numerous cases. Again, it should be made clear that the capacity calculations are based on SDC guidelines and the axial force used is the most critical across the time history, whereas the peak shear demand does not necessarily occur at the instant of critical axial demand. Further, the frequency of the axial force fluctuation is considerably different from that of the lateral force variations, making this issue more complex to resolve without experimental calibration.

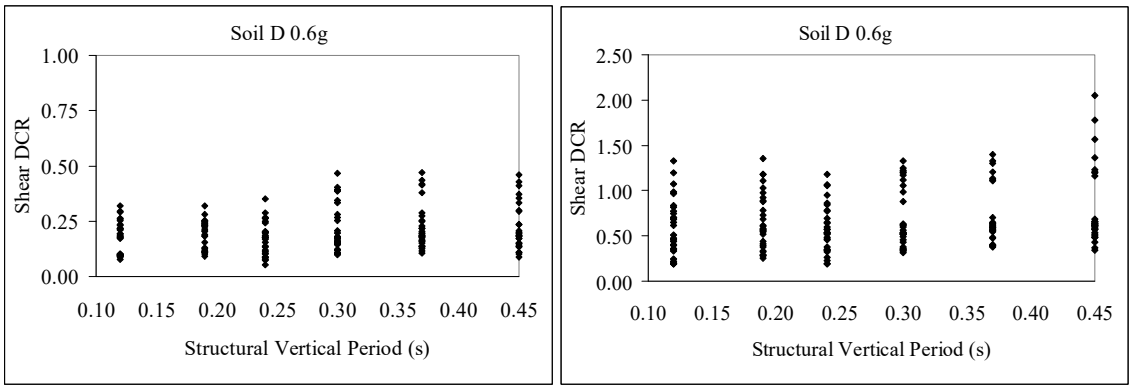

(a) (b)

Figure 4-4 – Shear demand-capacity-ratios (DCR) computed under combined horizontal and vertical excitations: (a) column shear span ratio =4.8; (b) column shear span ratio =1.5

Figure 4-5 depicts the variation of moment demand at the face of the bent cap as a function of the fundamental vertical period of the bridge. Also shown in Figure 4-5 are the design moment demand computed according to the provisions of the SDC-2006 (Caltrans 2006) and the moment capacity of the superstructure computed using classical section analysis. As in the case of axial force demand in the columns, increase in the support moment demand due to vertical ground motions are more pronounced for systems with low vertical periods and tends to decrease with an increase in the vertical period. The design moment demand computed using the guidelines of SDC-2006 which is based on a capacity design approach aiming to limit the plastification to the columns of bridge structures yields highly non-conservative results once the vertical ground motions are considered. The capacity of the superstructure computed using a moment-curvature analysis indicates that the provided capacity significantly exceeds the design moment demand at the support due to various reasons including the minimum reinforcement requirements, material over-strength, etc… Hence, the authors believe that using the actual moment capacity of the systems is more appropriate in assessing the effects of vertical ground motions. Figure 4-5 shows that the vertical ground motions result in support moment demands higher than the capacity for a number of cases with short vertical periods. However, the demand-capacity-ratio (DCR) for the limited number of cases considered in this investigation does not exceed 1.5. In the

computation of support moment capacity, material strengths specified in the design drawings were used. At this point, it will be safe to assume that the on-site material strengths at the time of a strong ground motion will be higher than the values specified in the design drawings. Taking this fact into account and recalling that the DCR values are limited to 1.5, it can be stated that, although the vertical ground motions may test the validity of the assumption that the superstructures will remain elastic throughout all the stages of seismic loading, they are not likely to induce significant damage at the face of the bent cap.

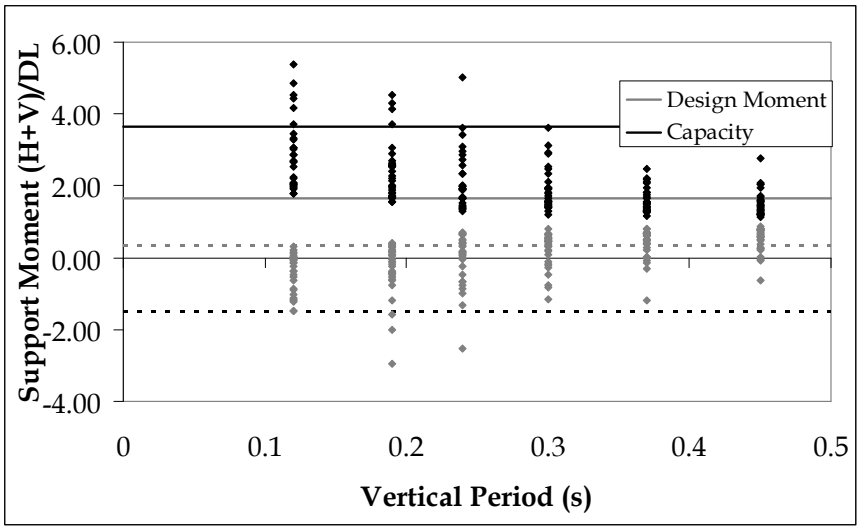

Figure 4-5 – Variation of moment demand at the face of the bent cap with vertical period for unscaled ground motions

Figure 4-6 presents the variation of moment demand at the mid-span with the vertical period of the bridge. Also depicted in Figure 4-6 are the design moment and the capacity of the girder section at the mid-span under both positive and negative bending. As in the case of axial force demand in the column and the support moment demand, the increase in the moment demand at the mid-span due to vertical ground motions decreases with an increase in the vertical period. The moment capacity of the superstructure at the mid-span is much higher than the design moment in positive bending whereas these two values are very close under negative bending. In case of positive bending, the capacity provided is higher than the moment demand even in the

most adverse case indicating that the vertical components of ground motions are unlikely to result in significant damage at the mid-span under positive bending. However, under negative bending, the capacity of the girder is very limited. This may be attributed to very low moment demands in negative bending computed using the SDC-2006 approach resulting in very low amounts of steel provided at the mid-span (25% of the dead load). Therefore, as is evident from Figure 4-6, vertical effects resulting from high intensity near-fault shaking can result in negative moment demands consistently exceeding the capacity available in the girder at the mid-span. Different than the case of positive support moment, in which the DCR values are limited to 1.5, the DCR values in case of negative span moment can reach values as high as 12 for system with a vertical period of 0.12 seconds (note that an elastic stiffness is used for the superstructure hence the demand is not limited by strength capacity). Moreover, although the vertical effects tend to diminish with an increase in the vertical period, the low negative moment capacity provided results in demands higher than the capacity for the cases with vertical periods as high as 0.45 seconds. High demand-capacity-ratios obtained particularly for short period systems suggest that damage is likely to occur under negative bending at the mid-span due to vertical component of near-fault ground motions.

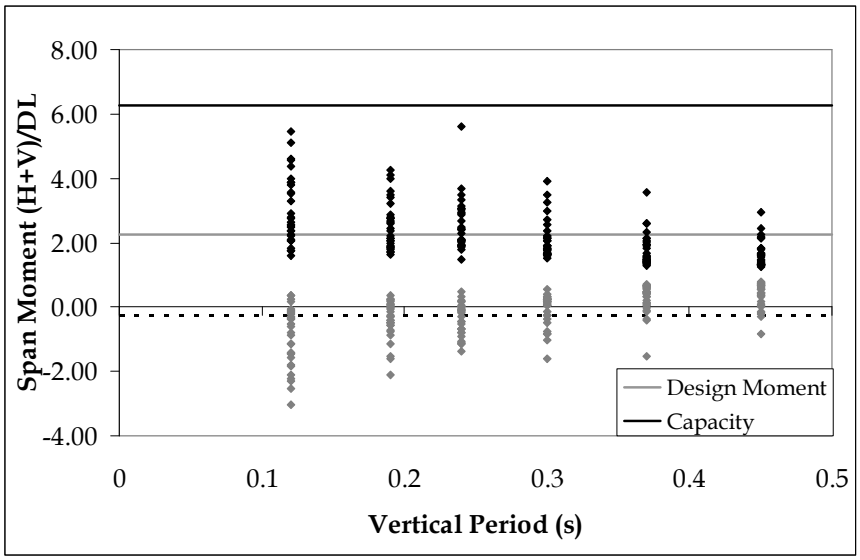

Figure 4-6 - Variation of moment demand at the mid-span with vertical period for unscaled ground motions

A set of response spectra referred to as ARS curves are used by Caltrans (2006) in the seismic design of ordinary standard bridges. A unique design spectrum is defined for each soil type, earthquake magnitude and peak rock acceleration. SDC-2006 requires the vertical components of ground motions included in the design process if the peak rock acceleration is at least 0.6g. To be able to check the validity of this assumption and to standardize the ground motions by matching the horizontal component to a prescribed design spectrum, the ground motions were scaled to match the ARS curve proposed for site class D, earthquake magnitude of 8.0 and peak rock acceleration of 0.5g and 0.6g. Figure 4-7 displays typical spectra of the horizontal component of the ground motions scaled to match the ARS curve for ground motions with a PGA 0.5g and site class D together with the corresponding vertical spectra.

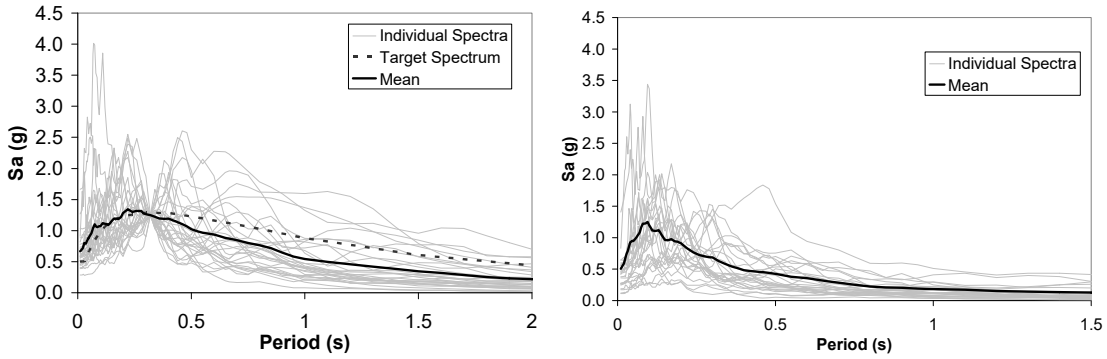

(a) (b)

Figure 4-7 – Spectra of the (a) horizontal component of ground motions scaled to ARS curve (soil type D, magnitude 8.0 and PGA 0.5g) at the fundamental longitudinal period of base configuration and (b) corresponding vertical component

Figure 4-8 shows the maxima of the normalized axial force demand in column, support moment demand and mid-span support moment in girder for each vertical period along with the mean and mean plus standard deviation of these points for peak rock acceleration of 0.5g and 0.6g. Also plotted in Figure 4-8 are the mean plus standard deviation of the corresponding response obtained under horizontal ground motions only. Moreover, in Figure 4-8 (b) and (c) moment capacity of the girder under positive and negative bending at the support and mid-span are also depicted. Figure 4-8 clearly indicates that the vertical ground motions amplify all the parameters investigated for the vertical period range considered. As in the case of unscaled ground motions, the amplification of each response quantity due to vertical ground motions tend to decrease with an increase in the vertical period. The comparison of the graphs for a PGA of 0.5g and 0.6g shows a marginal increase in the effect of vertical ground motions for all the parameters considered.

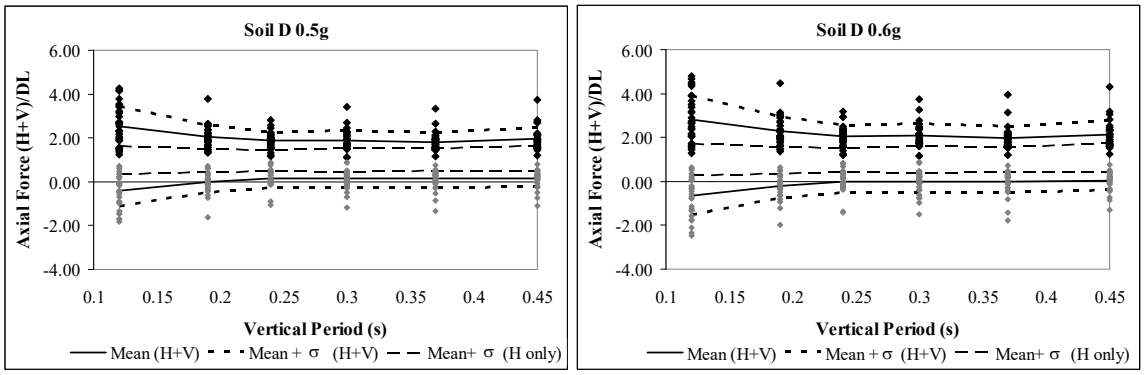

(a)

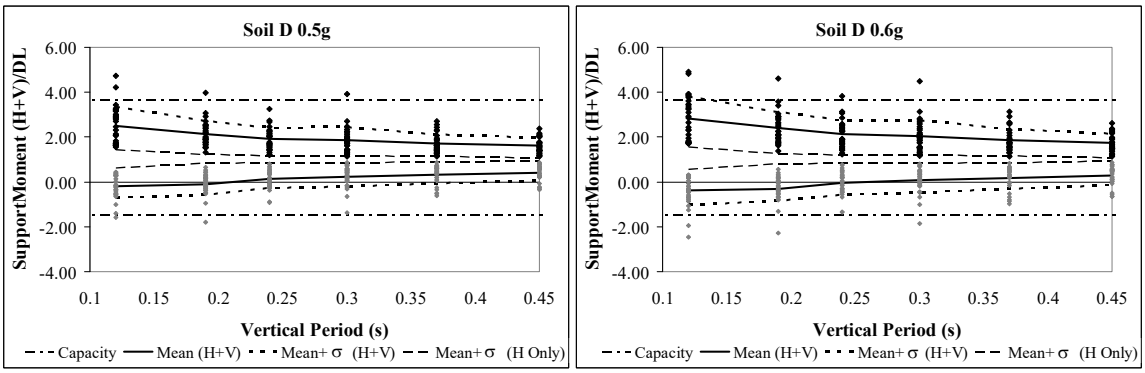

(b)

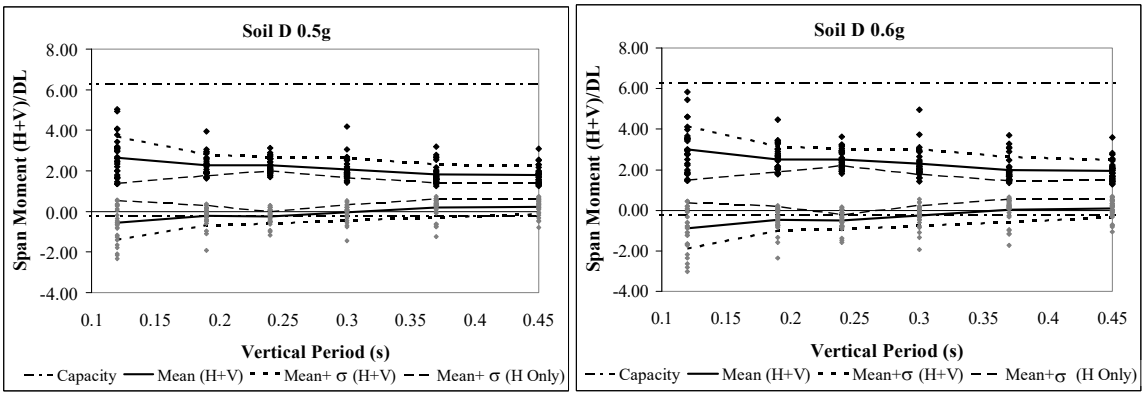

(c)

Figure 4-8 – Variation of normalized (a) axial force demand in columns (b) support moment demand (c) mid-span moment demand with vertical period for ground motions scaled to match ARS curves

Although both the axial force demand in the columns and the moment demand at the mid-span are significantly amplified by vertical effects, this amplification does not suggest the occurrence of any significant damage in the girder due to vertical effects. However in the case of negative mid-span moments, the amplification due to vertical ground motions may result in significant damage due to the very limited

confinement provided in the superstructures of ordinary standard bridges. Figure 4-8 also depicts that, although the amplification due to vertical effects is slightly lower for the ground motions scaled to ARS curves for a PGA of 0.5g than those for 0.6g, it is clear that the former case can also result in damage in the mid-span of the girder under negative bending. This observation points to the fact that the current PGA threshold of 0.6g is not a suitable parameter to delineate the inclusion of vertical effects in design.

To assess the degree of damage occurring in the concrete section at mid-span, the bridge deck was modeled using non-linear fiber beam sections and the response history analyses were repeated on the original configuration. Figure 4-9 presents the strains in the longitudinal reinforcement of the girder due to vertical effects. As expected, the strains in the bottom reinforcement at mid-span of the bridge are within the elastic limit, whereas the strains in the top-reinforcement cause yielding in a significant number of cases with peak strain reach about 1.5%. However, this strain level is acceptable for capacity protected members according to SDC-2006 provisions which set a strain limit of 9% for bars smaller than #10 and 6% for bars larger than #10 in the capacity definition of bridge superstructures. Figure 4-9 also reveals that the compressive strains experienced at the top section of the superstructure at the mid-span exceeds the concrete crushing strain of 0.3% set by SDC-2006 frequently and reaches values up to 1.5% suggesting that significant cracking and crushing can be expected in concrete at the top section of the mid-span under the vertical components of ground motions. Recalling that the girders in a highway bridge are designed to remain elastic under seismic action, these demands need to be evaluated carefully to assess their significance in the context of the overall system performance. Consider also the fact that the top slab section of the girder has limited plastic rotation capacity since they are essentially unconfined.

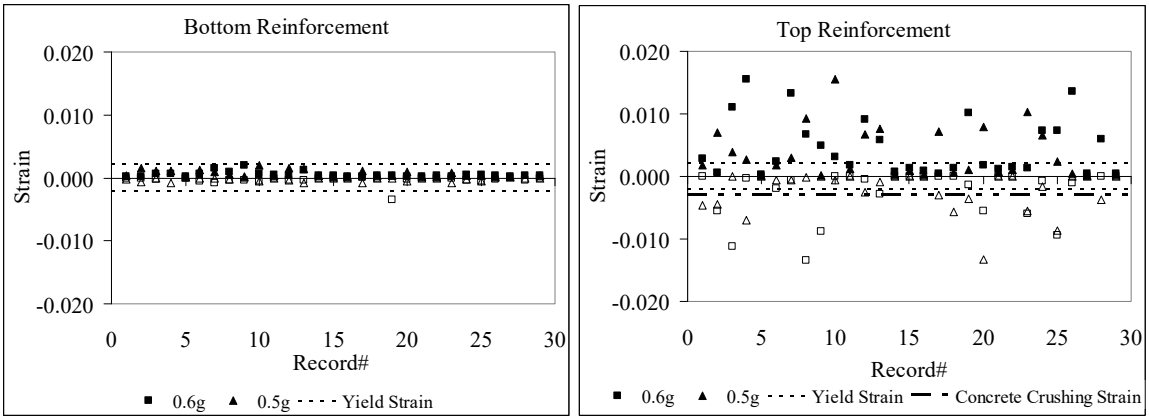

Figure 4-9 - Strains in the longitudinal reinforcement of the girder at mid-span (unfilled markers indicate corresponding peak negative strains)

4.1.2 Response Spectrum Analysis

Nonlinear time history analysis, despite being the most reliable tool to determine the seismic demands on structures under a given ground motion, is not suitable for design purposes. First of all, it is a rather time consuming and involved procedure requiring a comprehensive understanding of nonlinear material behavior. Moreover, the choice of appropriate ground motions for use in seismic evaluation at the expected design event is difficult and subject to speculation and subjective judgment. Therefore, studies have been carried out to come up with a simple procedure that can be used to determine the effects of vertical ground motions on the bridges.

Figure 4-10 plots the time history plot of the normalized mid-span moment demands obtained considering only horizontal components, only vertical component and all three components of a sample ground motion. It is evident that virtually all the mid-span moment demands are a result of the vertical ground motions. As a direct result of this observation, it can be stated that the vertical effects can be uncoupled from horizontal effects. Since the girders were modeled to remain elastic at all stages of the loading as per the capacity design approach of SDC-2006 (Caltrans 2006) and the behavior of the columns in the vertical direction is governed by the axial response which is essentially elastic for the investigated bridge and the considered ground motions, it can be concluded that the behavior of the bridge under vertical ground

motions is generally elastic. Combining these two observations, i.e. the vertical effects can be uncoupled from horizontal effects and the behavior of the bridge under vertical ground motions results in a primarily elastic response, leads to one major conclusion: The effects of vertical components of ground motions on seismic demands of ordinary standard bridges can be estimated using elastic response history analysis, and, in turn, by *elastic response spectrum analysis (RSA)* once sufficient number of modes are included. RSA is not only easy to apply and available in most, if not all, commercial software but also is suitable for use along with the design spectrum.

In order to investigate the effectiveness of RSA on the determination of vertical effects on highway over-crossings, RSA were carried out on the base configuration of Camino del Norte Bridge using the ground motions scaled to match the ARS curve for an earthquake of magnitude 8.0, soil type D and PGA of 0.5g, Figure 4-7. In the RSA analyses, CQC modal combination technique was used to combine the modal responses in each direction and SRSS modal combination rule was used to combine the responses obtained under different directions. Figure 4-11 depicts the approximate normalized axial force, span moment and support moment demands obtained from RSA along with the corresponding "exact" demands obtained from nonlinear NTH for each record. Shown also in Figure 4-11 are the mean values of these demands. Moreover,

Figure 4-12 presents the mean and 84 percentile (mean plus standard deviation, σ) envelope girder moment diagrams obtained from NTH along with the girder moment diagram obtained from RSA. The demands obtained from RSA and NTH for each ground motion for each response parameter as well as the mean value of all the ground motions presented in Figure 4-11 and the girder moment diagrams shown in

Figure 4-12 are close enough to be able to state that the elastic response spectrum analysis is an effective approximate procedure to estimate the effects of vertical ground motions on the column axial force, span moment and support moment demand of ordinary standard bridges.

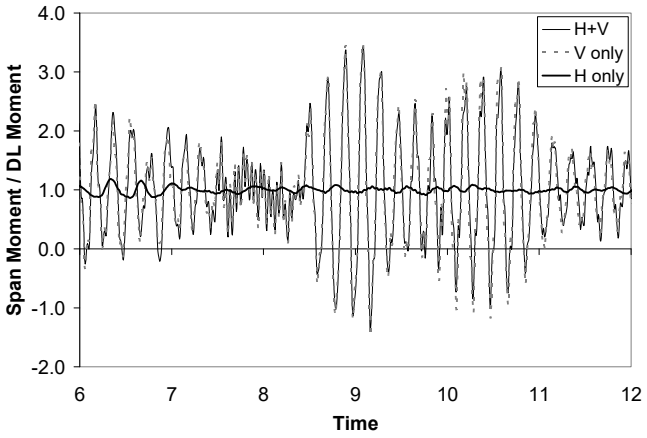

Figure 4-10 – A sample time history of moment demands at mid-span showing contribution of vertical ground motions

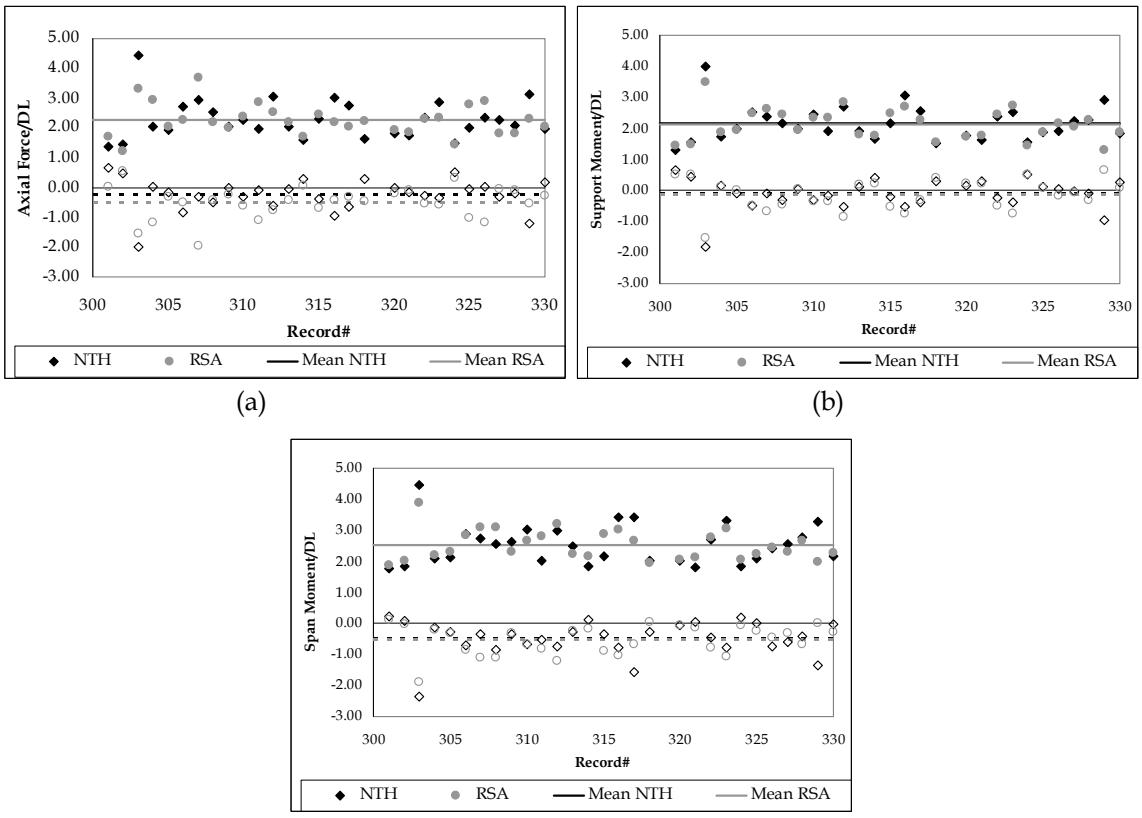

Figure 4-11 – Comparison of NTH and RSA for Camino Del Norte Bridge for ground motions scaled to match spectral value of the ARS curve at the fundamental period of the bridge

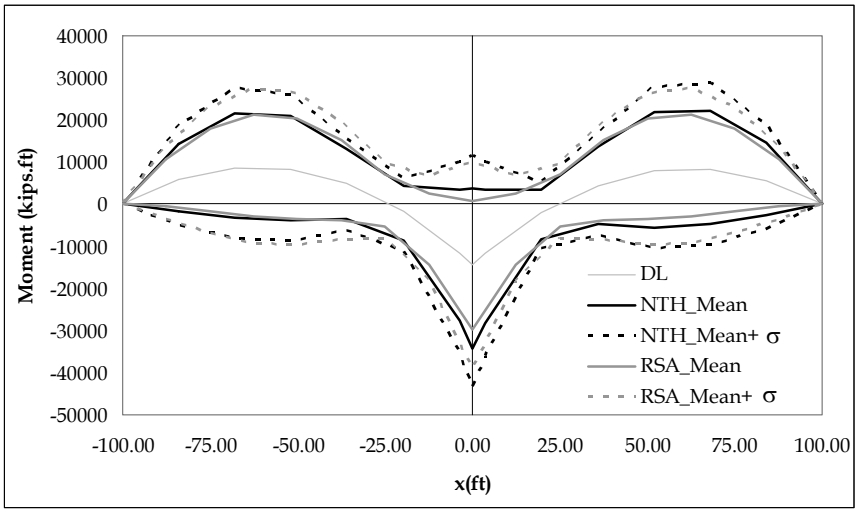

Figure 4-12 – Mean and 84 percentile moment diagrams obtained from NTH and RSA

4.2 NUMERICAL SIMULATIONS ON MULTI-SPAN HIGHWAY BRIDGES

Multi-span highway bridges (described in Chapter 2) were subjected to horizontal and combined horizontal and vertical components of near-fault ground motions to evaluate the effect of vertical ground motions on these systems.

Figure 4-13 depicts the time history response of the moment demand at the mid-span and at the support along with the axial force demand in the column for two cases: (a) neglecting and (b) including the vertical component of a sample ground motion. The results presented in

Figure 4-13 show that the vertical ground motions affect the demand parameters considered in this study, significantly. However, for the ground motion given, the moment demand at the mid-span is more susceptible to vertical effects than the support moment demand and the axial force demand.

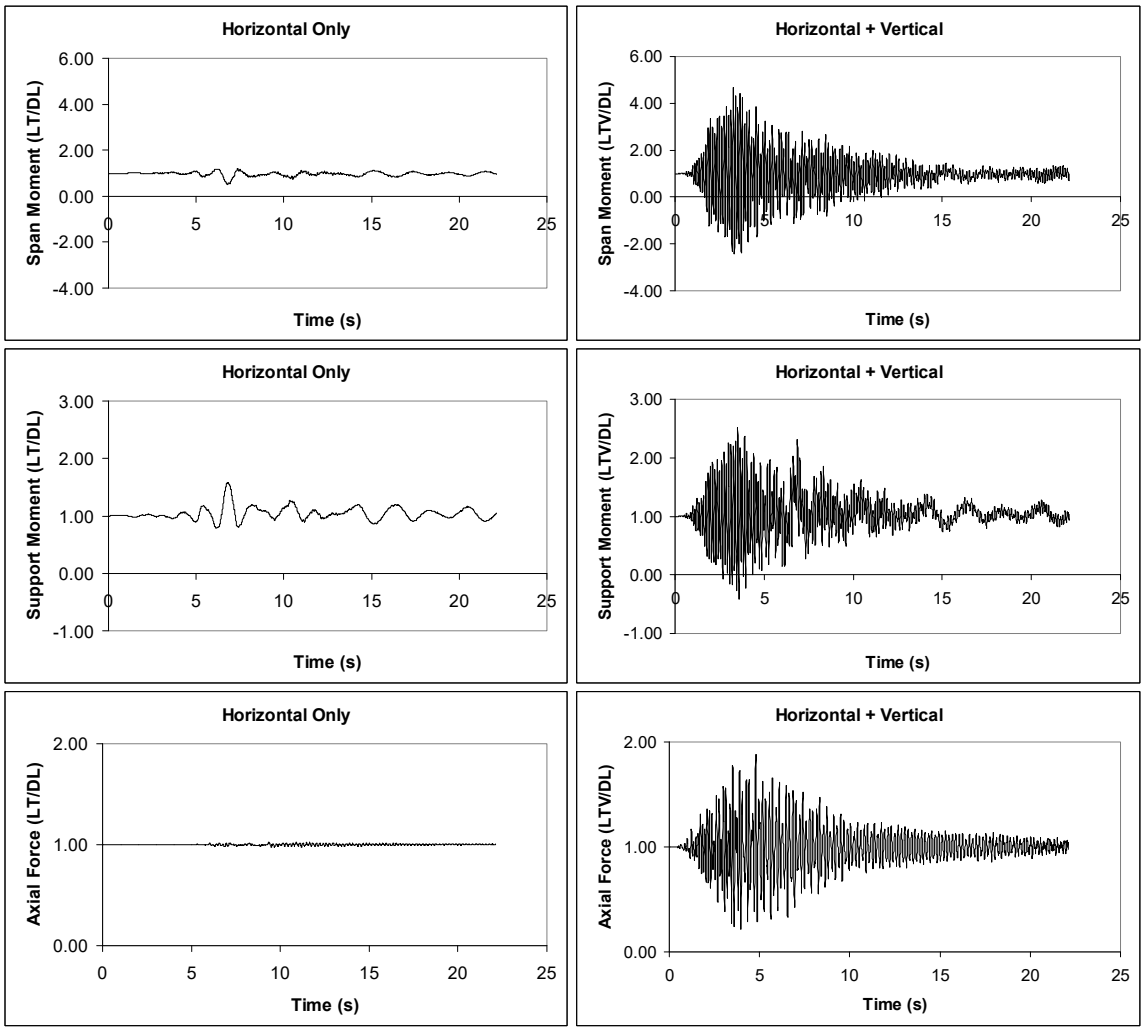

Figure 4-13 – Time history response of selected parameters under horizontal and combined horizontal and vertical components of a sample ground motion

Figure 4-14 presents the variation of extreme values of moment demand at the mid-span for (a) interior and (b) exterior spans as a function of the fundamental vertical period. Figure 4-14 clearly shows that, as in the case of highway overpass systems, the amplification in the mid-span moment demands tend to decrease with an increase in the fundamental vertical period. Moreover, for a multi-span bridge system, the amplification in mid-span moment demands due to vertical effects are more pronounced for exterior spans than interior spans, which are generally designed to be longer than the exterior spans. The difference in the amplification between exterior and

interior spans can be, on average, as high as 65% for the case of the system with a fundamental vertical period of 0.23 seconds and tend to decrease with an increase in T_V.

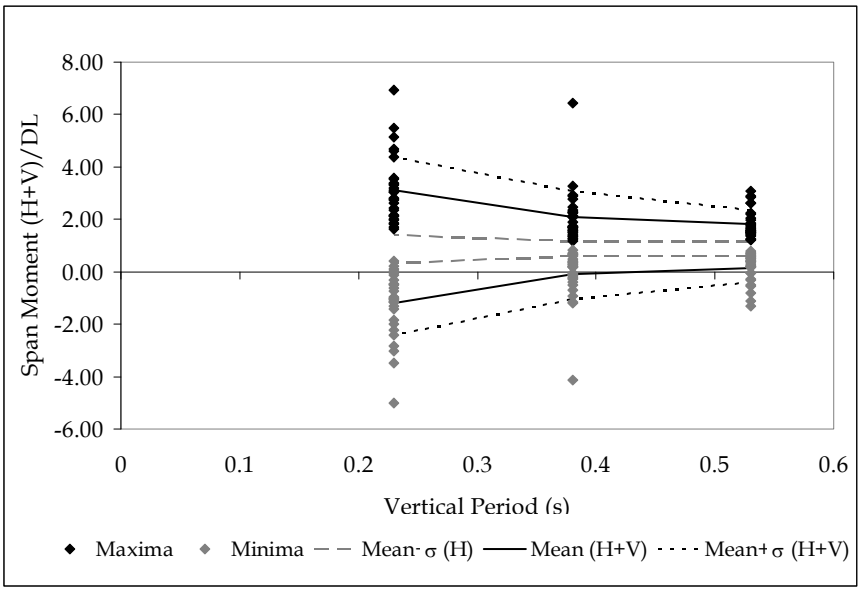

(a)

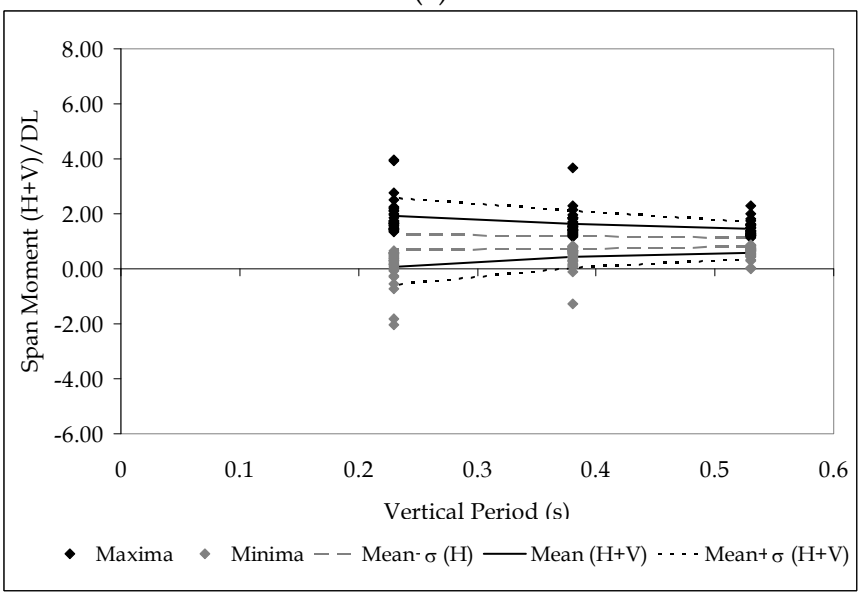

(b)

Figure 4-14 – Variation of extreme values of mid-span moment demand at (a) the exterior span and (b) interior span with vertical period

Shown in

Figure 4-15 are the moment demands at the face of the bent cap of (a) the exterior column and (b) the interior column. In both cases, the amplification due to vertical

effects decreases with an increase in the fundamental vertical period. Moreover, it can be stated that, for both cases the support moment demands obtained considering vertical effects are not significantly higher than the support moment demands obtained when vertical effects are neglected.

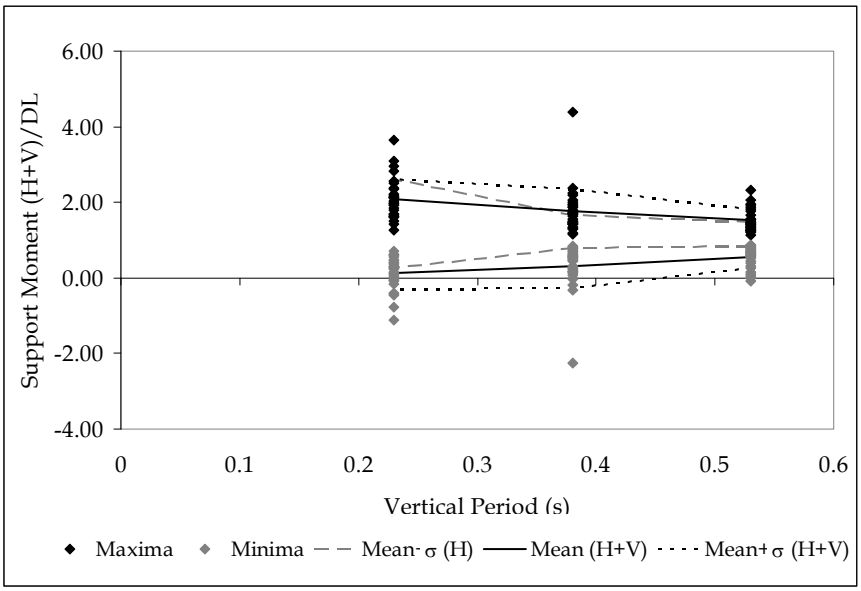

(a)

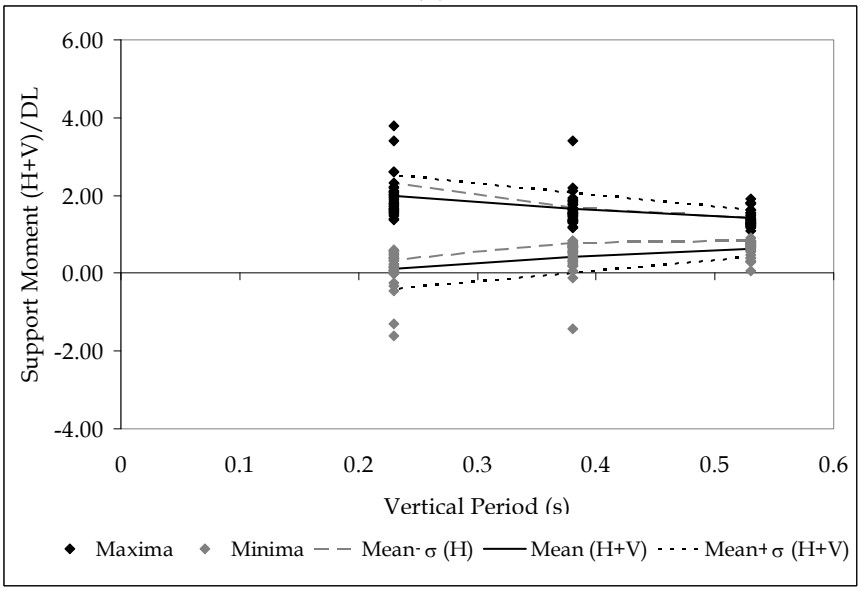

(b)

Figure 4-15 - Variation of extreme values of support moment demand at (a) the exterior support and (b) interior support with vertical period

Figure 4-16 presents the variation of extreme values of axial force demands in the middle column with the fundamental vertical period. As in all the cases investigated so far, the highest amplification due to vertical effects is observed for high frequency systems and the amplification tends to diminish with increasing vertical period.

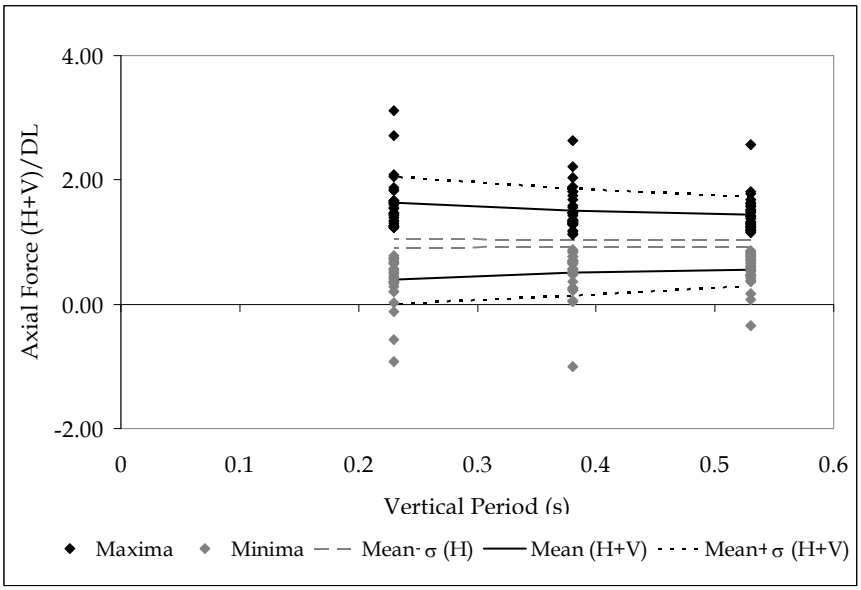

Figure 4-16 – Variation of extreme values of axial force demand in the middle column

Similar to the simulations carried out for highway over-crossings, the multi-span highway systems were also subjected to ground motions scaled to match the design spectra at the fundamental period of the system. However, unlike the prior case where the horizontal components of the ground motions applied in the longitudinal direction of the bridge were scaled to match the horizontal design spectra and the same scale factor was applied to the other two components, in the case of multi-span bridges, the vertical components of the ground motions were scaled separately to match the vertical design spectra and the scale factors obtained this way was applied to the horizontal components of the ground motions.

Figure 4-17 depicts the normalized extreme values of span moment demands, support moment demands and axial force demands obtained for each ground motion

and each system under combined effects of vertical and horizontal ground motions. Shown also in Figure 4-17 are the mean and 84 percentile (mean plus standard deviation, σ) values along with the 84 percentile values obtained considering horizontal components of the ground motions only.

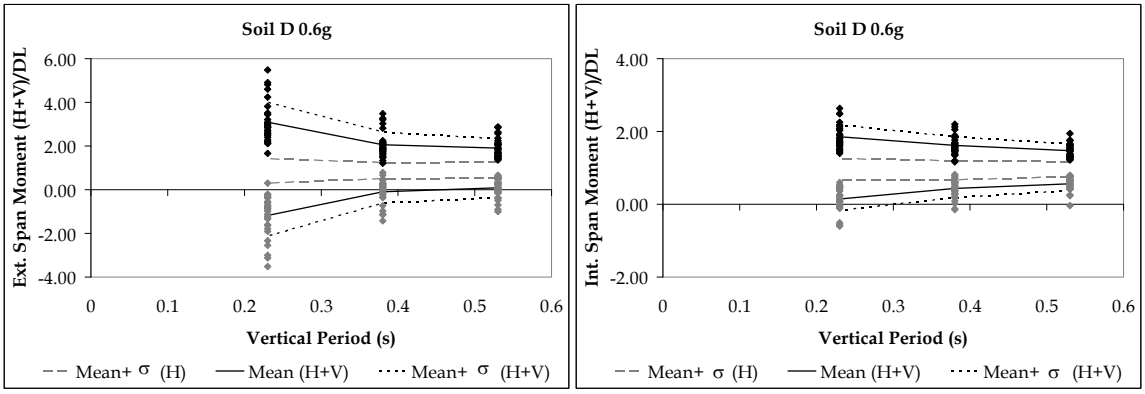

(a)

(b)

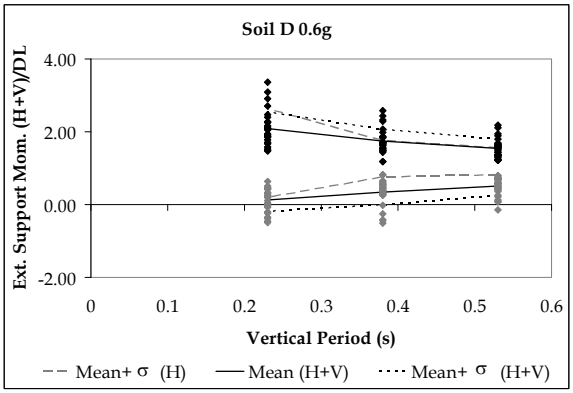

(c)

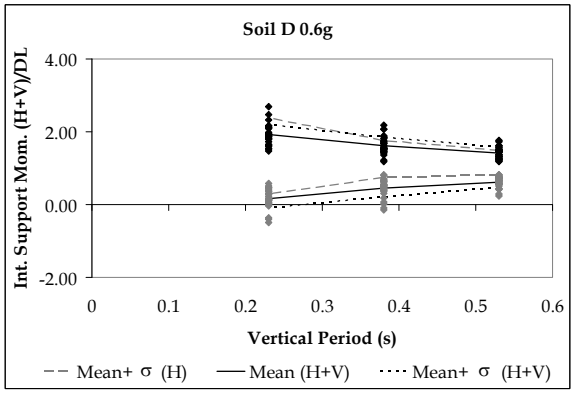

(d)

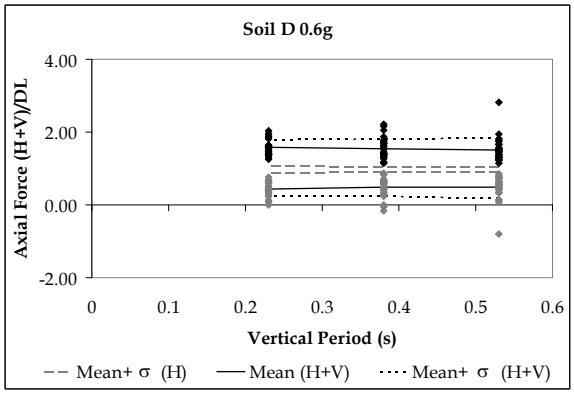

(e)

Figure 4-17 - Variation of extreme values of span moment demand as a function of vertical period at (a) the exterior span, (b) interior span, support moment demand at (c) exterior support, (d) interior support and (e) axial force demand in the middle column

Figure 4.17 (c) and (d) clearly shows that support moment demands obtained considering vertical components of ground motions are only slightly higher than those obtained neglecting the vertical components indicating that the effect of vertical component of ground motions in the moment demands at the face of the bent caps of multi-span bridges is insignificant.

The normalized axial force demands in the middle column of the Amador Creek Bridge shown in Figure 4.17 (e) points out that the vertical component of ground motions amplifies the axial force demands in the columns. However, the level of the amplification in the axial force demands is only marginal and the increased demands do exceed the axial capacity of the column.

Figure 4.17 (a) and (b) summarizes the normalized moment demands at the mid-span of the interior and exterior spans, respectively. The amplification of the moment demands in the exterior span due to vertical ground motions is significantly higher than the amplification in the interior span. The maximum negative exterior span moment demands obtained considering vertical ground motions is significantly high suggesting that yielding in these zones is probable and ignoring the vertical effects may lead to structural damage in these regions.

For the multi-span highway span bridge systems, the amplification in the column axial force demands (Figure 4-16 and Figure 4.17 (e)) are lower than those obtained for highway over-crossings (see Figure 4-2 for comparison). Of the 180 cases investigated for various configurations, tension was observed in only 9 of them and the level of maximum tensile forces is not significant. The same observation is also valid for support moment demands and moment demands in the interior spans. This might be attributed to higher fundamental vertical periods of multi-span highway bridges.

Here, it must be noted that the multi-span highway bridge system with the highest vertical period (T_V=0.53 seconds) used in this study can be considered to be in

the boundary line between reinforced concrete and pre-stressed concrete bridge systems in terms of span length (L=54.0 m). The bridges with higher span lengths are generally constructed using pre-stressed concrete. An increase in the span length tends to increase the vertical period of the bridge system, which, in turn, results in a decrease in the amplification of force demands due to vertical effects. Consequently, based on the observations from the simulations carried out in this study, the vertical component of ground motions are not expected to have a significant effect on the seismic behavior of pre-stressed concrete bridge systems.

5 PROBABILISTIC SEISMIC DEMAND MODELS

In this phase of the study, a careful and comprehensive investigation of the characteristics of vertical ground motions that most significantly influence the response of bridge systems was conducted. The characteristics of vertical ground motion have been examined by a number of researchers as discussed in Section 3 of this report. Studies by Niazi and Bozorgnia [1992] and Silva [1997] found that V/H ratios have a maximum at periods of 0.05 – 0.1 seconds and a minimum between periods of 0.4 – 0.8 seconds. At longer periods V/H slowly increases with period. Additionally, Ambraseys and Douglas [2003] pointed out the importance of estimating the ground motion parameters useful for proper structural design. They examined the peak and spectral values of the vertical acceleration relative to horizontal in the frequency and time domain to answer the question of whether the vertical component of ground motion constitutes a significant proportion of the inertial loading that has to be resisted by a building and its foundations. Results of their study are similar to the previous ones mentioned except the fact that they have claimed that the ratio of vertical response at the time of maximum horizontal response should be used to estimate the loading conditions during an earthquake. Most of the studies in the past, however, have not explored the relationship between proposed models and structural response parameters. In order to define a possible relation between the ground motion characteristics and structural response, characteristics of the ground motions which produced the largest adverse effects are studied systematically in order to address the features of ground motions that influence the structural response.

For this purpose a series of response analyses in respective time windows were carried out in order to search for the possible parameters representing the relative phasing between the horizontal and vertical components. As the first step, the response spectra for horizontal and vertical components of each ground motion were constructed. Inspired by the previous studies in the literature, the ratio of vertical spectral acceleration to horizontal spectral acceleration (Sa_V/Sa_H) was selected as one of

the variables to explain the influence of vertical ground motions. Different than the other studies, vertical spectral acceleration at the vertical period of the bridge SaV (at $T=T_v$), and horizontal spectral acceleration at the transverse and longitudinal periods of the bridge SaH (at $T=T_H$) were used for correlations.

The ratio of the axial load (AL), positive and negative span moments (PSpanM and NSpanM) and positive and negative support moments (PSupM and NSupM) with and without the vertical component were selected as the structural response variables explaining the effect of vertical component on overall response. Figure 5-1 to Figure 5-5 are prepared using the results of the simulations of typical overcrossings reported in Chapter 4 (Configuration 1, T_{long}=0.27, T_{trans}=0.46 and T_{vert}=0.12). The ratio of axial load at the column with and without vertical ground motion, defined as **amplification factor (AF)** for axial load, are plotted with respect to the vertical to horizontal spectral acceleration ratio of the corresponding ground motion record in Figure 5-1 (a) and(b) in logarithmic scale. Similarly, Figure 5-2 to Figure 5-5 shows the correlation between the amplification factor of moment at the span or at the support and the vertical to horizontal spectral acceleration ratio. The negative moment values are normalized using the dead load moments for consistency, therefore these amplification factors are defined as the **normalized amplification factors (NAF)**. These figures show that the axial load & moment at the column or at the span may increase up to 300% when the vertical excitations are applied for earthquakes have a SaV/SaH greater than 1. Evidently, all of the structural variables increase as the vertical to horizontal spectral acceleration ratio increases. For each structural parameter, an increase in the correlation coefficient is observed when the horizontal spectral acceleration at the longitudinal period was used instead of the horizontal spectral acceleration at the transverse period for this bridge configuration. Better correlations are expected when the earthquakes are scaled to the same horizontal excitation level. This example shows that the ratio of the vertical spectral acceleration at the vertical period of the bridge to the horizontal spectral acceleration at the longitudinal period of the bridge would be a good indication of the effect of vertical ground excitation on bridge structures. A new set of analyses are

done using a new set of ground motions selected using this property. 56 recordings having the biggest and smallest average SaV/SaH ratio were selected from the dataset, (named as Set 2) and used in non-linear bridge simulations.

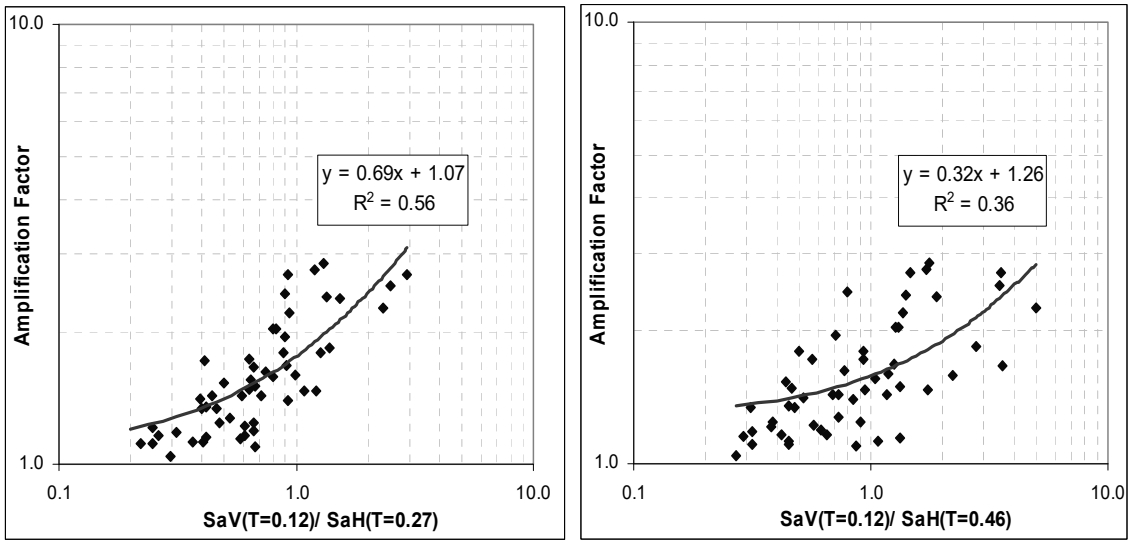

(a) (b)

Figure 5-1 - Correlation between Amplification Factor and Spectral Acceleration Ratio for Axial Load a) using longitudinal period, b) using transverse period for horizontal spectral value

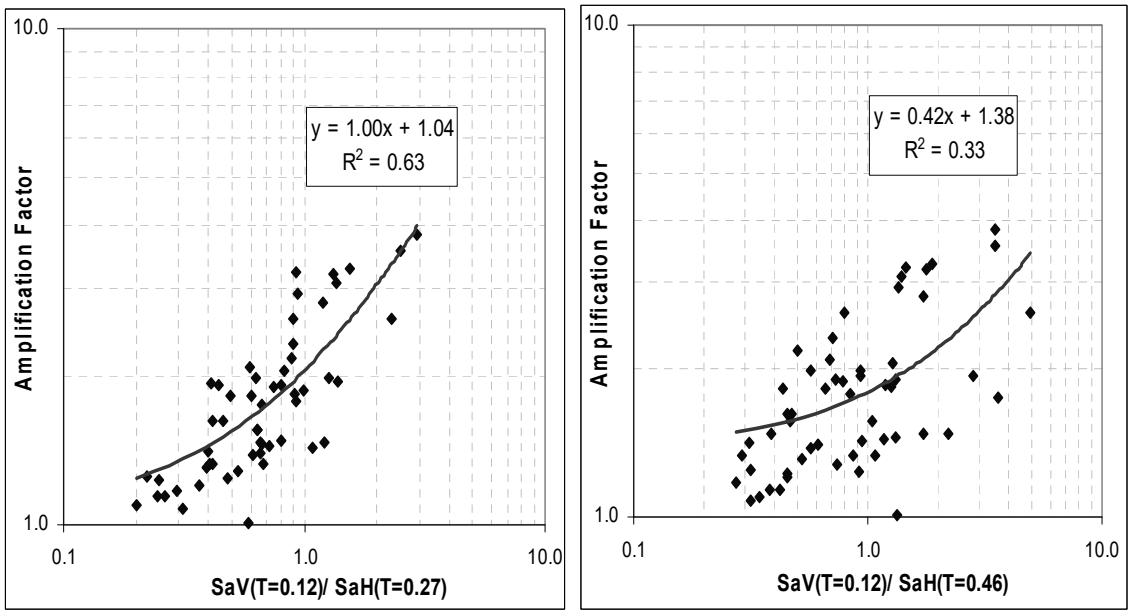

(a) (b)

Figure 5-2 - Correlation between Amplification Factor and Spectral Acceleration Ratio for positive span moment a) using longitudinal period, b) using transverse period for horizontal spectral acceleration

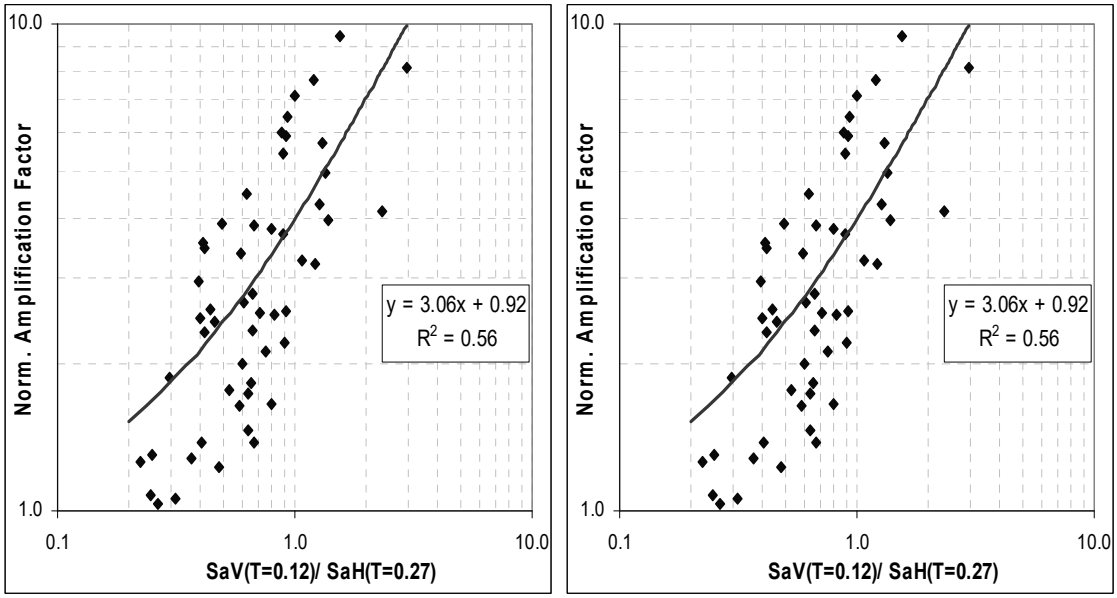

(a) (b)

Figure 5-3 - Correlation between Normalized Amplification Factor and Spectral Acceleration Ratio for negative span moment a) using longitudinal period, b) using transverse period for horizontal spectral acceleration value

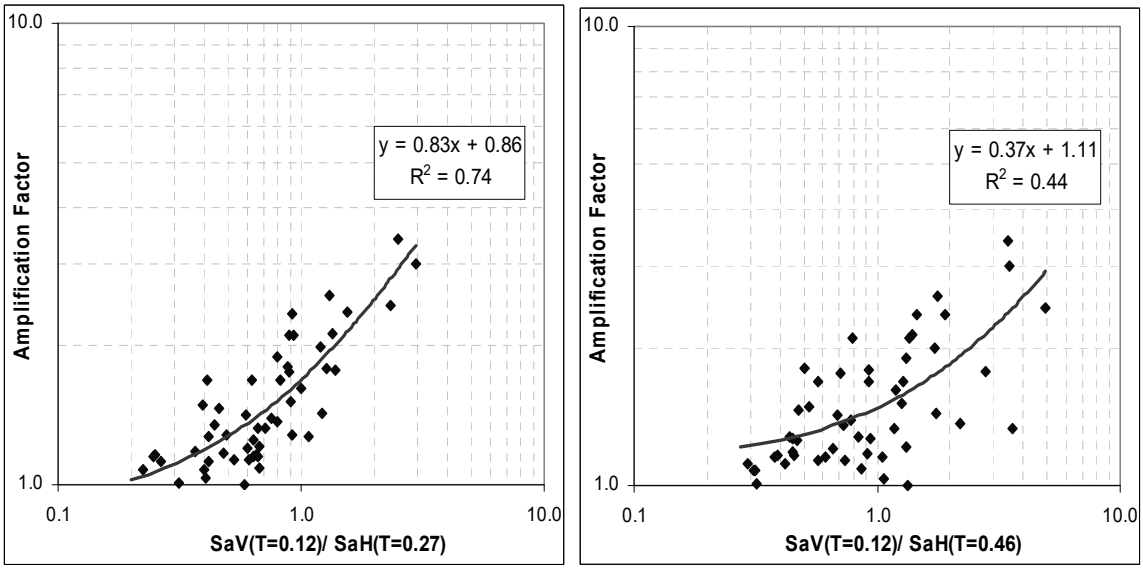

(a) (b)

Figure 5-4 - Correlation between Amplification Factor and Spectral Acceleration Ratio for positive support moment a) using longitudinal period, b) using transverse period for horizontal spectral acceleration value

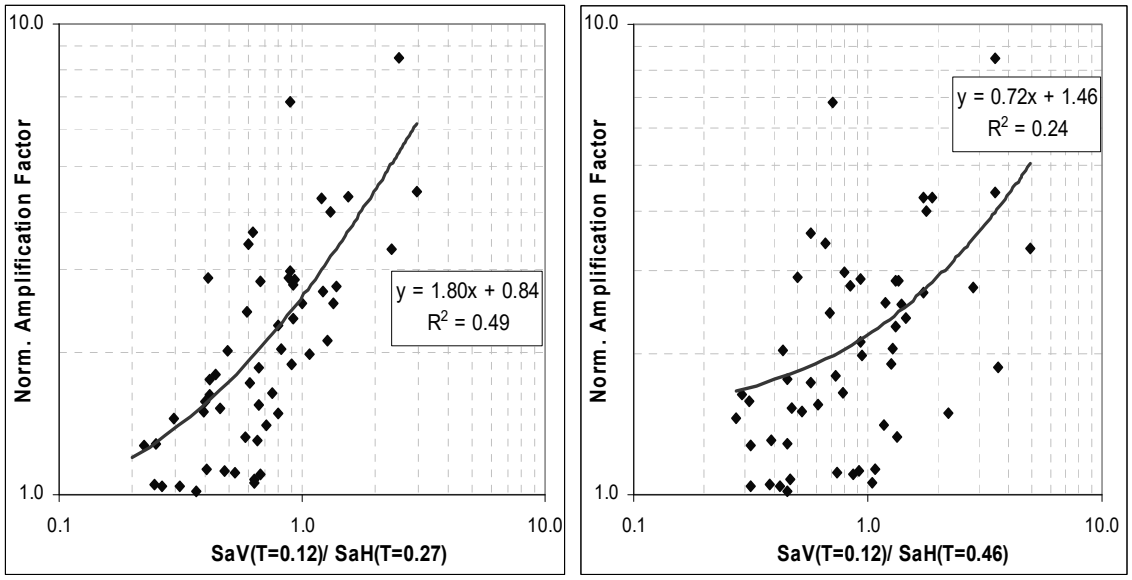

(a) (b)

Figure 5-5 - Correlation between Normalized Amplification Factor and Spectral Acceleration Ratio for negative support moment a) using longitudinal period, b) using transverse period for horizontal spectral acceleration value

Table 5-1 - List of second set of ground motions used in nonlinear simulations (Set 2)

Earthquake Name	Station Name	PGA (g)	PGV (inch/sec)	PGD (inch)	Earthquake Magnitude	Closest Distance (miles)
Cape Mendocino	Rio Dell Overpass - FF	0.42	18.88	6.68	7.01	8.90
Cape Mendocino	Shelter Cove Airport	0.20	2.39	0.16	7.01	17.88
Chi-Chi, Taiwan	CHY026	0.08	13.84	11.03	7.62	18.35
Chi-Chi, Taiwan	CHY036	0.26	14.66	10.18	7.62	9.98
Chi-Chi, Taiwan	CHY041	0.46	10.92	3.87	7.62	12.32
Chi-Chi, Taiwan	CHY086	0.15	6.27	2.86	7.62	17.66
Chi-Chi, Taiwan	CHY092	0.10	17.24	13.07	7.62	14.11
Chi-Chi, Taiwan	TCU059	0.16	23.05	23.03	7.62	10.64
Chi-Chi, Taiwan	TCU103	0.16	17.19	21.64	7.62	3.79
Chi-Chi, Taiwan	TCU118	0.10	12.10	11.59	7.62	16.68
Chi-Chi, Taiwan	TCU122	0.24	15.27	14.47	7.62	5.81
Chi-Chi, Taiwan	TCU141	0.09	14.39	11.13	7.62	15.04
Chi-Chi, Taiwan-03	CHY028	0.15	8.88	3.48	6.20	15.15
Chi-Chi, Taiwan-03	CHY080	0.33	18.56	3.50	6.20	13.90
Chi-Chi, Taiwan-03	TCU065	0.28	10.52	2.34	6.20	16.19
Chi-Chi, Taiwan-03	TCU074	0.04	1.29	0.22	6.20	10.33
Chi-Chi, Taiwan-03	TCU116	0.13	9.51	3.35	6.20	13.75
Chi-Chi, Taiwan-04	TCU116	0.10	4.08	0.99	6.20	17.87
Chi-Chi, Taiwan-06	TCU075	0.08	1.85	0.56	6.30	16.35
Chi-Chi, Taiwan-06	TCU076	0.13	3.39	1.45	6.30	16.06
Imperial Valley-06	Aeropuerto Mexicali	0.34	11.97	3.00	6.53	0.21
Imperial Valley-06	Agrarias	0.29	13.33	3.73	6.53	0.40
Imperial Valley-06	El Centro Array #6	0.43	32.73	17.69	6.53	0.84
Imperial Valley-06	El Centro Array #7	0.42	31.57	16.15	6.53	0.35
Imperial Valley-06	El Centro Array #13	0.12	6.06	2.51	6.53	13.66
Imperial Valley-06	El Centro Differential Array	0.43	21.78	13.01	6.53	3.16
Irpinia, Italy-01	Bisaccia	0.08	7.07	3.45	6.90	13.21
Irpinia, Italy-01	Mercato San Severino	0.12	4.07	0.60	6.90	18.52
Irpinia, Italy-02	Calitri	0.18	9.61	2.67	6.20	5.49
Irpinia, Italy-02	Sturno	0.08	1.71	0.33	6.20	12.67
Kobe, Japan	Port Island (0 m)	0.26	24.54	11.65	6.90	2.06
Kobe, Japan	Shin-Osaka	0.23	13.54	3.26	6.90	11.90
Loma Prieta	Capitola	0.48	13.59	2.81	6.93	9.46
Loma Prieta	Coyote Lake Dam (SW Abut)	0.29	11.26	4.47	6.93	12.64
Mammoth Lakes-01	Convict Creek	0.43	9.55	1.99	6.06	4.12
Mammoth Lakes-01	Long Valley Dam (Upr L Abut)	0.34	7.86	2.10	6.06	9.61
Morgan Hill	Gilroy Array #2	0.19	3.37	0.68	6.19	8.51
Morgan Hill	Gilroy Array #3	0.19	4.95	1.12	6.19	8.09
Morgan Hill	Gilroy Array #4	0.28	6.65	1.42	6.19	7.17
Morgan Hill	Gilroy Array #7	0.14	2.79	0.67	6.19	7.50
Morgan Hill	Hollister Diff Array #1	0.09	4.30	0.64	6.19	16.42

Earthquake Name	Station Name	PGA (g)	PGV (inch/sec)	PGD (inch)	Earthquake Magnitude	Closest Distance (miles)
Morgan Hill	Hollister Diff Array #3	0.08	3.39	0.65	6.19	16.42
Morgan Hill	Hollister Diff Array #4	0.10	4.11	0.69	6.19	16.42
Morgan Hill	Hollister Diff Array #5	0.09	4.09	0.72	6.19	16.42
Morgan Hill	Hollister Diff. Array	0.09	3.94	0.67	6.19	16.42
Morgan Hill	San Juan Bautista, 24 Polk St	0.04	1.63	0.61	6.19	16.87
N. Palm Springs	Cabazon	0.22	4.91	0.83	6.06	4.87
N. Palm Springs	Morongo Valley	0.21	14.27	4.48	6.06	7.50
Nahanni, Canada	Site 3	0.16	2.09	0.84	6.76	3.31
Northridge-01	Arleta - Nordhoff Fire Sta	0.33	12.11	5.02	6.69	5.38
Northridge-01	Sunland - Mt Gleason Ave	0.14	6.10	1.57	6.69	8.30
Northridge-01	Pacoima Dam (downstr)	0.41	14.42	1.86	6.69	4.36
Northridge-01	Santa Monica City Hall	0.59	12.31	4.16	6.69	16.44
Northridge-01	LA - N Westmoreland	0.37	9.34	1.36	6.69	16.61
Northridge-02	LA - Century City CC North	0.08	1.64	0.12	6.05	15.25
Northridge-02	LA - Hollywood Stor FF	0.16	1.99	0.12	6.05	15.50
Parkfield	Temblor pre-1969	0.30	6.95	1.41	6.19	9.92
Superstition Hills-02	Wildlife Liquef. Array	0.19	12.68	8.11	6.54	14.82
Explanations:* indicates that the epicentral distance is used instead of closest distance.						

5.1 CONSTRUCTION OF THE ANALYTICAL EXPRESSIONS FOR STRUCTURAL PARAMETERS

In this phase of the study, a simple model explaining the effect of vertical excitation on the structural response of the bridge is constructed using ground motion parameters. The positive and negative extremes of the time history of axial load at the column and the moments at the span & support for the case that only horizontal earthquake components were applied, are normalized by the dead load values and defined as Rsp(Honly). Similarly the extreme values of the axial load at the column and the moments at the span & support for the case that all three earthquake components were applied are defined as Rsp(H+V). For the positive extreme values of the time histories amplification factor (AF) was defined before as:

$$AF = \frac{Rsp(H+V)}{Rsp(Honly)} \tag{5.1}$$

Similarly a normalized amplification factor was defined for the negative extremes of the moment time histories using the dead load moment value (DLM) as:

$$NAF = \frac{DLM - Rsp(H+V)}{DLM - Rsp(Honly)} \tag{5.2}$$

$$\ln(Rsp(H+V)) = \ln(Rsp(Honly)) + \ln(AF) \tag{5.3}$$

$$\ln(Rsp(H+V)) = \ln(Rsp(H_{only})) + \ln(NAF) \tag{5.4}$$

By taking the natural logarithm of both sides of Eq. 5.1 and 5.2 and redistributing the terms, Eq. 5.3 and 5.4 were established. Both elements in the right hand side of Eq. 5.3 and 5.4 were modeled separately. According to the sensitivity analyses, Rsp(Honly) can be modeled using only one variable - the horizontal spectral acceleration (SaH). Both the positive moment demand in the span and at the support and the axial force demand in the column increases non-linearly with increasing horizontal spectral acceleration at the horizontal periods of the bridge as defined below in Eq. 5.5 and 5.6.

$$\ln(Rsp(Honly)) = f(SaH) \pm \sigma_{Honly} \tag{5.5}$$

$$\ln(Rsp(Honly)) = b_{1\times(}\ln(SaH) - b_{2)}{}^{2} \pm \sigma_{Honly} \tag{5.6}$$

Negative moment demand in the span and at the support increases linearly with increasing horizontal spectral acceleration at the horizontal periods of the bridge as defined below in Eq. 5.7.

$$\ln(Rsp(Honly)) = b_{1+}\, b_2 \ln(SaH) \pm \sigma_{Honly} \tag{5.7}$$

According to the formulas given above, non-linear regression models were built to determine the response parameters (Rsp(Honly)) using horizontal spectral acceleration in 5% to 20% error margin depending on the type of the parameter and the period of the structure. Example models for the negative span moment and column axial force response parameters are given in Figure 5-8 to Figure 5-10. (Actual data is shown with solid dots and the predictions are given in black lines).

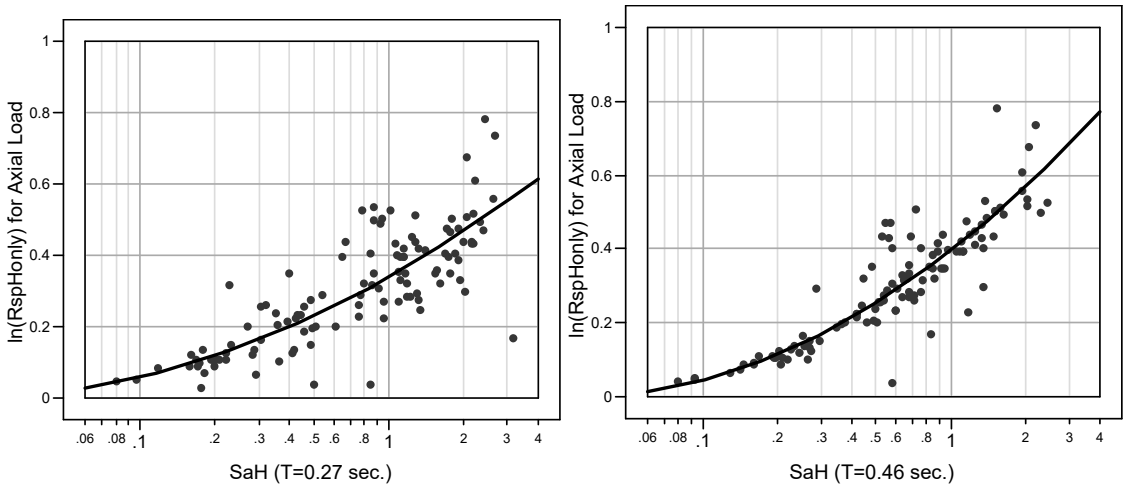

(a) (b)

Figure 5-6 - Correlation between Axial Force and Horizontal Spectral Acceleration a) using longitudinal period, b) using transverse period for horizontal spectral acceleration value

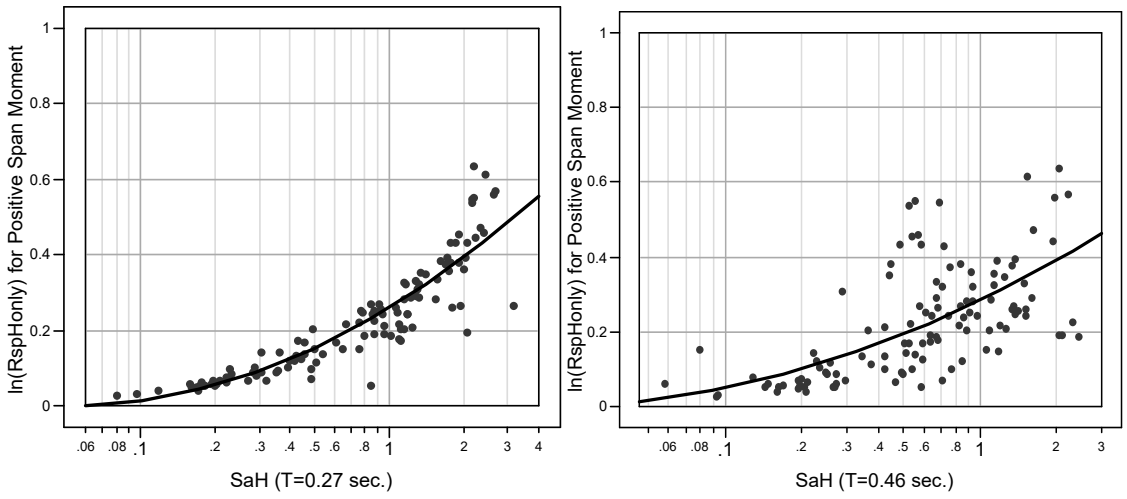

(a) (b)

Figure 5-7 - Correlation between Positive Span Moment and Horizontal Spectral Acceleration a) using longitudinal period, b) using transverse period for horizontal spectral acceleration value.

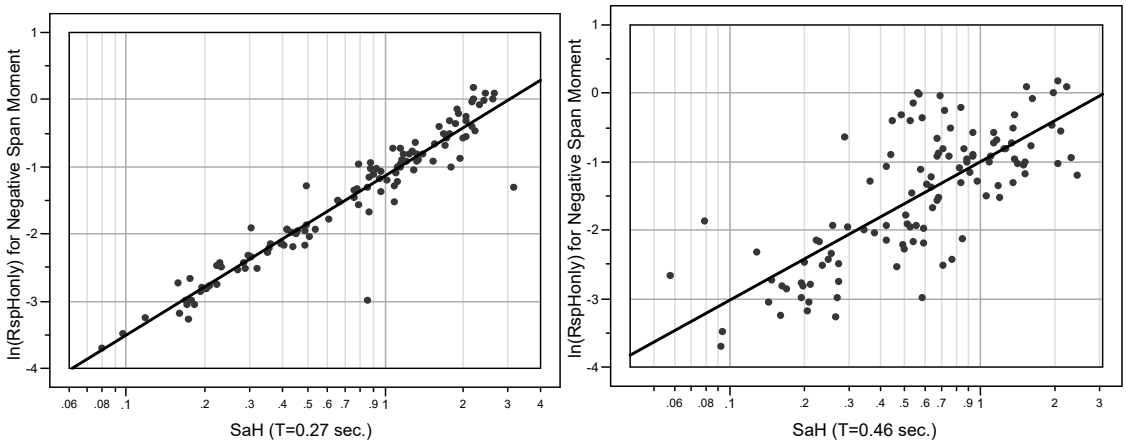

(a) (b)

Figure 5-8 - Correlation between Negative Span Moment and Horizontal Spectral Acceleration a) using longitudinal period, b) using transverse period for horizontal spectral acc. value

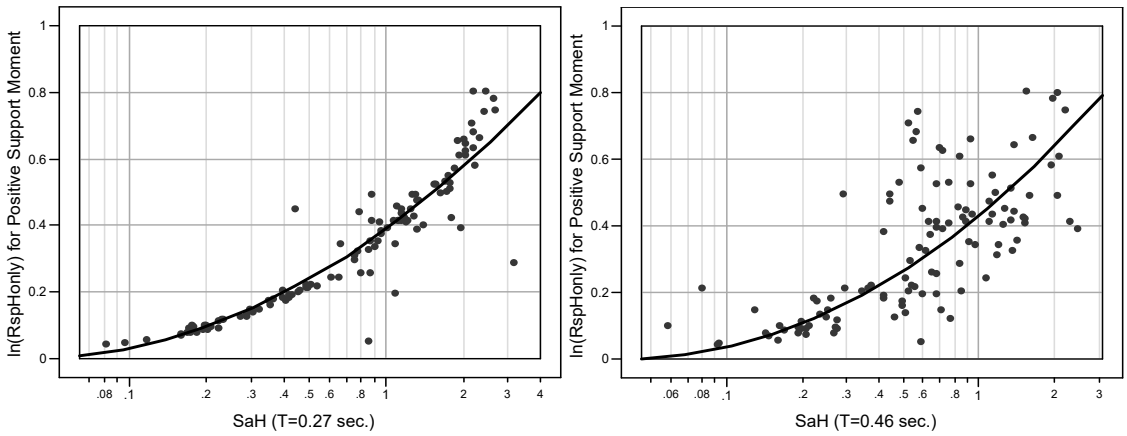

(a) (b)

Figure 5-9 - Correlation between Positive Support Moment and Horizontal Spectral Acceleration a) using longitudinal period, b) using transverse period for horizontal spectral acc. value

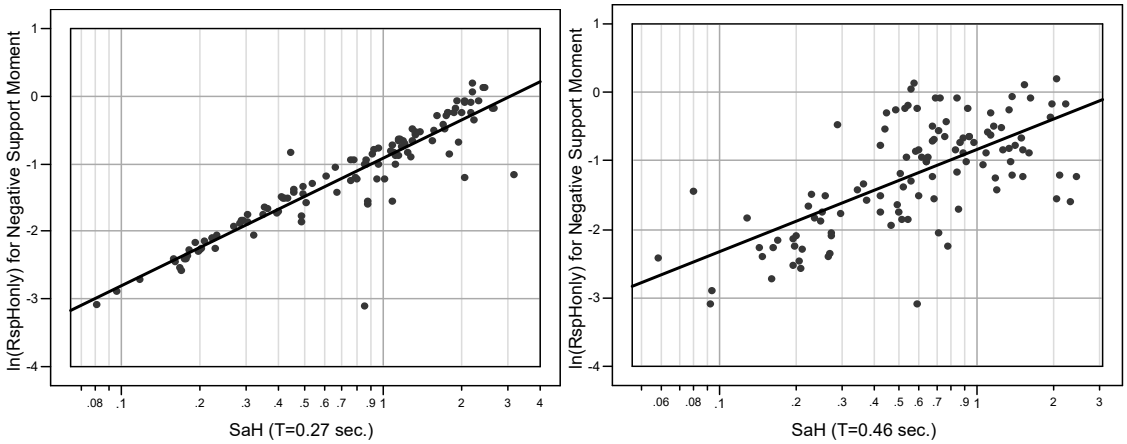

(a) (b)

Figure 5-10 - Correlation between Negative Support Moment and Horizontal Spectral Acceleration a) using longitudinal period, b) using transverse period for horizontal spectral acc. value

Similar models are constructed for all the bridge configurations considered in this study. The parameters and the root mean square error values for the proposed models are summarized in Table 5-2 to Table 5-4.

Table 5-2 - List of parameters and the root mean square error values for Axial Load and Positive Span Moment Models

Configuration No	Vertical Period (sec)	Horizontal Period (sec)	Axial Load Model Parameters			Positive Span Moment Model Parameters		
			b1	b2	RMSE	b1	b2	RMSE
0	0.19	0.32	0.0173	-4.0	0.0966	0.0448	-3.0	0.0958
0	0.19	0.55	0.0215	-4.0	0.0485	0.0369	-3.5	0.1872
1	0.12	0.27	0.0212	-4.0	0.0983	0.0288	-3.0	0.0629
1	0.12	0.46	0.0323	-3.5	0.0733	0.0177	-4.0	0.1163
2	0.30	0.43	0.0163	-4.2	0.0923	0.0313	-3.5	0.0818
2	0.30	0.64	0.0189	-4.2	0.0562	0.0252	-4.0	0.1475
3	0.37	0.53	0.0167	-4.2	0.0809	0.0205	-3.5	0.0536
3	0.37	0.68	0.0187	-4.2	0.0545	0.0165	-4.0	0.0773
4	0.45	0.62	0.0145	-4.5	0.0697	0.0178	-3.2	0.0429
4	0.45	0.75	0.0159	-4.5	0.0525	0.0158	-3.5	0.0544
5	0.24	0.35	0.0154	-4.2	0.0919	0.0419	-3.5	0.1131
5	0.24	0.59	0.0206	-4.0	0.0518	0.0274	-4.5	0.2137

Table 5-3 - List of parameters and the root mean square error values for Negative Span Moment and Positive Support Moment Models

Conf No	Vertical Period (sec)	Horizontal Period (sec)	Negative Span Moment Model Parameters			Axial Force Model Parameters		
			b1	b2	RMSE	b1	b2	RMSE
0	0.19	0.32	-0.8254	0.8521	0.3233	0.0173	-4.0	0.0966
0	0.19	0.55	-0.7339	0.6032	0.6217	0.0215	-4.0	0.0485
1	0.12	0.27	-1.1371	1.0287	0.2833	0.0212	-4.0	0.0983
1	0.12	0.46	-0.9987	0.8769	0.6419	0.0323	-3.5	0.0733
2	0.30	0.43	-0.8278	0.8301	0.3523	0.0163	-4.2	0.0923
2	0.30	0.64	-0.7958	0.6302	0.5992	0.0189	-4.2	0.0562
3	0.37	0.53	-1.3216	0.8065	0.3878	0.0167	-4.2	0.0809
3	0.37	0.68	-1.2694	0.7143	0.5309	0.0187	-4.2	0.0545
4	0.45	0.62	-1.7206	0.7842	0.4088	0.0145	-4.5	0.0697
4	0.45	0.75	-1.6538	0.7536	0.5092	0.0159	-4.5	0.0525
5	0.24	0.35	-0.4765	0.8666	0.3820	0.0154	-4.2	0.0919
5	0.24	0.59	-0.3965	0.6114	0.6608	0.0206	-4.0	0.0518

On the other hand, the amplification factor (AF) for the positive moment demand and the axial force demand is found to be a more complex function of both horizontal spectral acceleration (SaH) and ratio of vertical spectral acceleration to horizontal spectral acceleration (SaV/SaH). For ground motions that have smaller horizontal spectral accelerations or small ratios of vertical spectral acceleration to horizontal spectral acceleration, the amplification factor has a negligible value as defined below in

Eq 5.8 and 5.9. If (SaV/SaH) is bigger than the cut-off value, the normalized amplification factor for negative moment demand in the span and at the support increases linearly with increasing ratio of vertical spectral acceleration to horizontal spectral acceleration (SaV/SaH) (See Eq. 5.9).

Table 5-4 - List of parameters and the root mean square error values for Negative Support Moment Model

Configuration No	Vertical Period (sec)	Horizontal Period (sec)	Negative Support Model Parameters		
			b1	b2	RMSE
0	0.19	0.32	-1.7677	0.7967	0.3070
0	0.19	0.55	-1.6476	0.6152	0.5415
1	0.12	0.27	-0.9226	0.8211	0.3103
1	0.12	0.46	-0.8401	0.6496	0.5944
2	0.30	0.43	-1.9529	0.7546	0.3697
2	0.30	0.64	-1.8653	0.6483	0.5055
3	0.37	0.53	-1.9836	0.7790	0.4291
3	0.37	0.68	-1.9114	0.7168	0.5252
4	0.45	0.62	-2.1692	0.7054	0.4818
4	0.45	0.75	-2.1138	0.6724	0.5592
5	0.24	0.35	-1.9701	0.7959	0.3292
5	0.24	0.59	-1.8404	0.6399	0.5261

$$\ln(AF) = f(SaH, V/H) \pm \sigma_{af} \tag{5.8}$$

$$\ln(AF) = if \begin{vmatrix} \frac{SaV}{SaH} \le \ln(b_1) \rightarrow 0 \\ elseif \begin{vmatrix} SaH \le 0.1 \rightarrow 0 \\ else \rightarrow (\ln(\frac{SaV}{SaH}) - \ln(b_1)) \times (b_2 + b_3 \times \ln(SaH)) \end{vmatrix} \end{vmatrix} \tag{5.9}$$

$$\ln(NAF) = if \begin{vmatrix} \frac{SaV}{SaH} \le \ln(b_1) \rightarrow 0 \\ else \rightarrow b_2 + b_3 \times \ln(\frac{SaV}{SaH}) \end{vmatrix} \tag{5.10}$$

Using the proposed models, the amplification in the structural response due to vertical excitation can be determined using vertical and horizontal spectral accelerations at related structural periods within the range of 16% to 30% error. Example models for column axial force and negative span moment are given in Figure 5-11 to Figure 5-14.

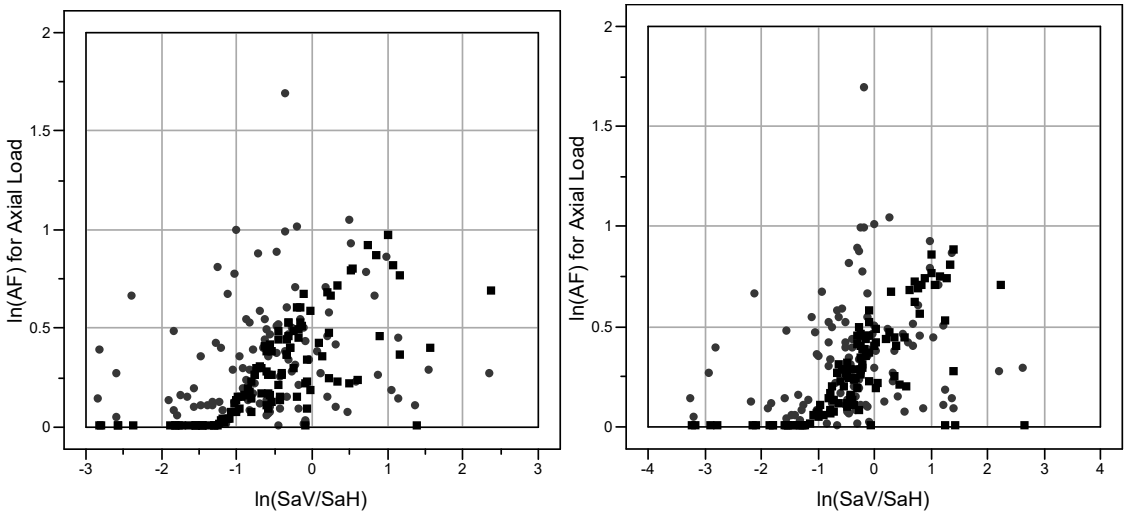

(a) (b)

Figure 5-11 - Correlation between Axial Force and ratio of vertical to horizontal spectral acceleration a) using longitudinal period, b) using transverse period for horizontal spectral acceleration value

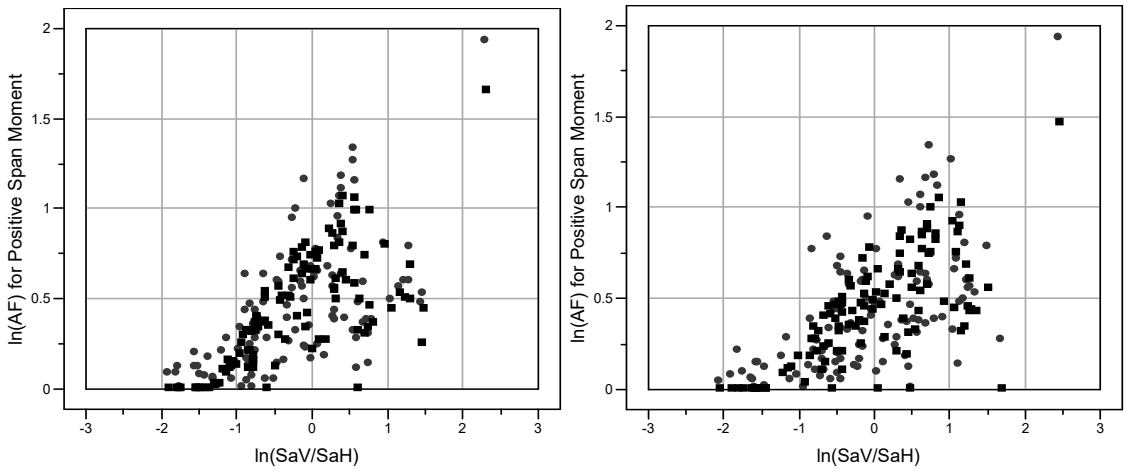

(a) (b)

Figure 5-12 - Correlation between Positive Span Moment and ratio of vertical to horizontal spectral acceleration a) using longitudinal period, b) using transverse period for horizontal spectral acceleration value

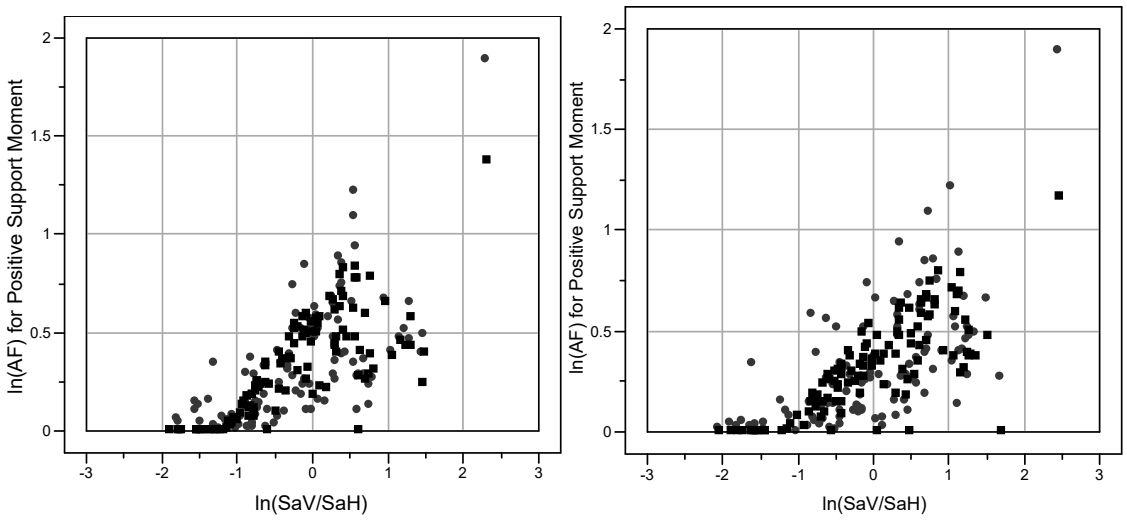

(a) (b)

Figure 5-13 - Correlation between Positive Support Moment and ratio of vertical to horizontal spectral acceleration a) using longitudinal period, b) using transverse period for horizontal spectral acceleration value

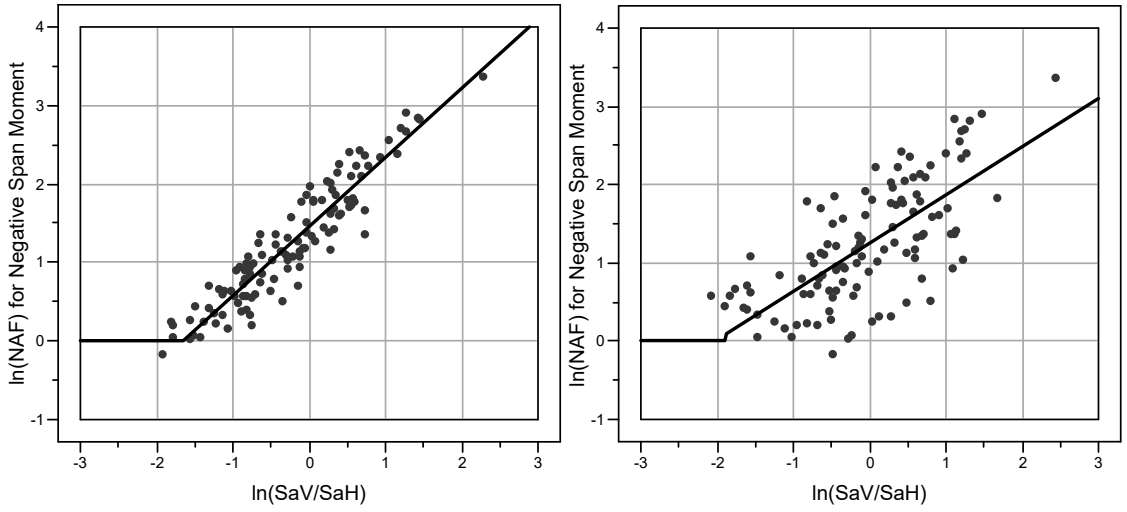

(a) (b)

Figure 5-14 - Correlation between Negative Span Moment and ratio of vertical to horizontal spectral acceleration a) using longitudinal period, b) using transverse period for horizontal spectral acceleration value.

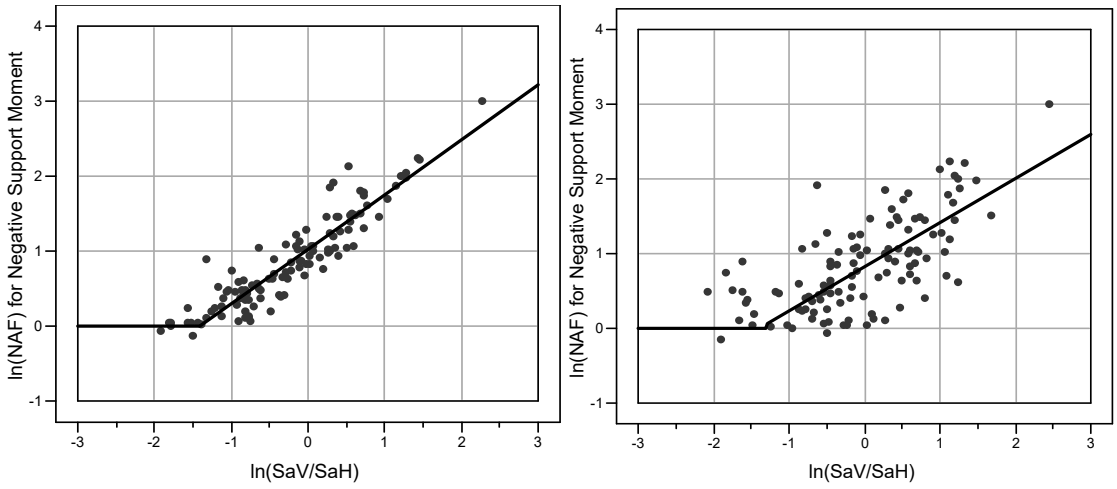

(a) (b)

Figure 5-15 - Correlation between Negative Support Moment and ratio of vertical to horizontal spectral acceleration a) using longitudinal period, b) using transverse period for horizontal spectral acceleration value.

Similar models are constructed for all the bridge configurations considered in this study. The parameters and the root mean square error values for the proposed models are summarized in Table 5-5 to Table 5-7

Table 5-5 - List of parameters and the root mean square error values for Axial Force and Positive Span Moment Models

Conf No	T_v (sec)	T_H (sec)	Axial Load Model Parameters				Positive Span Moment Model Parameters			
			b1	b2	b3	RMSE	b1	b2	b3	RMSE
0	0.19	0.32	0.19	0.2882	0.1263	0.1384	0.30	0.3514	0.1165	0.1139
0	0.19	0.55	0.33	0.3914	0.1500	0.1153	0.29	0.2741	0.0865	0.1477
1	0.12	0.27	0.28	0.4333	0.1682	0.1425	0.25	0.4948	0.1901	0.1603
1	0.12	0.46	0.30	0.4068	0.1548	0.1626	0.25	0.4534	0.1799	0.1940
2	0.30	0.43	0.18	0.2072	0.0884	0.1050	0.30	0.3630	0.1560	0.0829
2	0.30	0.64	0.21	0.2118	0.0815	0.1038	0.33	0.3233	0.1331	0.1067
3	0.37	0.53	0.15	0.1692	0.0702	0.0975	0.25	0.3337	0.1392	0.0899
3	0.37	0.68	0.19	0.1952	0.0789	0.0911	0.23	0.2870	0.1249	0.0954
4	0.45	0.62	0.11	0.1459	0.0673	0.0946	0.15	0.2427	0.1056	0.0917
4	0.45	0.75	0.15	0.1756	0.0774	0.0926	0.15	0.2375	0.1064	0.0889
5	0.24	0.35	0.26	0.3274	0.1343	0.1092	0.35	0.3506	0.1166	0.0992
5	0.24	0.59	0.25	0.2771	0.0986	0.0970	0.35	0.2779	0.0865	0.1109

Table 5-6 - List of parameters and the root mean square error values for Negative Span Moment and Positive Support Moment Models

Conf No	T_v (sec)	T_H (sec)	Negative Span Moment Model Parameters				Positive Support Model Parameters			
			b1	b2	b3	RMSE	b1	b2	b3	RMSE
0	0.19	0.32	0.20	0.3732	0.1376	0.1238	0.19	0.2882	0.1263	0.1384
0	0.19	0.55	0.23	0.3638	0.1250	0.1355	0.33	0.3914	0.1500	0.1153
1	0.12	0.27	0.30	0.4299	0.1588	0.1469	0.28	0.4333	0.1682	0.1425
1	0.12	0.46	0.30	0.3728	0.1362	0.1881	0.30	0.4068	0.1548	0.1626
2	0.30	0.43	0.22	0.3757	0.1666	0.0917	0.18	0.2072	0.0884	0.1050
2	0.30	0.64	0.23	0.3496	0.1479	0.1014	0.21	0.2118	0.0815	0.1038
3	0.37	0.53	0.19	0.2898	0.1245	0.0808	0.15	0.1692	0.0702	0.0975
3	0.37	0.68	0.19	0.2782	0.1216	0.0783	0.19	0.1952	0.0789	0.0911
4	0.45	0.62	0.15	0.2395	0.1092	0.0797	0.11	0.1459	0.0673	0.0946
4	0.45	0.75	0.16	0.2470	0.1155	0.0747	0.15	0.1756	0.0774	0.0926
5	0.24	0.35	0.24	0.4415	0.1752	0.1099	0.26	0.3274	0.1343	0.1092
5	0.24	0.59	0.29	0.4458	0.1653	0.1088	0.25	0.2771	0.0986	0.0970

Table 5-7 - List of parameters and the root mean square error values for Negative Support Moment Models

Configuration No	Vertical Period (sec)	Horizontal Period (sec)	Negative Support Model Parameters			
			b1	b2	b3	RMSE
0	0.19	0.32	0.12	1.8313	0.8455	0.2674
0	0.19	0.55	0.07	1.5358	0.5607	0.4837
1	0.12	0.27	0.26	1.0194	0.7337	0.2405
1	0.12	0.46	0.27	0.8209	0.5903	0.4535
2	0.30	0.43	0.13	1.7572	0.8270	0.3348
2	0.30	0.64	0.08	1.4992	0.6019	0.4399
3	0.37	0.53	0.11	1.6318	0.7233	0.3839
3	0.37	0.68	0.08	1.4265	0.5412	0.4633
4	0.45	0.62	0.09	1.6631	0.6828	0.4165
4	0.45	0.75	0.07	1.5037	0.5556	0.4665
5	0.24	0.35	0.12	1.9303	0.8853	0.3183
5	0.24	0.59	0.10	1.6153	0.6898	0.5014

6 VECTOR PSHA FOR THE EFFECT OF VERTICAL GROUND MOTIONS ON THE SEISMIC RESPONSE OF HIGHWAY OVERCROSSINGS

The primary objective of this study is to identify the effects of near fault vertical ground motions on the seismic response of ordinary highway bridges. The initial step was building the probabilistic seismic demand models for one class of bridges, viz., highway overcrossings, under the influence of the vertical and horizontal time histories. The engineering demand parameters (EDP) were selected as the 'axial load demand at the columns' and the 'moment demand at the girder and at the support' after carefully screening the nonlinear time history analysis results. Sensitivity analysis showed that the increase in these EDP's is a result of increasing horizontal spectral accelerations at the transverse and longitudinal period of the bridge and vertical spectral acceleration at the vertical period of the bridge. The vertical and horizontal spectral accelerations at the spectral periods of the bridge were identified as the intensity measures (IM) which are defined by ground motion equations. Abrahamson and Silva (2008) NGA model is selected and used among many available horizontal ground motion models for this study. A new NGA vertical ground motion model consistent with the horizontal model is constructed. The key question of when the vertical component should be incorporated in design will be answered by the probabilistic seismic hazard assessment study incorporating the probabilistic seismic demand models and ground motion models. Within the contents of this chapter, a vector valued probabilistic seismic hazard assessment study is conducted using the available resources. Structural demand hazard curves are generated for selected engineering demand parameters for an example bridge configuration and compared to the capacity to predict the probability of exceeding the capacity. Probability of exceeding the capacity of negative span moment and the positive and negative support moments is found to be

substantial if the vertical effects are included. Analyses are replicated for the negative span moment demand for different bridge configurations to investigate the effect of the spectral period of the structure on the importance of vertical excitation. Finally, series of hazard curves developed and presented for different locations in Bay Area for soil site conditions to provide a roadmap for the prediction of these features for future earthquakes.

6.1 VECTOR HAZARD CONCEPT

The basic methodology of PHSA involves computing how often a specified level of ground motion will be exceeded at the site. Specifically, in a PSHA, the annual rate of events that produce a ground motion parameter, A, that exceeds a specified level, z, at the site is computed. This annual rate, γ, is also called the "annual rate of exceedance". Traditionally, the equation for a seismic hazard analysis due to a single source has been given by Equation 6.1:

$$\gamma(A > z) = N_{\min} \cdot \int_M \int_R f_M(M) \times f_R(M,R) \times P(A > z | M,R) \times dM \times dR \qquad (6.1)$$

where R is the distance from the source to site, M is the earthquake magnitude; N_{min} is the annual rate of earthquake with magnitude greater than or equal to the minimum magnitude, f_M (M) and f_R (M, R) are the probability density functions for the magnitude and distance and P (A>z | M, R) is the probability of observing a ground motion greater than z for a given earthquake magnitude and distance. In essence, seismic hazard analysis is concerned with estimating the ground motions at a specific site due to a suite of earthquake scenarios. Each scenario is defined by the size of the earthquake (magnitude, M) and the location which defines the distance, R, from the site. The value of chosen ground motion parameter, A, is then obtained from a ground motion prediction equation. Since these equations define probabilistic distributions of the ground motion parameter, the scenario must also include a selected value of epsilon, ε (Bommer and Abrahamson, 2006), which leads to Equation 6.2:

$$\gamma(A > z) = N_{\min} \cdot \int_M \int_R \int_\varepsilon \begin{pmatrix} f_M(M) \times f_R(M,R) \times f_\varepsilon(\varepsilon) \\ \times P(A > z | M, R, \varepsilon) \times dM \times dR \times d\varepsilon \end{pmatrix} \tag{6.2}$$

To evaluate the seismic performance of bridge structures under the influence of vertical ground motions, uncertainties in the nonlinear structural responses also need to be considered. The probabilistic structural demand models defined in Chapter 2 are incorporated into the hazard integral to directly estimate earthquake damage. The concept is similar to the conventional probabilistic seismic hazard analysis (PSHA); merely the ground motion attenuation relationship is replaced with the more structure-specific one:

$$\gamma(EDP > A) = \begin{pmatrix} N_{\min} \cdot \int_M \int_R \int_\varepsilon \int_{\varepsilon_{EDP}} f_M(M) \times f_R(M,R) \times f_\varepsilon(\varepsilon) \times f_{EDP}(M,R,\varepsilon) \\ \times P(EDP > A | M, R, \varepsilon, \varepsilon_{EDP}) \times dM \times dR \times d\varepsilon \times d\varepsilon_{EDP} \end{pmatrix} \tag{6.3}$$

where EDP is the engineering demand parameter, $f_{EDP}(EDP)$ is the probabilistic seismic demand model for the engineering demand parameter, and ε_{EDP} is the number of standard deviations for the probabilistic seismic demand model.

In a standard PSHA, the hazard is computed for scalar intensity measures, such as spectral acceleration at a single period and peak ground acceleration. In vector hazard, the PSHA is conducted for two or more intensity measures. Since the response of structures can depend on more than one ground motion parameter, using vector hazard allows for more accurate predictions of the response by using more complete descriptions of the scenarios. Due to the nature of this project, intensity measures consisting of two parameters are used: horizontal spectral acceleration at the longitudinal or transverse period along with vertical spectral acceleration at the vertical period of the structure. The vector valued structural demand hazard equation is given by:

$$\gamma(EDP > A) = \left(\begin{array}{l} N_{\min} \cdot \int_{M}\int_{R}\int_{\varepsilon_H}\int_{\varepsilon_V}\int_{\varepsilon_{EDP}} f_M(M) \times f_R(M,R) \times f_{\varepsilon_H}(\varepsilon_H) \\ \times f_{\varepsilon_V}(\varepsilon_H, \varepsilon_V) \times f_{EDP}(M,R,\varepsilon) \times P(EDP > A | M, R, \varepsilon_H, \varepsilon_V, \varepsilon_{EDP}) \\ \times dM \times dR \times d\varepsilon_H \times d\varepsilon_V \times d\varepsilon_{EDP} \end{array} \right) \quad (6.4)$$

where Sa_H is the horizontal spectral acceleration at the horizontal period of the structure, Sa_V is the vertical spectral acceleration at the vertical period of the structure, ε_H is the number of standard deviations for horizontal ground motion model, ε_V is the number of standard deviations for vertical ground motion model, $f_{\varepsilon H}(\varepsilon_H)$ and $f_{\varepsilon v}(\varepsilon_H, \varepsilon_V)$ are the probability density functions for ε_H and ε_V.

The probability density functions for ε_{EDP}, ε_H and ε_V are characterized by the standard deviations of the residuals and expressed with standard normal distribution (the normal distribution that mean is equal to zero and standard deviation is equal to one). In addition to the median and standard deviations of the ground motion the parameters of interest, the covariance of the ground motion parameters is also needed. The covariance of vertical spectral acceleration with respect to horizontal spectral acceleration is computed from the correlation of the residuals for related spectral periods. Figure 6.1 shows a sketch of correlation between the normalized residuals (epsilons) for vertical ground motion model at $T=T_V$ and the normalized residuals for horizontal ground motion model at $T=T_H$. The red lines in Figure 6.1 would be flat if there is no correlation between the epsilons of two models whereas; a positive slope shows that there is a tendency of increase in the vertical spectral accelerations at $T=T_V$ when the horizontal spectral values at $T=T_H$ increase and vice versa. The epsilons for the vertical model can be defined as a function of horizontal model epsilons as in Equation 6.5:

$$\varepsilon_v(T = T_v) = c \times \varepsilon_H(T = T_H) \pm \sigma_c \quad (6.5)$$

Correlation coefficients (c) and standard deviations (σ_c) are determined for the vertical and horizontal periods of each bridge configuration and given in Table 6.1.

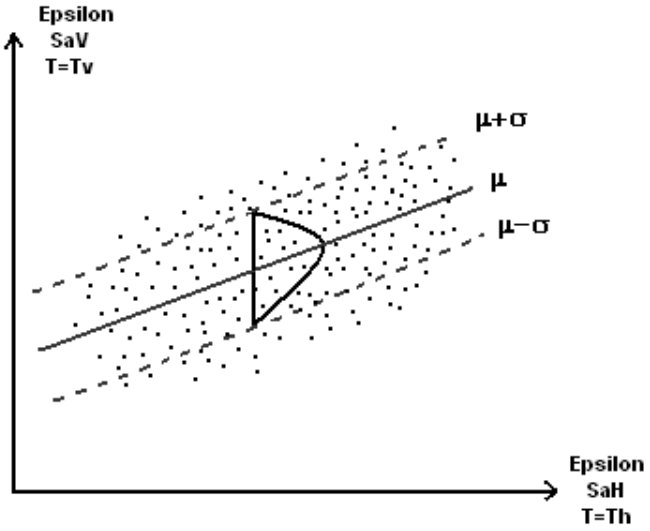

Figure 6-1 - Correlation of residuals of vertical and horizontal models

Table 6-1 - List of parameters and the root mean square error values SaV/SaH Model

Configuration #	Vertical Period	Horizontal Period	Correlation Coefficient (c)	Standard Deviation (σ_c)
0	0.19	0.32	0.385	0.718
0	0.19	0.55	0.262	0.788
1	0.12	0.27	0.353	0.803
1	0.12	0.46	0.221	0.881
2	0.30	0.43	0.428	0.675
2	0.30	0.64	0.346	0.722
3	0.37	0.53	0.430	0.655
3	0.37	0.68	0.368	0.690
4	0.45	0.62	0.432	0.648
4	0.45	0.75	0.396	0.668
5	0.24	0.35	0.422	0.680
5	0.24	0.59	0.301	0.747

6.2 STRUCTURAL DEMAND HAZARD CURVES

Figures 6.2 to 6.6 shows the hazard curves for the axial load demand and the positive and negative moment demand at the span and in the girder, respectively. Similar to the nonlinear time history analyses, the PSHA study was also done in two stages. First, the effects of vertical excitement were neglected.

For these calculations, the probabilistic seismic demand models built by considering only the horizontal ground motions (mentioned as $Rsp_{(Honly)}$) in Chapter 5.1) were applied. Results are given by the gray curves in each figure. The gray broken line on each figure indicates the capacity for that engineering demand parameter. Figures 6.2 to 6.4 show that neither the axial load demand nor the positive moment demands exceed the capacity, if the effects of verticals are neglected. Analyses show that there is a small change of exceeding the capacity for negative span and support moment demands, but these possibilities are negligible for the life time of these particular structures. For the second stage, vertical effects are taken into account by using probabilistic seismic demand models built for all three components of ground motions including the vertical component (mentioned as $Rsp_{(H+V)}$ in Chapter 5.1) (shown by black curves on each graph). Figures 6.2 and 6.3 indicate that the probability of exceeding the axial load capacity at the column and the positive span moment capacity increased significantly but still below the capacity. The annual probability of exceeding the support moment capacity (both on the positive and negative sides) are found to be 0.001 if the vertical effects are included (Figure 6.4 and 6.6). Negative span moment demand is identified as the most critical parameter under the influence of vertical accelerations. Annual probability of exceeding the negative span moment capacity is around 0.01 if the vertical effects are considered (Figure 6.5). We compared the results to the NEHRP Guidelines for Seismic Rehabilitation of Buildings (FEMA-273) design criteria since FEMA-273 defines the ground motion hazard levels in probabilistic basis. Life Safety performance level is defined in FEMA-273 as the demand from Basic Safety Earthquake (BSE-1) that has a return period of 474 years (or 10% changes in 50 years). Similarly, Collapse Prevention performance level is defined as the demand from Basic Safety Earthquake (BSE-2) that has a return period of 2475 years (or 2% changes in 50 years). The annual rates of exceeding the Life Safety performance level and the Collapse Prevention level correspond to 0.002 and

0.0004, respectively. Results show that the annual probability of exceeding the capacity of three parameters (negative span and support moments and positive support moment) exceeds the Collapse Prevention performance level when the vertical ground motions included in the analysis. Probability of exceeding positive and negative support moment capacity values are slightly under the Life Safety performance level, but the probability of exceeding the negative span moment capacity is significantly larger than the limits.

After the preliminary analysis, the negative span moment is found to be the most critical parameter under the influence of vertical ground motions; therefore, negative span moment hazard curves are constructed for all bridge configurations. Results are presented in Figures 6.7-6.12. Two sets of hazard curves are given for all configurations; for the black curves, the transverse period of the structure is used as the horizontal period and for the gray curves, the longitudinal period of the structure is used as the horizontal period. Broken lines in each figure represent the analysis done without the vertical component and the solid lines show the analysis including the vertical component. According to Figures 6.7 to 6.12, probability of exceeding the negative span moment capacity is proportional to the period of the structure. The probabilities calculated by using the transverse period of the structure as the horizontal period are higher than the probabilities calculated by using the longitudinal period of the structure as the horizontal period for each configuration. Probability of exceeding the negative span moment capacity also varies significantly between different bridge configurations, for example, the annual probability of exceeding the capacity is close to 1% for Configuration #1 but this value decreases to 0.1% for Configuration #4, which has higher horizontal and vertical periods than Configuration #1. The probabilities of exceeding the capacity for each configuration are plotted with respect to transverse and vertical periods in Figures 6.13 and 6.14, respectively. As these figures implies, the bridges with smaller horizontal and vertical periods are more susceptible to the effects of near

fault vertical ground motions than the bridges with larger horizontal and vertical periods. The number of bridge configurations examined for this study is not enough to support an empirical relation between the period of the structure and the probability of exceeding the negative span moment capacity, but such a relation can be suggested if more data points included by examining different bridge configurations.

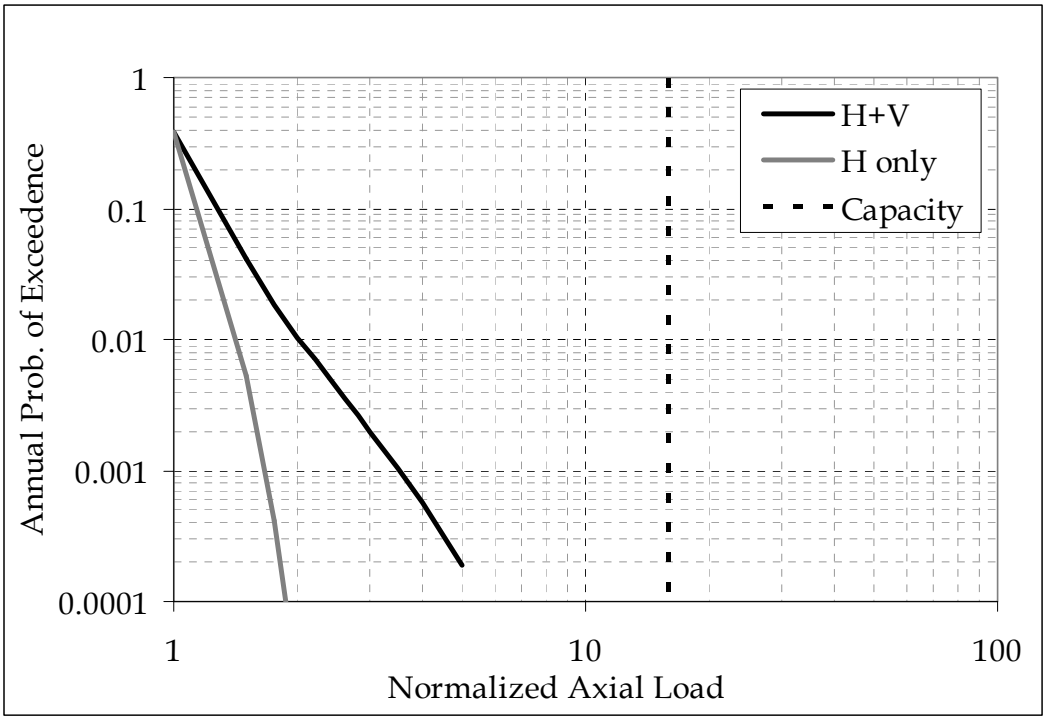

Figure 6-2 - Axial Load Demand Hazard Curve for Berkeley (Configuration #1, T_v=0.12 seconds and T_h=0.27 seconds)

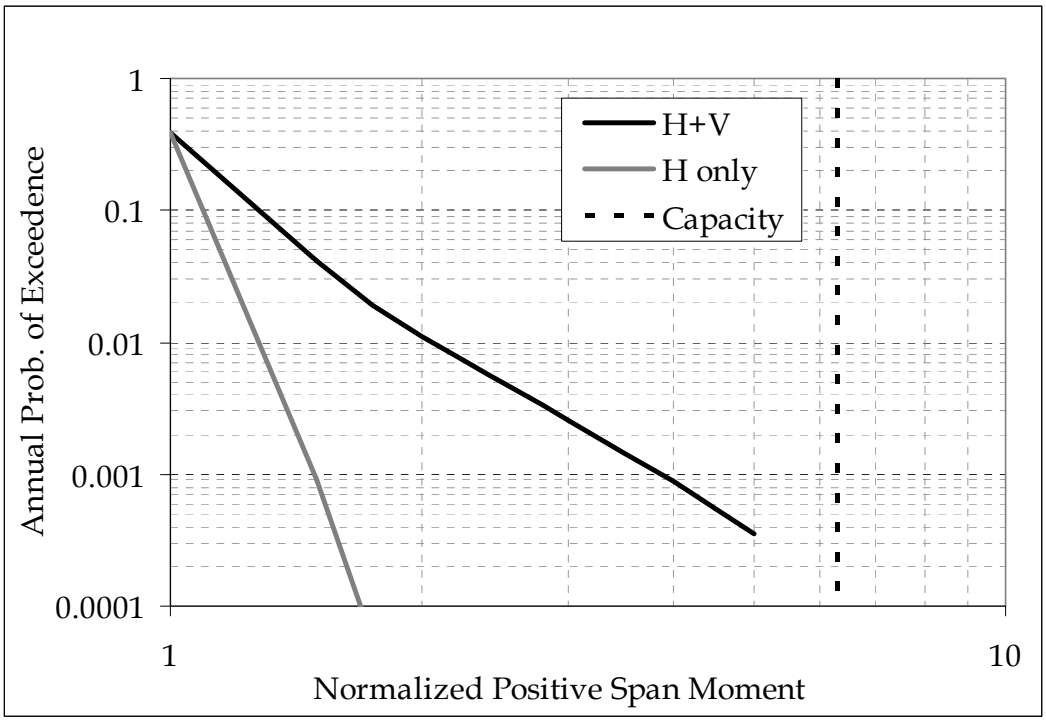

Figure 6-3 – Positive Span Moment Demand Hazard Curve for Berkeley (Configuration #1, T_v=0.12 seconds and T_h=0.27 seconds)

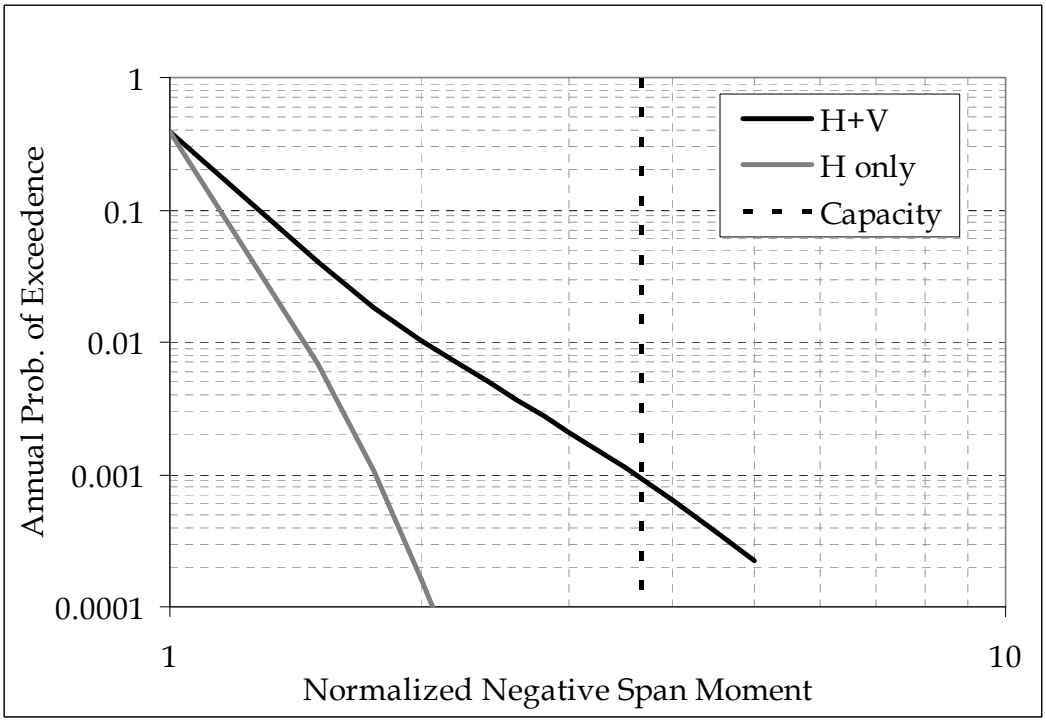

Figure 6-4 - Positive Support Moment Demand Hazard Curve for Berkeley (Configuration #1, T_v=0.12 seconds and T_h=0.27 seconds)

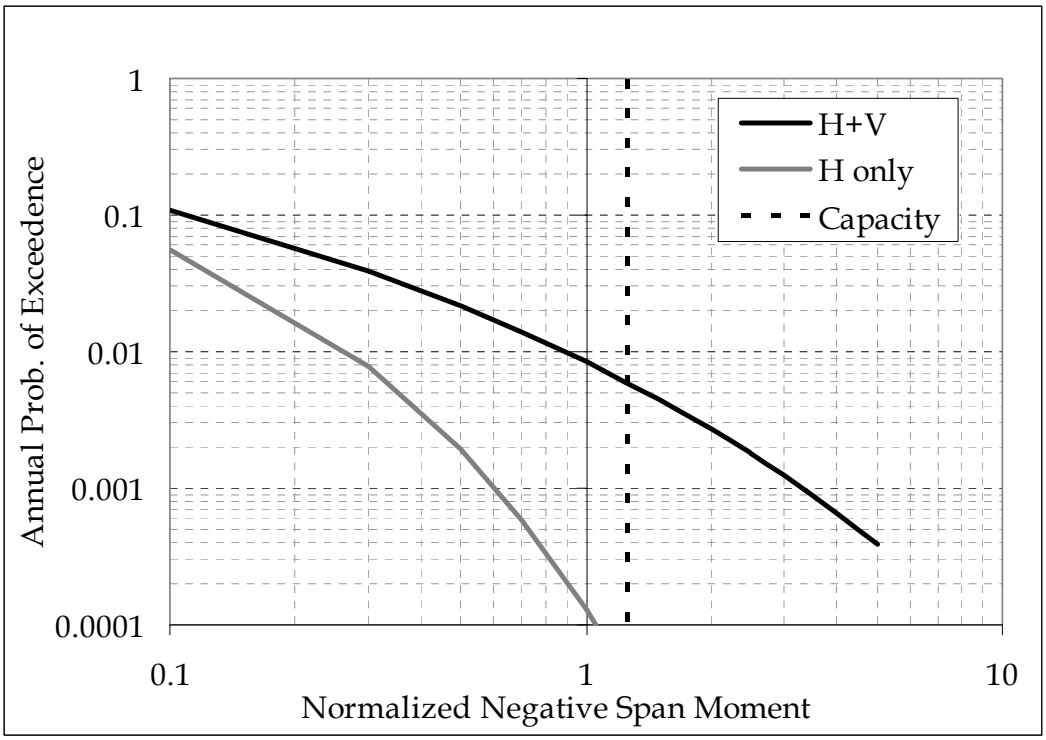

Figure 6-5 - Negative Span Moment Demand Hazard Curve for Berkeley (Configuration #1, T_v=0.12 seconds and T_h=0.27 seconds)

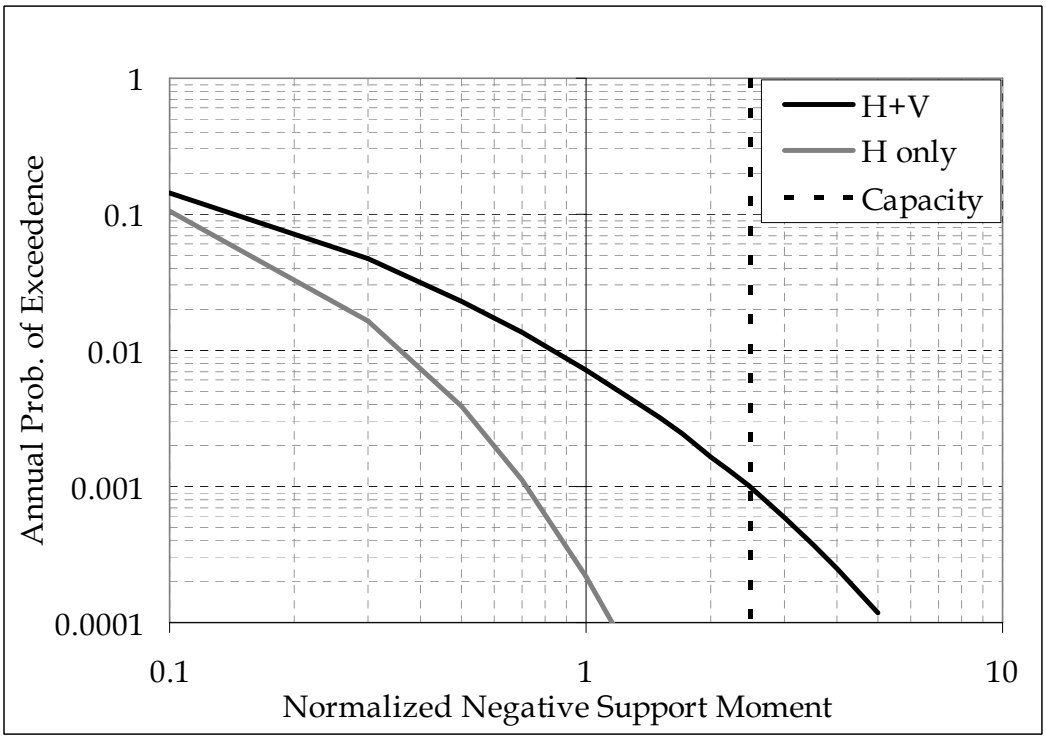

Figure 6-6 - Negative Support Moment Demand Hazard Curve for Berkeley (Configuration #1, T_v=0.12 seconds and T_h=0.27 seconds)

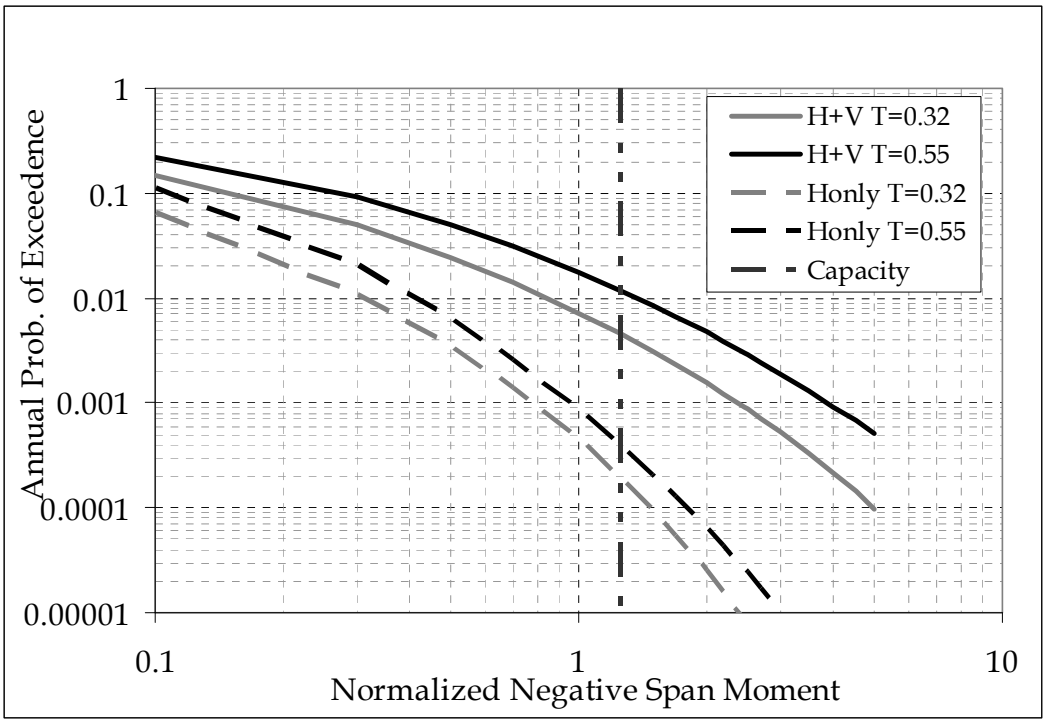

Figure 6-7 - Negative Span Moment Hazard Curve for Berkeley (Configuration #0, T_v=0.19 seconds, T_{long}=0.32 seconds and T_{trans} =0.55 seconds)

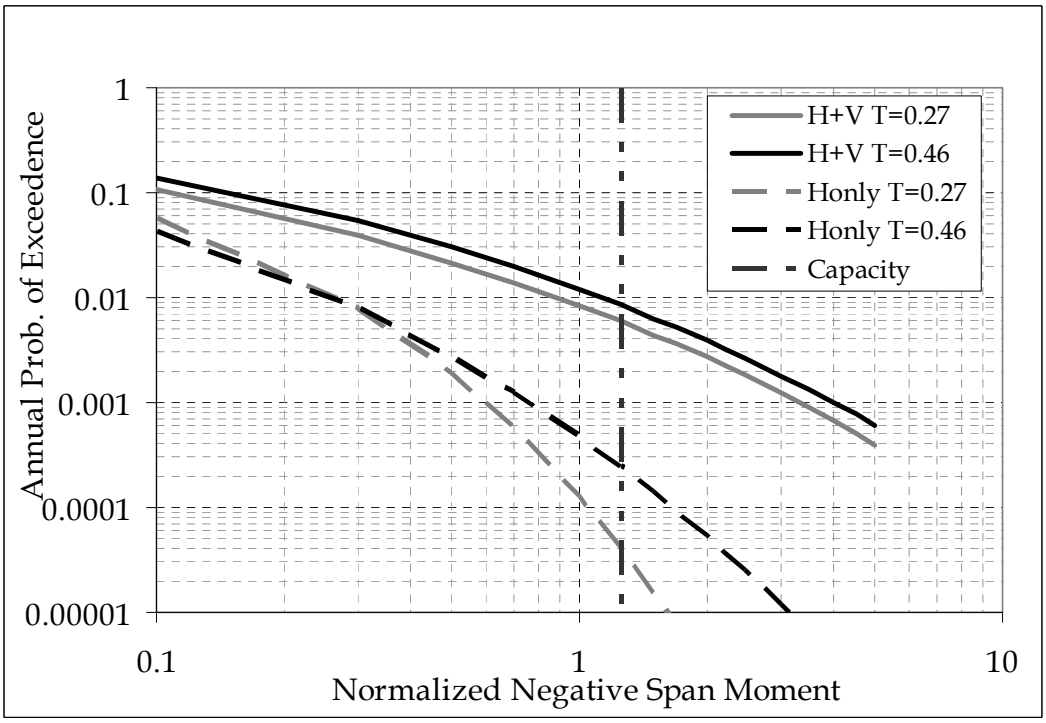

Figure 6-8 - Negative Span Moment Hazard Curve for Berkeley (Configuration #1, T_v=0.12 seconds, T_{long}=0.27 seconds and T_{trans} =0.46 seconds)

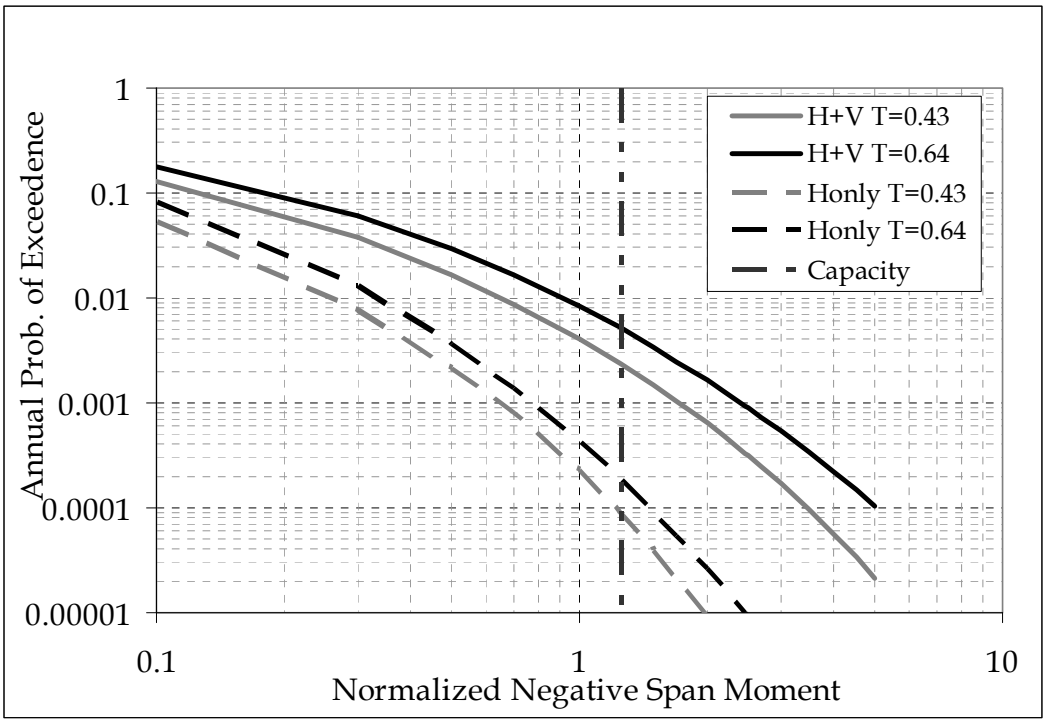

Figure 6-9 - Negative Span Moment Hazard Curve for Berkeley (Configuration #2, T_v=0.30 seconds, T_{long}=0.43 seconds and T_{trans} =0.64 seconds)

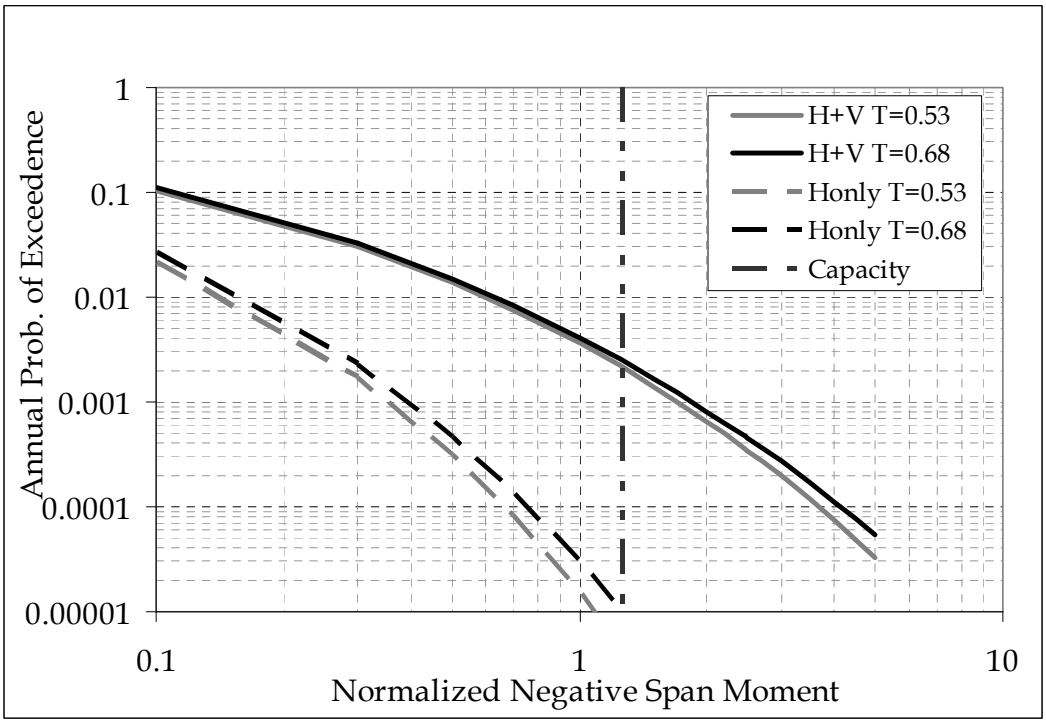

Figure 6-10 - Negative Span Moment Hazard Curve for Berkeley (Configuration #3, T_v=0.37 seconds, T_{long}=0.53 seconds and T_{trans} =0.68 seconds)

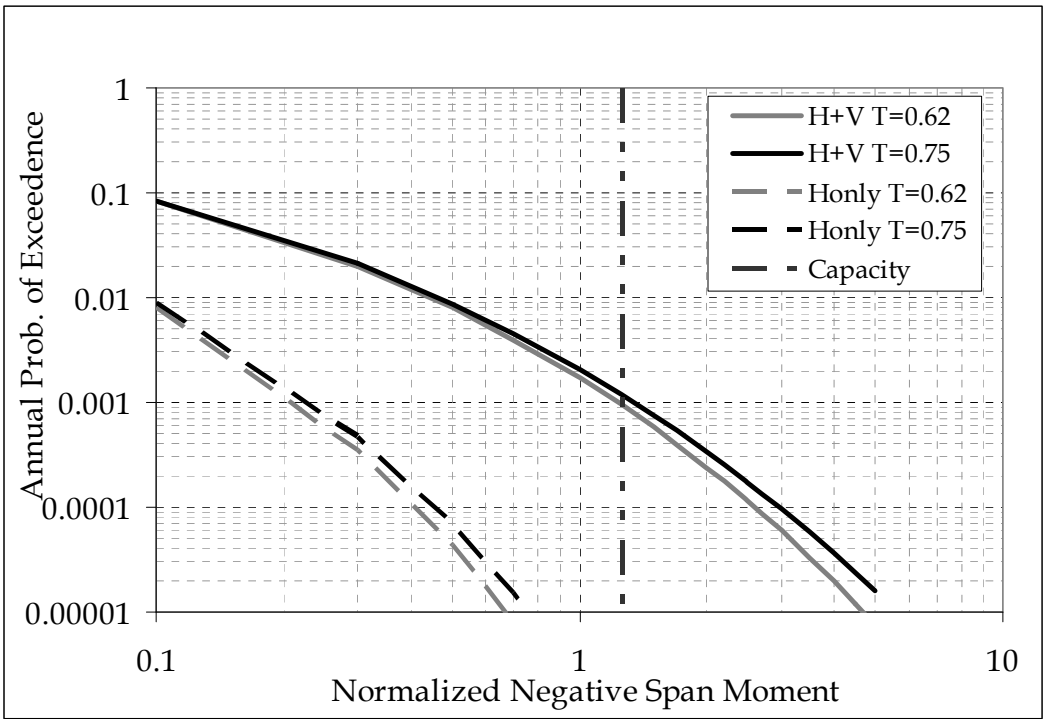

Figure 6-11 - Negative Span Moment Hazard Curve for Berkeley (Configuration #4, T_v=0.45 seconds, T_{long}=0.62 seconds and T_{trans} =0.75 seconds)

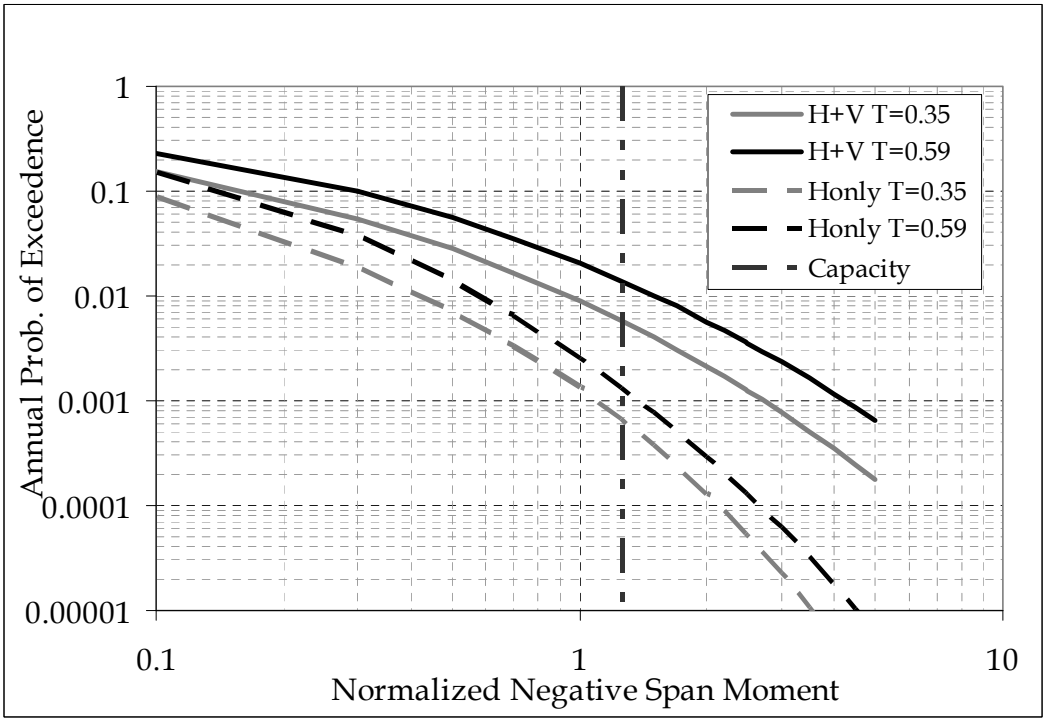

Figure 6-12 - Negative Span Moment Hazard Curve for Berkeley (Configuration #5, T_v=0.45 seconds, T_{long}=0.35 seconds and T_{trans}=0.59 seconds)

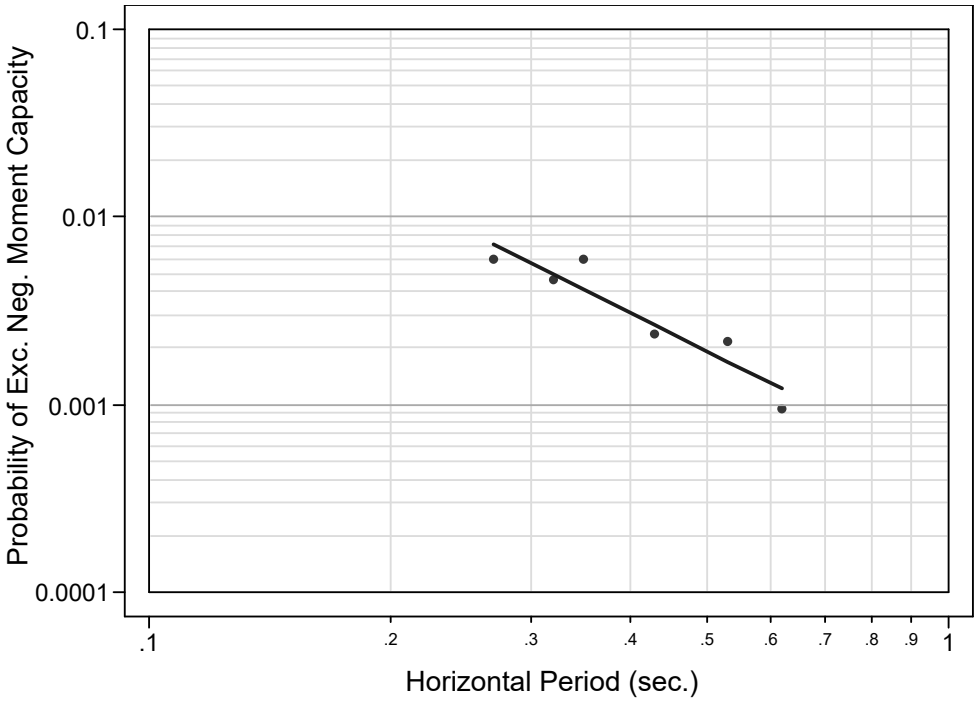

Figure 6-13 - Annual Probability of Exceeding Negative Span Moment Capacity vs. Horizontal (transverse) Period of the Structure.

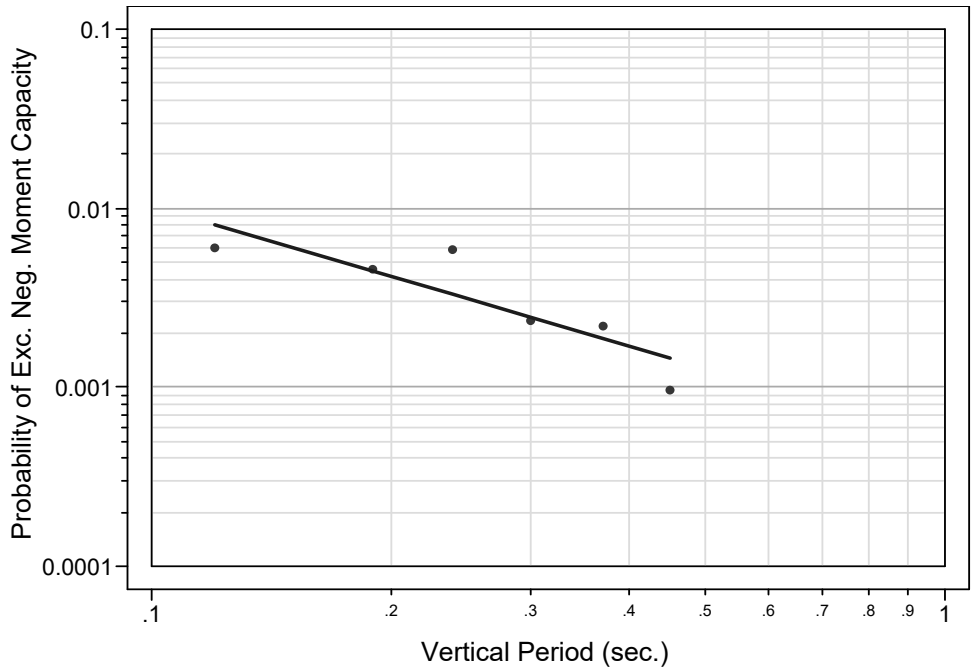

Figure 6-14 - Annual Probability of Exceeding Negative Span Moment Capacity vs. Vertical Period of the Structure.

Negative span moment hazard assessment is repeated for various sites in Northern California. The names, coordinates (in latitudes and longitudes) of the

sites and the probability of exceeding the negative span moment capacity for each site are listed in Table 6.2. Negative span moment hazard curves including vertical effects for Sites 1 - 10 and 11 – 18 are shown in Figure 6.15 and 6.16, respectively. We assumed all the sites have the same soil conditions for these analyses (V_{s30} value is assumed as 270 m/s), therefore the results does not reflect the differences due to site specific soil conditions. According to the results, the probability of exceeding the negative span moment capacity is pretty low even if the vertical effects included in the analysis for far field sites like Sacramento, Davis, and Stockton. Being within the near proximity of Hayward Fault; Berkeley, Richmond, Emeryville, and Hayward are the sites that have the bigger changes of exceeding the structural capacity due to vertical ground motions.

Table 6-2 - Names, Coordinates and Probability of Exceeding the Negative Span Moment Capacity of the Analyzed Sites in Northern California

Site Number	Site Name	Latitude	Longitude	Prob. Of Exceeding the Capacity
1	Sacramento	-121.53	38.58	0.00007
2	Davis	-121.74	38.54	0.00044
3	Dixon	-121.82	38.44	0.00127
4	Vacaville	-121.99	38.35	0.00458
5	Fairfield	-122.04	38.25	0.00580
6	Vallejo	-122.25	38.10	0.00385
7	Rodeo	-122.27	38.03	0.00432
8	Richmond	-122.35	37.93	0.00490
9	Berkeley	-122.27	37.87	0.00595
10	Emeryville	-122.28	37.83	0.00471
11	San Francisco	-122.42	37.77	0.00173
12	Daly City	-122.46	37.70	0.00247
13	San Mateo	-122.18	37.33	0.00236
14	Hayward	-122.04	37.38	0.00151
15	Dublin	-121.54	37.42	0.00475
16	Livermore	-121.45	37.41	0.00478
17	Brentwood	-121.42	37.56	0.00369
18	Stockton	-121.18	37.58	0.00127

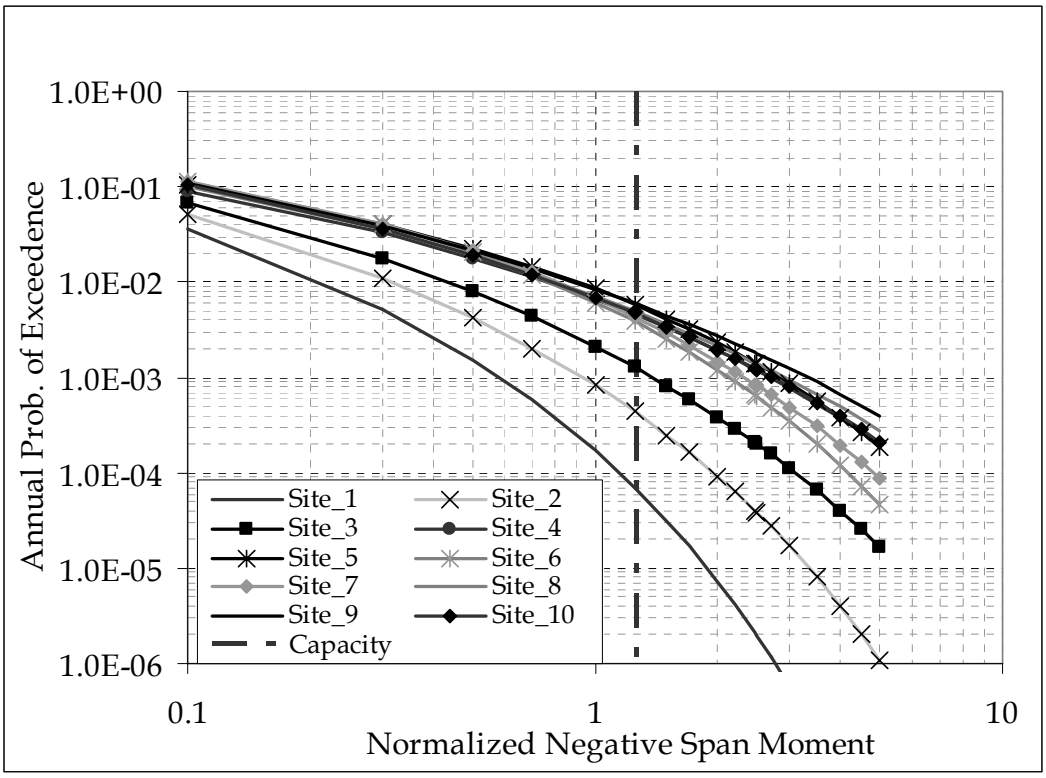

Figure 6-15 - Negative Span Moment Hazard Curves (Configuration #1) for Sites 1 to 10

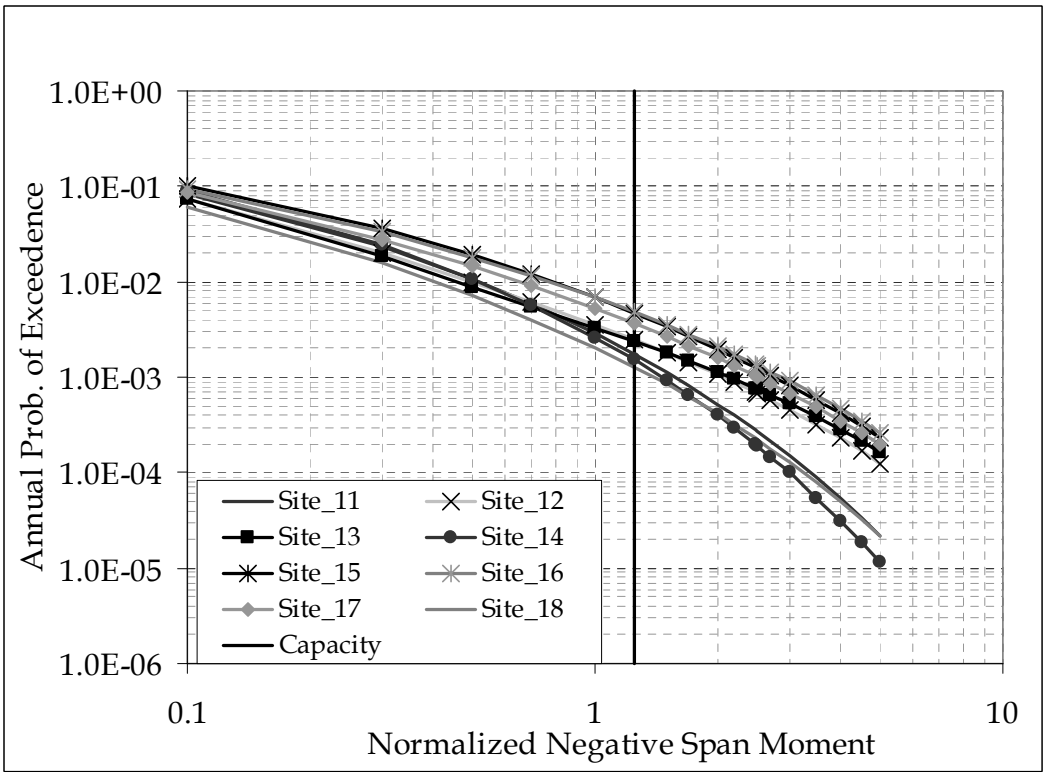

Figure 6-16 - Negative Span Moment Hazard Curves (Configuration #1) for Sites 11 to 18

6.3 SEMI-DETERMINISTIC SEISMIC HAZARD ASSESSMENT

For ordinary standard bridges constructed on sites where the horizontal peak ground acceleration is expected to be more than 0.6g, SDC-2006 requires consideration of vertical effects. Currently, the horizontal peak ground acceleration values obtained from the Caltrans Deterministic Seismic Hazard Map (1996). To evaluate the simplified procedure employed by Caltrans in SDC-2006 to account for the effect of vertical component of ground motions in the design of ordinary highway bridges, we conducted a semi deterministic seismic hazard assessment study in addition to the PSHA. For this analysis, we used the deterministic earthquake scenarios (earthquake magnitude and location are specified) but included the variability of both horizontal and vertical ground motions. The probabilities of exceeding the negative span moment capacity for soil (V_{s30}=270 m/s) and rock (V_{s30}=760 m/s) sites are calculated for different deterministic scenarios, magnitude varying between 5.5 to 8 for distances from 1 km to 100 km. Abrahamson and Silva (2008) NGA horizontal ground motion and proposed NGA vertical ground motion model are used for this study. The probability of exceeding the negative span moment capacity for soil sites and rock sites with respect to distance is given in Figures 6.17 and 6.18, respectively. These curves show that the probability of exceeding the negative moment capacity increases as the site getting closer to the fault and as the magnitude of the expected earthquake increases. Soil sites have higher chances of exceeding the capacity when compared to the rock sites. Both figures indicate that the vertical effects are substantial in near fault regions (0-20 km) but fade away at larger distances. Figures 6.19 and 6.20 show the probability of exceeding the negative span moment capacity for soil sites and rock sites with respect to median horizontal peak ground acceleration. According to these figures, SDC-2006 requirement for consideration of vertical effects where the horizontal peak ground acceleration is expected to be more than 0.6g is unconservative.

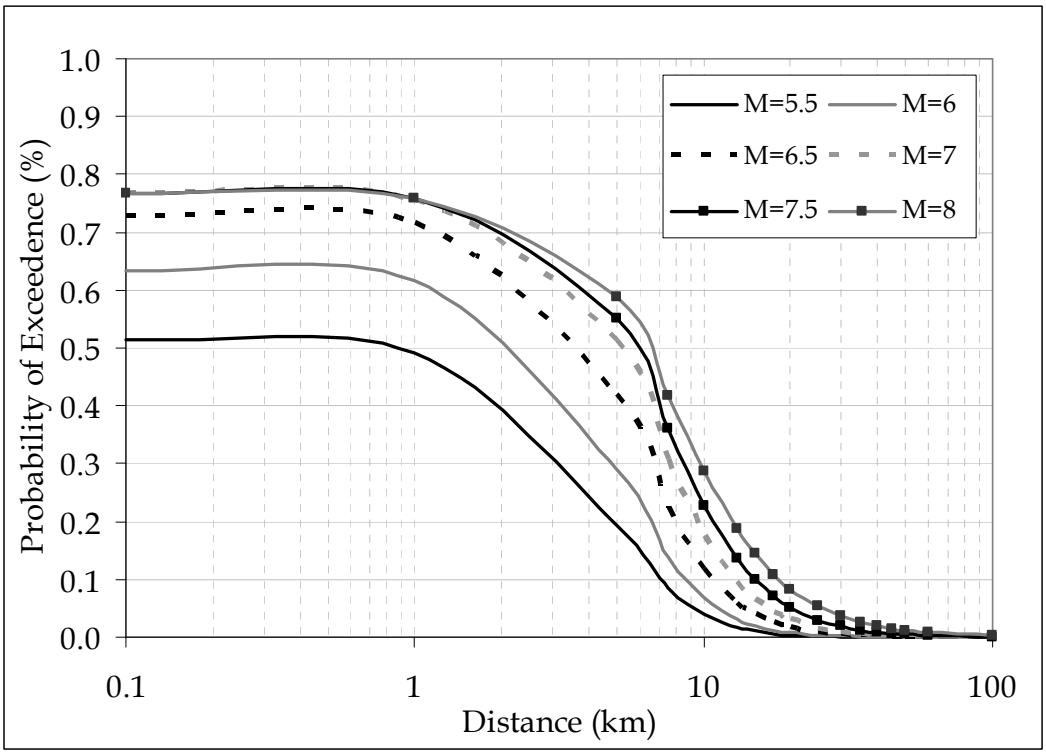

Figure 6-17 - Probability of exceeding the negative span moment capacity for soil sites with respect to distance (V_{s30}=270 m/s).

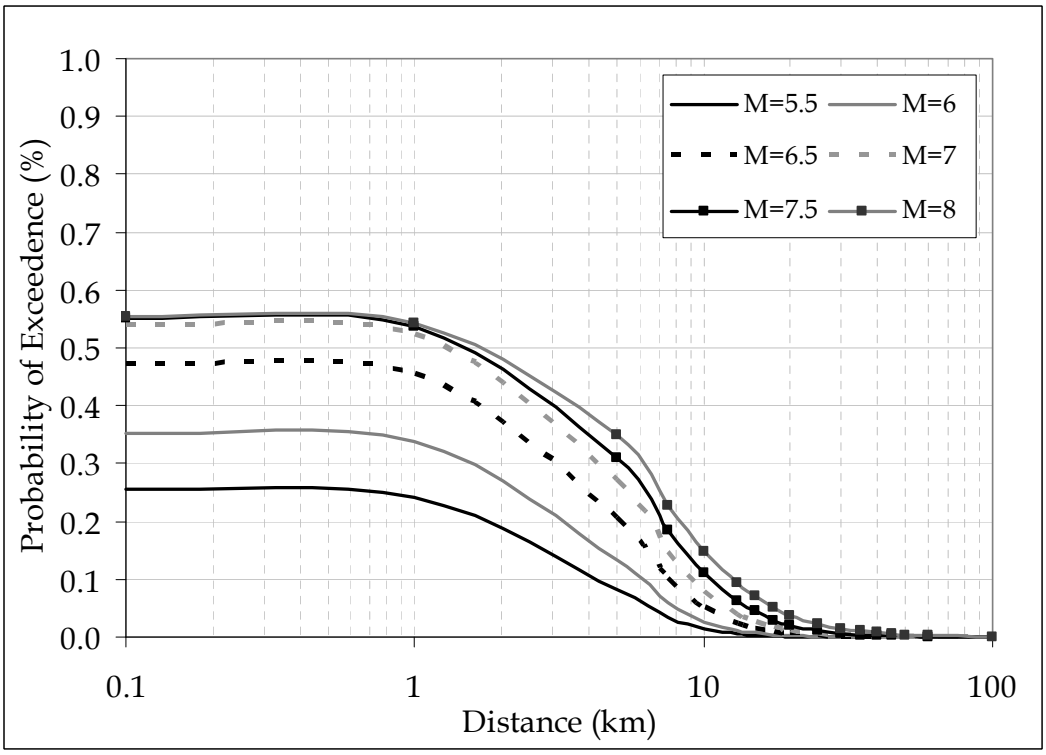

Figure 6-18 - Probability of exceeding the negative span moment capacity for rock sites with respect to distance (V_{s30}=760 m/s).

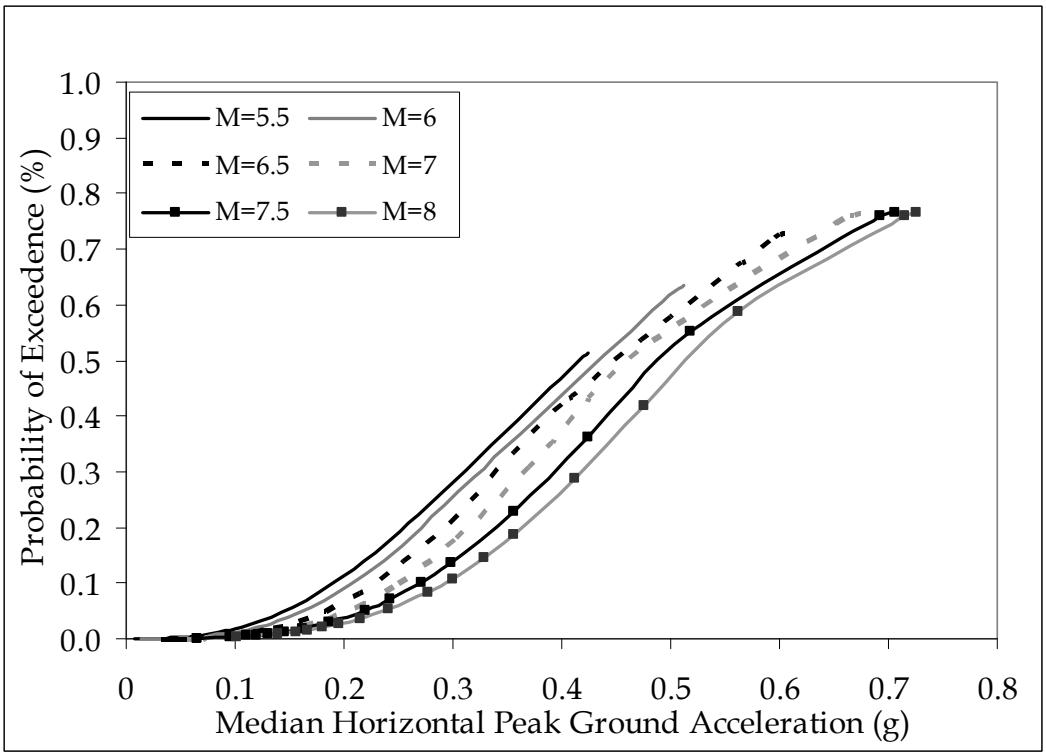

Figure 6-19 - Probability of exceeding the negative span moment capacity for soil sites with respect to median horizontal peak ground acceleration(V_{s30}=270 m/s).

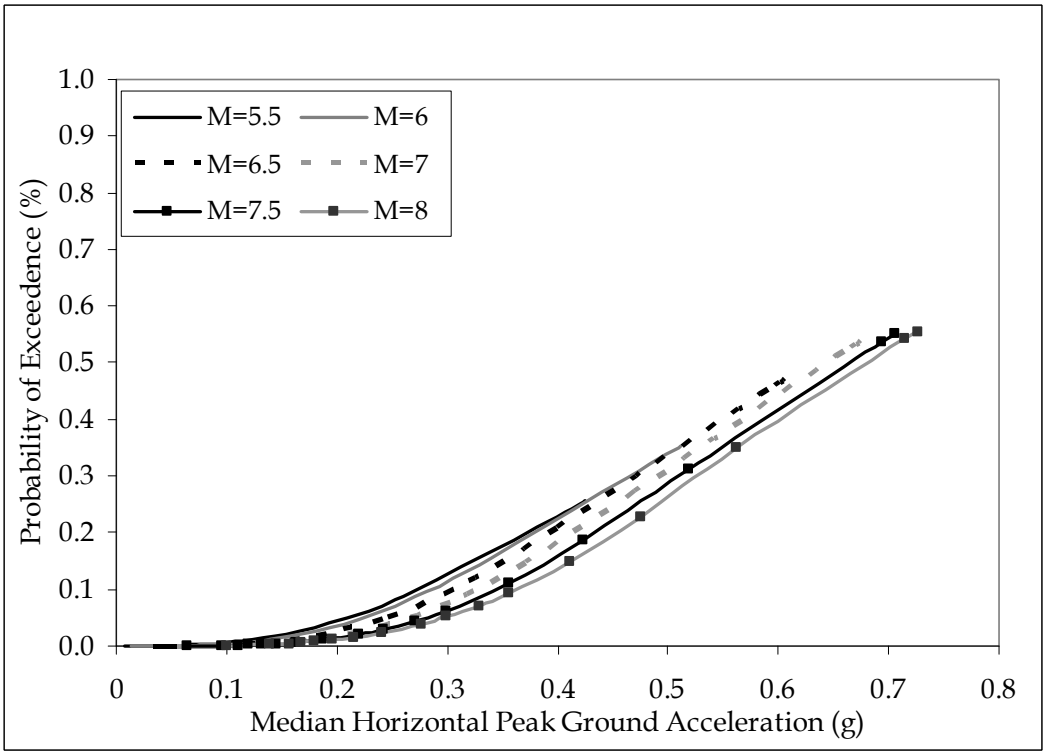

Figure 6-20 - Probability of exceeding the negative span moment capacity for rock sites with respect to median horizontal peak ground acceleration(V_{s30}=760 m/s).

6.4 VERTICAL DESIGN SPECTRUM

Some recent studies have focused on the shape of the vertical design spectrum. A design spectral shape for vertical ground motion has been proposed by Elnashai and Papazoglu in 1997. A simplified approach for developing vertical design spectra was proposed by Bozorgnia and Campbell (2004) based on V/H ratios that depend on distance, and site conditions. This simplified ratio is 0.5 at periods greater than 0.3 sec and increases for period between 0.1 and 0.3 sec. Bozorgnia and Campbell [2004] used attenuation relations to evaluate and validate their V/H ground motion model. In their study, they proposed a simplified V/H spectrum for practical engineering applications, Figure 6-21, and a tentative vertical spectrum consisting of a flat portion at short periods (0.05-0.15 sec) and a decaying spectral acceleration portion for periods longer than 0.15 sec, Figure 6-22.

An alternative method is proposed in this study in which the V/H ratios are dependent on magnitude, distance and soil conditions in addition to period. The average response spectra and median V/H ratios for the initially selected ground motion records are given in Figure 6-23 and Figure 6-24, respectively. In Figure 6.9, both the horizontal and vertical spectra are normalized by the PGA on the horizontal component. This figure shows that the peak in the vertical spectrum is shifted to shorter periods and that the commonly used 2/3 scaling of the horizontal component does not capture this period shift. This difference in spectral shape between the horizontal and vertical components is well known with the amplitude of the vertical peak at 0.1 sec period increasing as the earthquake magnitude increases or the distance decreases (Bozorgnia and Campbell, 2004). The short period vertical component is larger for soil sites than for rock sites, whereas, the short-period horizontal component is larger for rock sites. As a result, the V/H ratio at short periods is larger for soil sites than rock sites. Figure 6.10 indicates that, the V/H ratio peaks close to T=0.1 sec due to the

vertical peak at 0.1 second period and slowly decreases until the proximity of 0.3-0.5 sec. where the horizontal spectrum peaks.

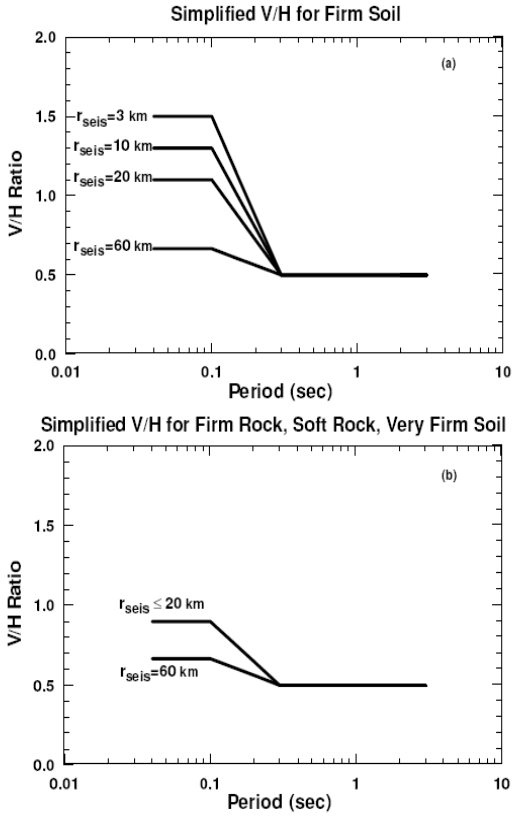

Figure 6-21 - **:** Simplified V/H response spectral ratio developed by Bozorgnia and Campbell (2004)

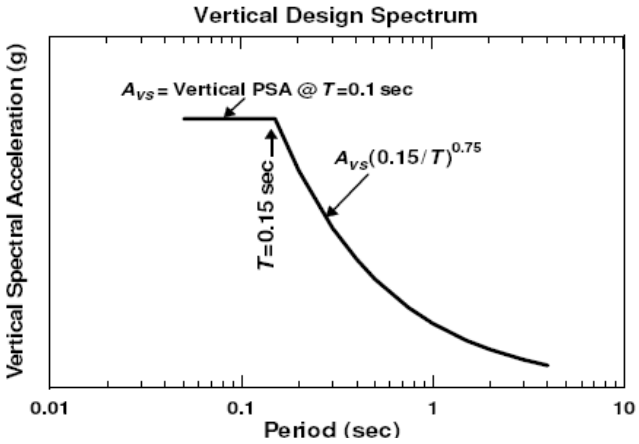

Figure 6-22 - Preliminary Vertical Design Spectrum Proposed by Bozorgnia and Campbell (2004)

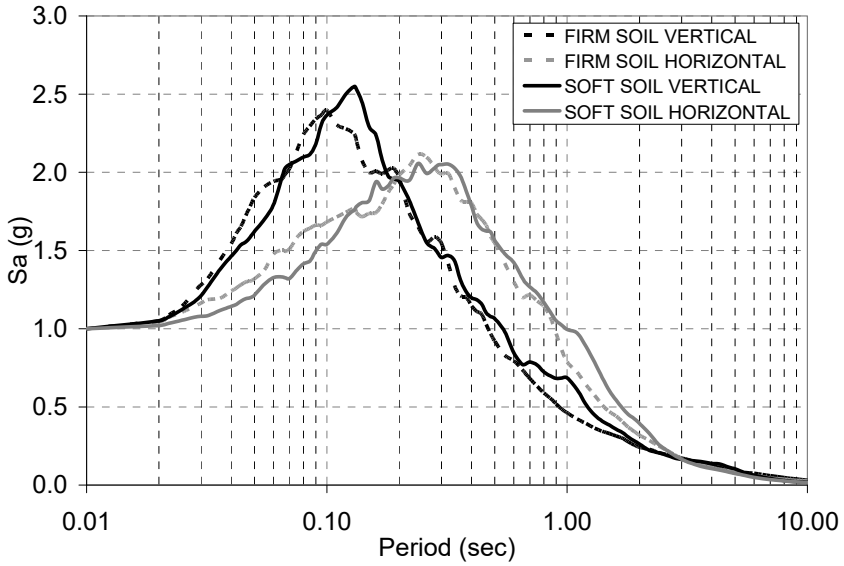

Figure 6-23 - Average Response Spectra for Records with Magnitude greater than 6 and closest distance to the rupture less than 30 km

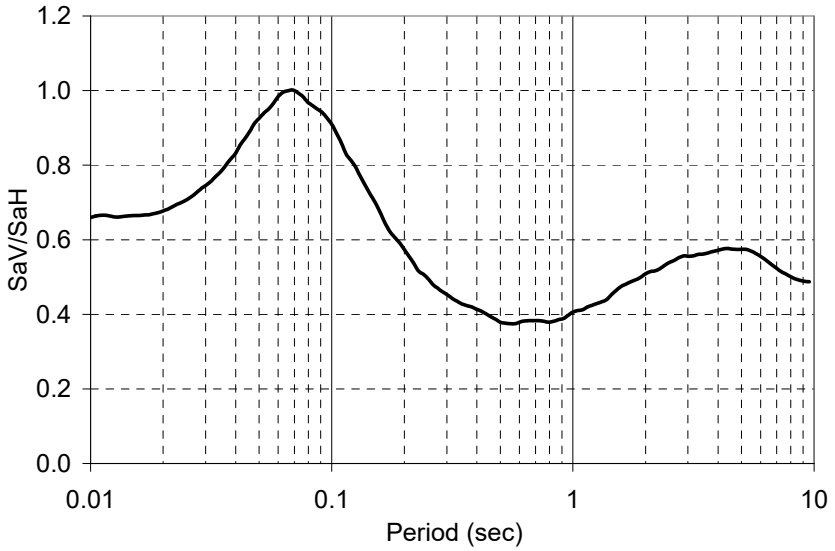

Figure 6-24 - Median SaV/SaH for Records with Magnitude greater than 6 and closest distance to the rupture less than 30 km

Inspired by the functional shape given in Equation 6.1 for SaV/SaH (where SaV is the vertical spectral acceleration at T=Tv and SaH is the horizontal spectral acceleration at T=Th), the V/H ratio (ratio of spectral accelerations at the

same period value) is modeled by the function given below. The coefficients for Equation 6.5 are summarized in Table 6-3.

$$\ln(V/H) = b_1 + b_2 \times (M-6) + b_3 \times \ln(D+5) + (b_4 + b_5 \times (\ln(PGA_{rock} + 0.05)) \times \ln(vs_{30}) + \sigma \quad (6.5)$$

The standard deviation estimated for the selected ground motions in this phase of the study is σ = 0.5. The inclusion of the standard deviation term is considered more appropriate for the ground motion hazard in California. The proposed V/H curves for a greater than 6 magnitude earthquake occurring less than 30 km away from the fault for different soil types are given in Figure 6-24. (Note: The PGA_{rock} values are calculated using the Abrahamson and Silva (1997) equations). Using the proposed V/H ratio model, new vertical ARS curves are constructed by scaling the horizontal ARS curves used by Caltrans. Figure 6-25 shows the proposed vertical ARS curves for all soil types. Vertical ARS curves are found to be alike the average response spectra given in Figure 6-23, the curves peak around 0.1 second period and the soft soil curves (soil type D) are lower than the firm soil curves (soil type B). All vertical ARS curves for different magnitudes and soil types are given in the Appendix for future reference.

Table 6-3 - List of parameters for V/H model

Period (sec)	b1	b2	b3	b4	b5
0.01	0.644	-0.039	-0.15	-0.073	0.0135
0.02	0.534	-0.058	-0.118	-0.046	0.024
0.03	1.185	-0.079	-0.118	-0.115	0.003
0.05	2.135	-0.076	-0.168	-0.241	0.0219
0.1	1.89	0.03	-0.111	-0.245	0.023
0.15	1.63	0.064	-0.191	-0.248	-0.003
0.2	0.488	0.048	-0.144	-0.11	-0.002
0.3	-1.03	0.051	-0.083	0.059	-0.012
0.4	-1.536	0.041	-0.068	0.107	-0.022
0.5	-2.264	0.033	-0.006	0.191	-0.02
0.75	-3	0.05	-0.015	0.287	-0.041
1	-2.83	0.053	-0.068	0.292	-0.042
1.5	-3.29	0.094	-0.116	0.398	-0.047
2	-3.39	0.103	-0.113	0.434	-0.04
3	-2.86	0.217	-0.092	0.338	-0.038

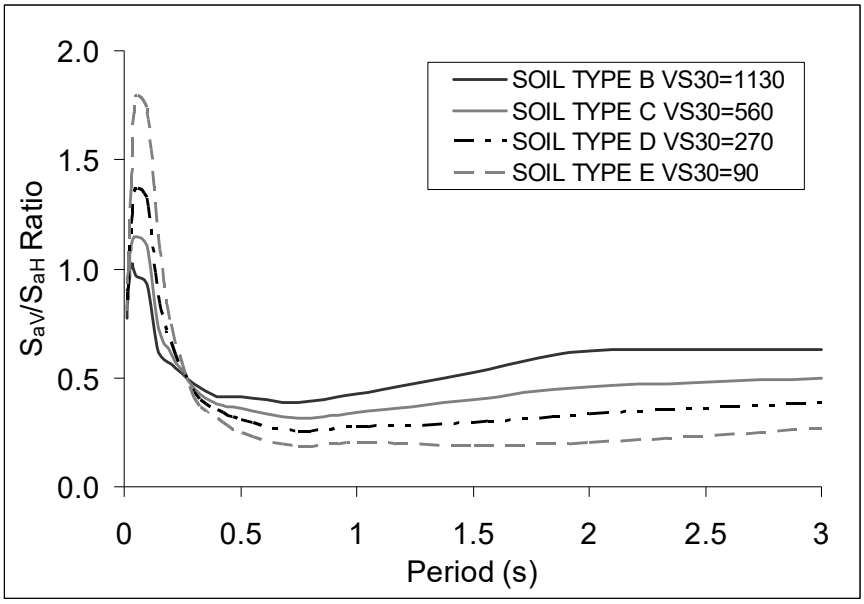

(a)

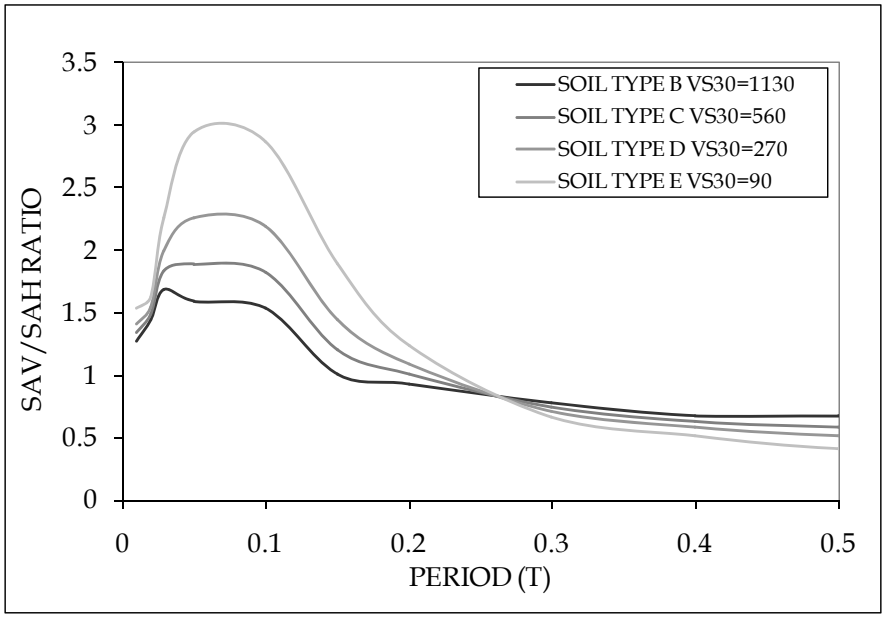

(b)

Figure 6-25 - The proposed V/H curves for a magnitude 7 earthquake occurring 3 miles away from the fault for different soil types: (a) period range up to T = 3.0 sec; (b) period range to 0.5s

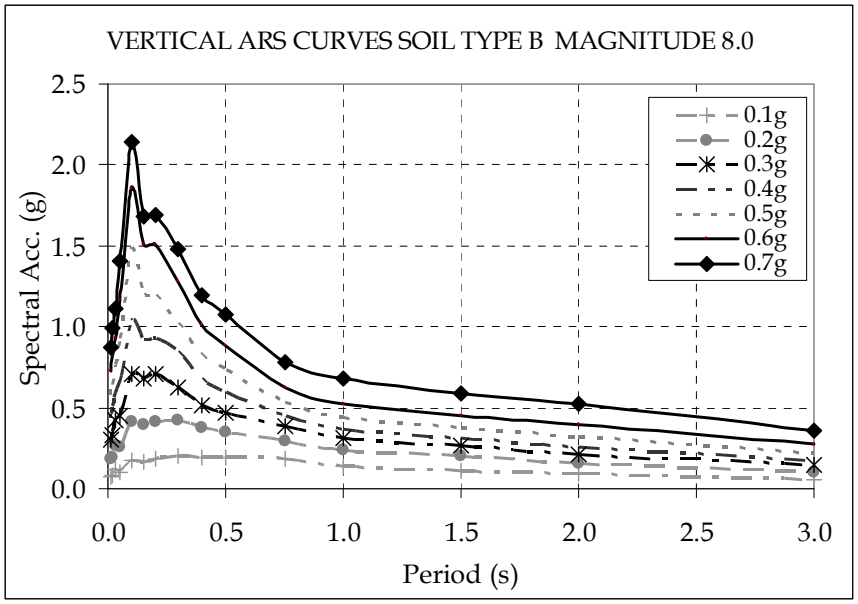

(a)

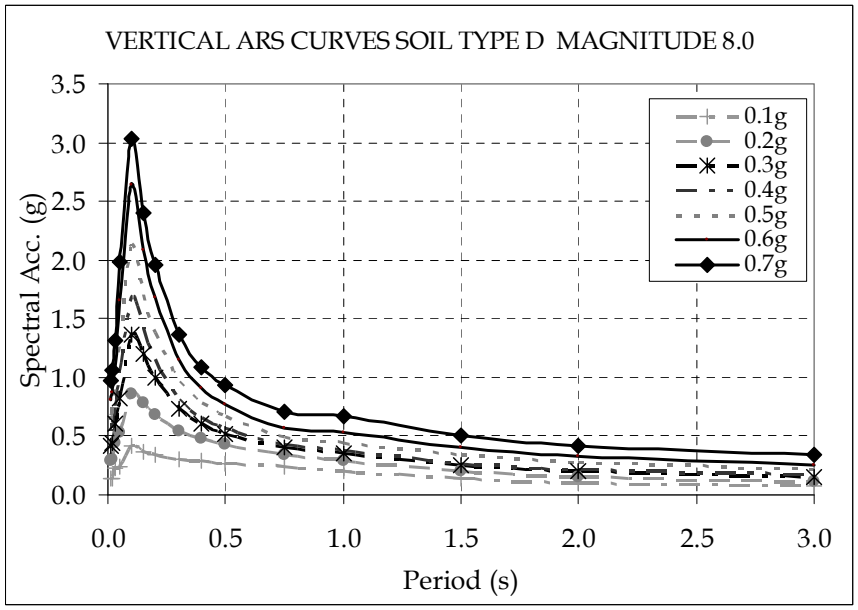

(b)

Figure 6-26 - Vertical ARS curves for magnitude 8.0 event (a) soil type B (b) soil type D

7 DESIGN RECOMMENDATIONS

Numerical analyses results presented in Chapter 4 of this report show that current design procedure employed in SDC-2006 (Caltrans 2006) for considering vertical ground motions is simplistic and may result in non-conservative designs for certain bridge configurations subject to near-fault ground motions. One of the significant findings from the numerical analyses carried out indicate that the current SDC criteria of considering the vertical components of ground motions only when the peak rock acceleration (PRA) is higher than 0.6g is not appropriate. Vertical components of ground motions with a PRA as low as 0.4g were shown to have significant effect on the seismic behavior of bridges, particularly with shorter periods. Although, a hazard analyses as summarized in chapter 6 is a complete and comprehensive way to decide whether the vertical effects should be included or not, it can be stated that considering the vertical components of ground motions with a PRA of 0.4g is a conservative and simple approach that can be implemented more readily in the design procedure.

The numerical analyses results also showed that the vertical components of ground motions on the selected parameters may well exceed the demands computed using 25% of dead load in both directions. Moreover, it is obvious that this effect differs from bridge to bridge depending primarily on the fundamental vertical period of the bridge. Hence, a design procedure that takes the dynamic properties of the structure into account is desirable.

In chapter 4, it was shown that the elastic response spectrum analysis is very effective in capturing the effects of vertical components of ground motions. In the light of this finding, an elastic response spectrum analysis using the vertical response spectra developed in chapter 6 may be a reasonable method for use in the design process of bridges subjected to combined effects of horizontal and vertical ground motions.

Figure 7-1 presents the girder moment diagram of the Camino del Norte Bridge obtained using a response spectrum analysis under a set of design spectra for a magnitude 8 event, site D and a PGA of 0.7g. In this figure, the response results for 5 independent cases are displayed: dead load only, dead load plus the longitudinal component, dead load plus the longitudinal and transverse components, dead load plus the longitudinal and vertical components, dead load plus all the three components. The ARS curve for the corresponding event taken from SDC-2006 was applied in the longitudinal and horizontal components whereas the vertical design spectrum developed in chapter 6 was applied in the vertical direction.

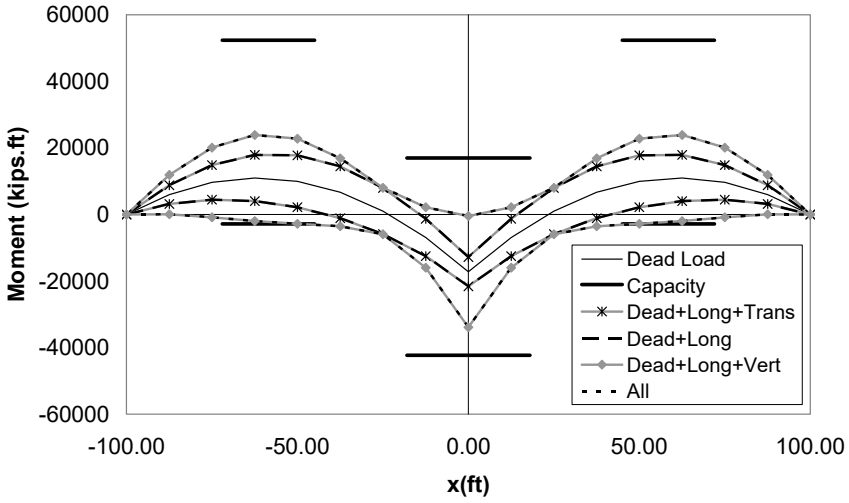

Figure 7-1 – Girder moment diagram obtained from response spectrum analysis.

One of the immediate observations drawn from Figure 7-1 is that the transverse component has no effect on the girder moment demands suggesting that considering only the longitudinal and vertical components is sufficient in determining the girder moment demands.

7.1 RECOMMENDED DESIGN PROCEDURE

Based on the studies carried out within the scope of this study, the following step by step design procedure is proposed:

1. Based on the location of the bridge, determine the design ground motion using current procedures.
2. If the expected peak rock acceleration is less than 0.4g, ignore the vertical components of ground motions and carry out the design according to the SDC-2006 guidelines.
3. If the expected peak rock acceleration is equal to higher than 0.4g, a 3D elastic computer model of the bridge should be developed.
4. Select the corresponding ARS curve based on the magnitude, peak rock acceleration of the design ground motion and site class. This spectrum will be applied in the longitudinal direction of the bridge (longitudinal spectrum).
5. Select the corresponding vertical design spectrum proposed in this document according to the same criteria. This spectrum will be applied in the vertical direction (vertical spectrum).
6. Carry out an elastic response spectrum using sufficient number of modes in each direction under longitudinal and vertical spectra. Combine the effect of each mode using CQC modal combination rule in each direction. The response quantities obtained from the analysis in vertical and horizontal directions will be combined using SRSS modal combination rule to determine the response under combined effects of horizontal and vertical ground motions. Combine the results of the elastic response spectrum analysis with the gravity analysis using the corresponding load combination.
7. Compare the moment demands with the moment demands obtained using the capacity design procedure employed in SDC-2006 and select the critical governing load case.
8. Design the longitudinal reinforcement of the girders based on the moment demands obtained from step 7.

Figure 7-2 shows the sample girder moment diagrams obtained from the elastic response spectrum analysis for Camino del Norte and Amador Creek bridges under selected events. The results obtained using the approximate procedure described above was found to compare well with nonlinear time-history estimates of the demand.

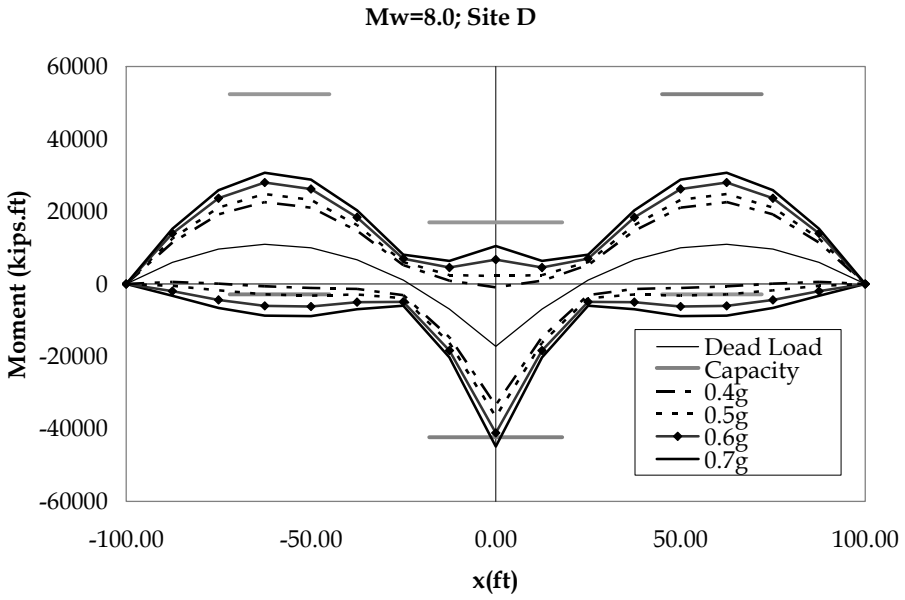

(a)

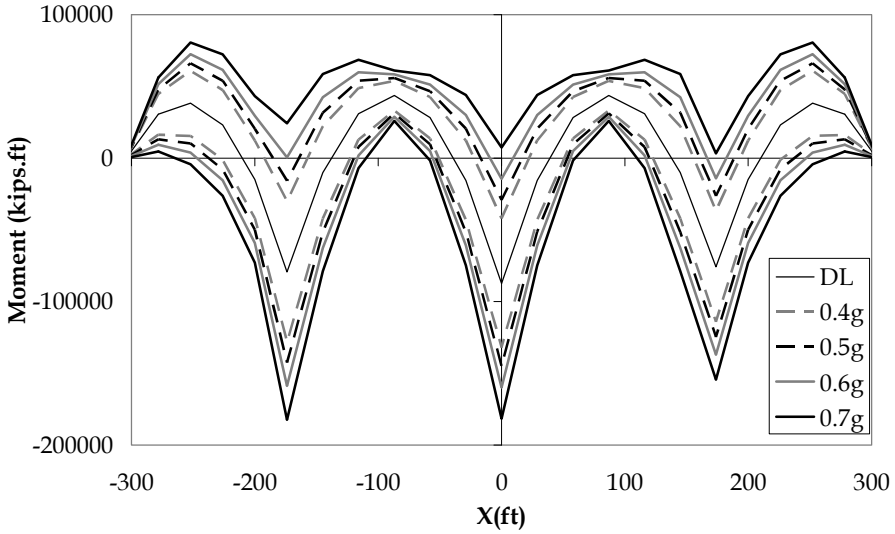

(b)

Figure 7-2 – Girder moment diagrams of (a)Camino del Norte (b) Amador Creek bridges under combined effects of longitudinal and vertical ground motions under various events

8 CONCLUSIONS

The influence of vertical components of ground motions on structural response have continued to remain a subject of debate since direct evidence of damage from vertical motions is difficult to establish. Studies in the past have clearly identified several potential issues that deserve additional attention. This study was undertaken with the objective of assessing the current provisions in SDC-2006 for incorporating vertical effects of ground motions in seismic evaluation and design of ordinary highway bridges. A comprehensive series of simulations was carried out on a range of over-crossing and multi-span bridge configurations to isolate the effects of vertical motions. The study indicated that the most vulnerable class of structures to vertical effects is highway over-crossings with vertical periods in the range of the predominant period of the vertical motions. This can however also be inferred from the results presented in Chapter 4 which show a diminishing demand with increasing vertical period.

Results of these analyses reveal that vertical ground motions do significantly affect (i) the axial force demand in columns; (ii) moment demands at the face of the bent cap, and (iii) moment demands at the middle of the span. The first two issues are found to be less of a concern in the present study since the axial capacity of the columns and the moment capacity of the girders at the face of the bent cap are generally adequate to resist the increase in the respective demands due to vertical effects. On the other hand, the amplification of negative moments in the mid-span section is identified as the primary issue that should be addressed in the context of existing seismic guidelines in SDC-2006. In particular, the current requirement that vertical ground motions be considered only for sites where the expected peak rock acceleration is at least 0.6g is not an adequate basis to assess the significance of vertical effects. A second SDC criteria that is in need of reexamination is the design specification for the consideration of vertical effects by means of a static load equivalent to 25% of the dead load applied in the

upward direction. The reinforcement resulting from this requirement is found to be inadequate for a significant number of cases examined in this study.

It was shown that elastic response spectrum analysis is an effective tool to determine the effects of vertical ground motions on the bridge superstructures. A set of vertical design spectra and a simplified design procedure that uses the proposed vertical elastic response spectrum as the seismic input in the vertical direction was proposed for seismic evaluation of ordinary highway bridges.

REFERENCES

Abrahamson, N.A. and Silva, W.J. [1997]. "Empirical Response Spectral Attenuation Relations for Shallow Crustal Earthquakes." *Seism. Soc. Am.,* 68(1), 94-127.

Bozorgnia, Y., M. Niazi. [1993]. "Distance Scaling of Vertical and Horizontal Response Spectra of the Loma Prieta Earthquake." Earthquake Engineering and Structural Dynamics 22: 695-707.

Bozorgnia, Y., Niazi, M. and Campbell, K. W. [1995] "Characteristics of Free-Field Vertical Ground Motion During the Northridge Earthquake," Earthquake Spectra 11, 515-525.

Bozorgnia, Y. M. and Campbell, K. W. [2004]. "The Vertical-to-Horizontal Response Spectral Ratio and Tentative Procedures for Developing Simplified V/H and Vertical Design Spectra," J. Earthquake Engineering, 8, 175-207.

Broekhuizen, D. S. (1996). "Effects of vertical acceleration on prestressed concrete bridges." MS thesis, Univ. of Texas at Austin, Texas.

Bureau, G. J. [1981] "Near-Source Peak Ground Acceleration," Earthquake Notes, 52-81.

Button, M.R., Cronin, C.J. and Mayes, R.L. (2002). "Effect of Vertical Motions on Seismic Response of Bridges." *ASCE Journal of Structural Engineering*, Vol.128 (12), 1551-1564.

California Department of Transportation (Caltrans) (2006), "Seismic design criteria", *SDC-2006*, Sacramento, CA

Collier C. J. and Elnashai A. S. (2001), "A procedure for combining vertical and horizontal seismic action effects." *Journal of Earthquake Engineering*, Vol. 5, No. 4, pp. 521-539, 2001.

Campbell, K. W. [1982] "A Study of the Near-Source Behavior of Peak Vertical Acceleration," EOS 63, 1037.

Chang, S.W., J.D. Bray and R.B. Seed [1996]. "Engineering Implications of Ground Motions from the Northridge Earthquake." *Bull. Seism. Soc. Am.,* 86(1B), S270-S288.

Electric Power Research Institute [1993]. "Guidelines for Determining Design Basis Ground Motions." Palo Alto, California: Electric Power Research Institute, vol. 1-5, EPRI TR-102293.

Elnashai, A. S. and Papazoglou, A. J. [1997] "Procedure and Spectra for Analysis of RC Structures Subjected to Strong Vertical Earthquake Loads," Journal of Earthquake Engineering 1, 121-155.

Gloyd, S. (1997). "Design of ordinary bridges for vertical seismic acceleration." *Proc., FHWA/NCEER Workshop on the National Representation of Seismic Ground Motion for New and Existing Highway Facilities, Tech. Rep. No. NCEER-97-0010*, National Center for Earthquake Engineering Research, State Univ. of New York at Buffalo, N.Y., pp.277–290.

Goel R. K. and Chopra A. K. (1997), "Evaluation of bridge abutment capacity and stiffness during earthquakes", Earthquake Spectra, 13(1), 1-23

Mander J.B. , Priestley M.J.N, and Park R. (1988) "Theoretical stress-strain model for confined concrete", *Journal of the Structural Division*, 114(ST8): 1804-1826

McCallen D.B. and Romstad K.M. (1994), "Dynamic analysis of a skewed short-span, box girder overpass", *Earthquake Spectra*, 10(4), 729-755

Niazi, M. and Bozorgnia, Y. [1989] "Behavior of Vertical Ground Motion Parameters in the Near Field," Seismological Research Letters 60, 4.

Niazi, M. and Bozorgnia, Y. [1990] "Observed Ratios of PGV/PGA and PGD/PGA for Deep Soil Sites across SMART-1 Array, Taiwan, Fourth US National Conference on Earthquake Engineering; Palm Springs; CA; Proceedings 1, 367-374.

Niazi, M. and Bozorgnia, Y. [1991] "Behavior of Near-Source Peak Vertical and Horizontal Ground Motions Over SMART-1 Array, Taiwan," Bulletin of the Seismological Society of America 81, 715-732.

Niazi, M. and Bozorgnia, Y. [1992] "Behavior of Near-Source Vertical and Horizontal Response Spectra at SMART-1 array, Taiwan," Earthquake Engineering and Structural Dynamics 21, 37-50.

Nigam, N. C. and Jennings, P. C. [1969] "Calculation of Response Spectra from Strong Motion Earthquake Records", Bulletin of the Seismological Society of America 59, 909-922.

Papazoglou A. J. and Elnashai A. S. (1996)., "Analytical and field evidence of the damaging effect of vertical earthquake ground motion", *Earthquake Engineering and Structural Dynamics*, Vol 25 pp 1109-1137

Price T. E. and Eberhard M. O. (2005), "Factors contributing to bridge-embankment interaction", *Journal of Structural Engineering*, 131(9), 1345-1354

Saadeghvaziri, M. A., and Foutch, D. A. (1991). "Dynamic behavior of R/C highway bridges under the combined effect of vertical and horizontal earthquake motions." *Earthquake Engineering and Structural Dynamics,*Vol 20, pp.535–549.

Silva, W. J. [1997]. "Characteristics of Vertical Ground Motions for Applications to Engineering Design." Proc., FHWA/NCEER Workshop on the National Representation of Seismic Ground Motion for New and Existing Highway Facilities, Tech. Rep. No. NCEER-97-0010, National Center for Earthquake Engineering Research, State Univ. of New York at Buffalo, N.Y., 205–252.

Somerville, P. [2000] "New Developments in Seismic Hazard Estimation," Sixth International Conference on Seismic Zonation; Palm Springs; CA

Veletzos M. J, Restrepo, J. I, Seible F. (2006). "Seismic response of precast segmental bridge superstructures" Report submitted to Caltrans – SSRP-06/18, University of California, San Diego

Yu, C-P., Broekhuizen, D. S., Roesset, J. M., Breen, J. E., and Kreger, M. E. (1997). "Effect of vertical ground motion on bridge deck response." *Proc., Workshop on Earthquake Engineering Frontiers in Transportation Facilities, Tech. Rep. No. NCEER-97-0005*, National Center for Earthquake Engineering Research, State Univ. of New York at Buffalo, N.Y., pp.249–263.

Zhang J. and Makris N., (2002), "Seismic response analysis of highway overcrossing including soil-structure interaction", *Earthquake Engineering and Structural Dynamics*, 31, 1967-1991

APPENDIX

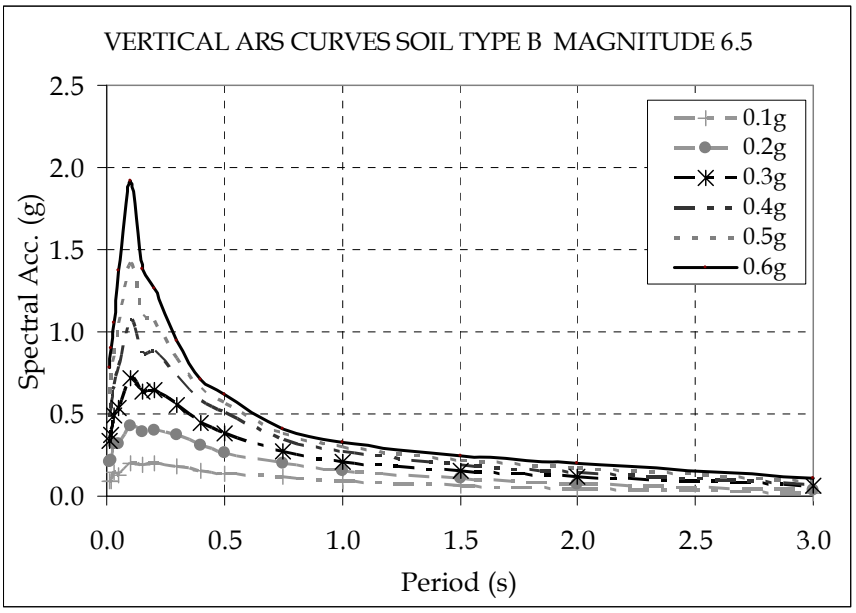

Figure A-8-1 - Proposed Vertical ARS Curves for Soil Type B Magnitude 6.5

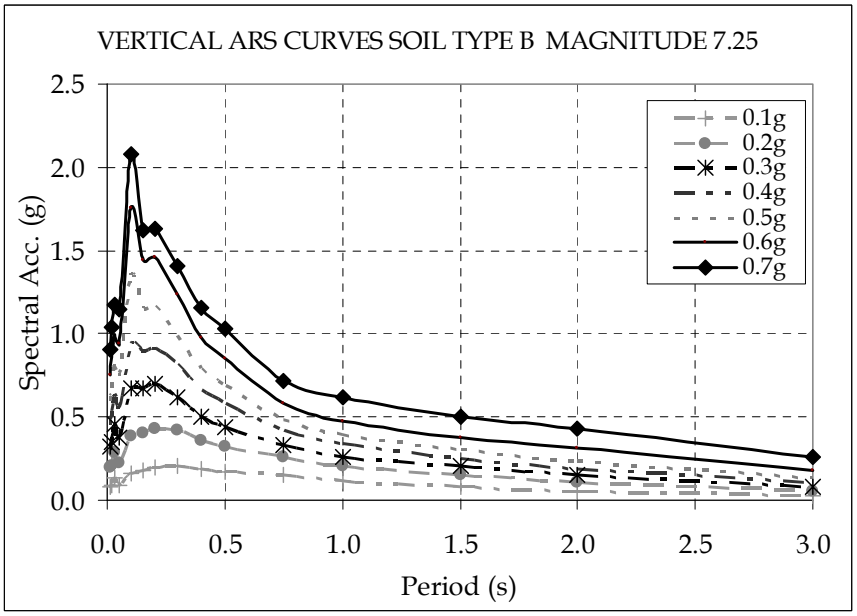

Figure A-8-2 - Proposed Vertical ARS Curves for Soil Type B Magnitude 7.25

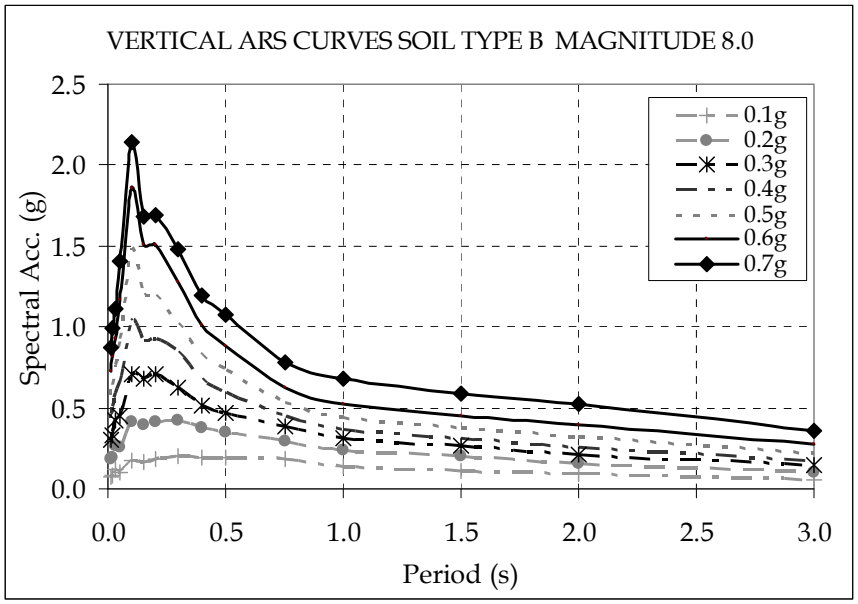

Figure A-8-3 - Proposed Vertical ARS Curves for Soil Type B Magnitude 8.0

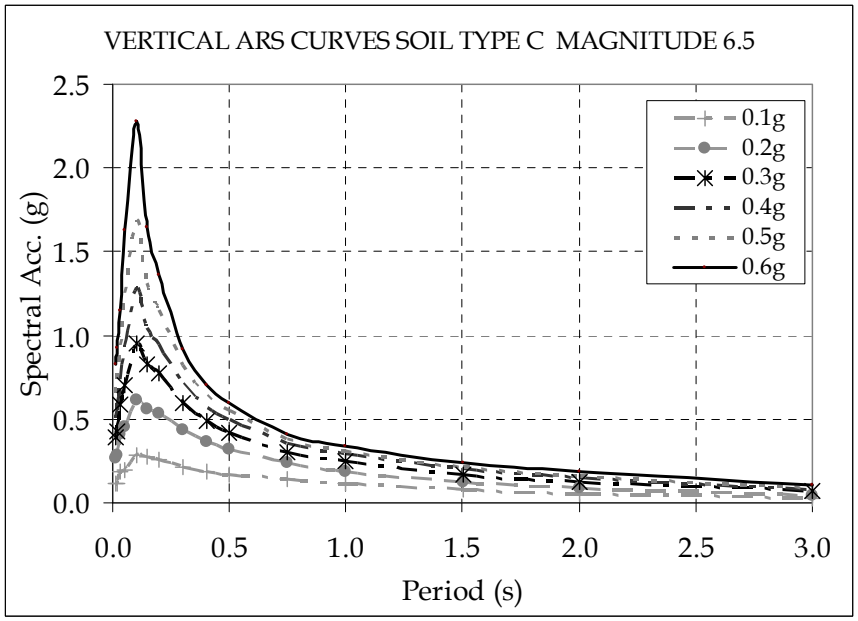

Figure A-8-4 - Proposed Vertical ARS Curves for Soil Type C Magnitude 6.5

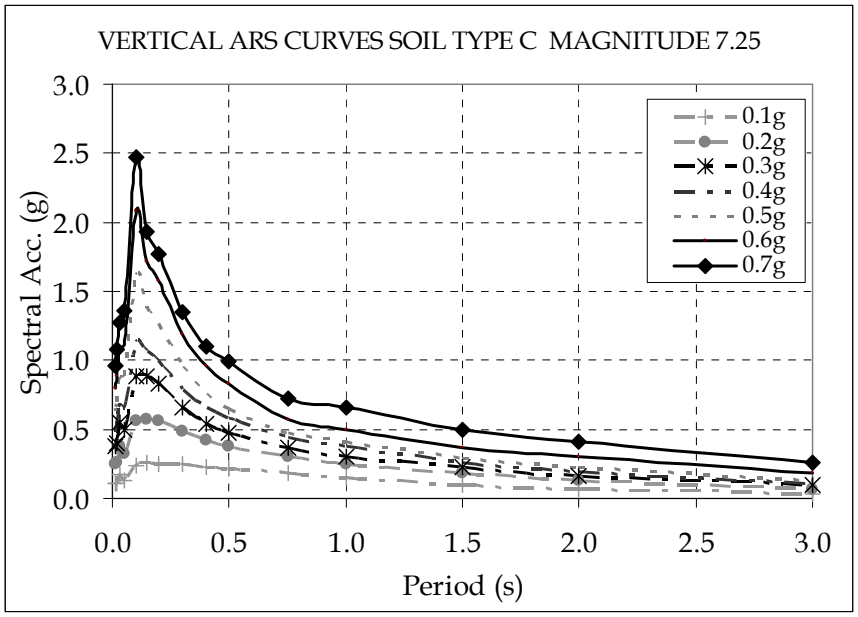

Figure A-8-5 - Proposed Vertical ARS Curves for Soil Type C Magnitude 7.25

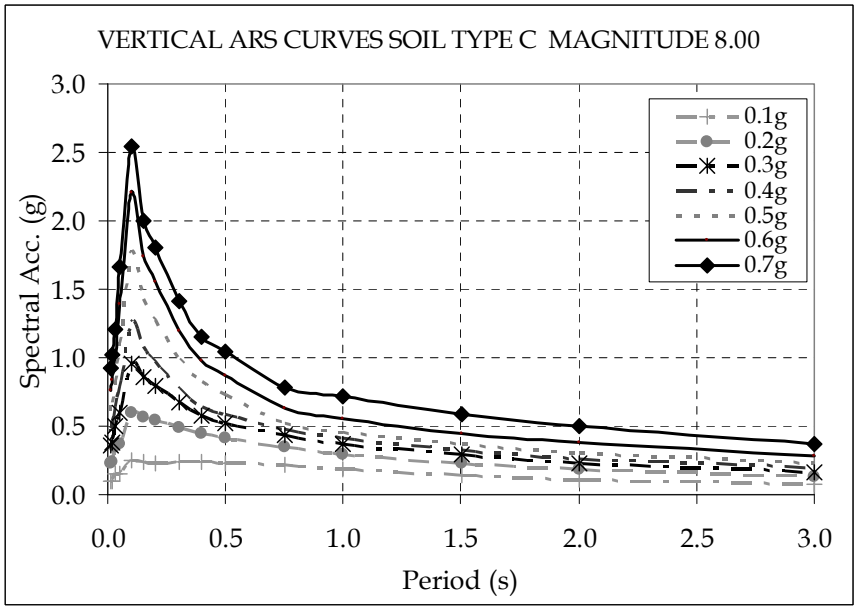

Figure A-8-6 - Proposed Vertical ARS Curves for Soil Type C Magnitude 8.0

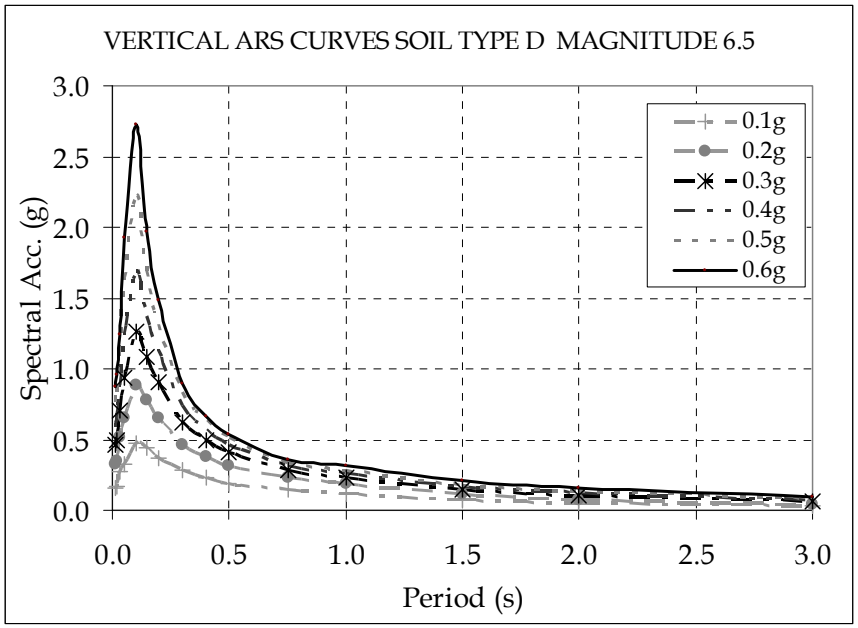

Figure A-8-7 - Proposed Vertical ARS Curves for Soil Type D Magnitude 6.5

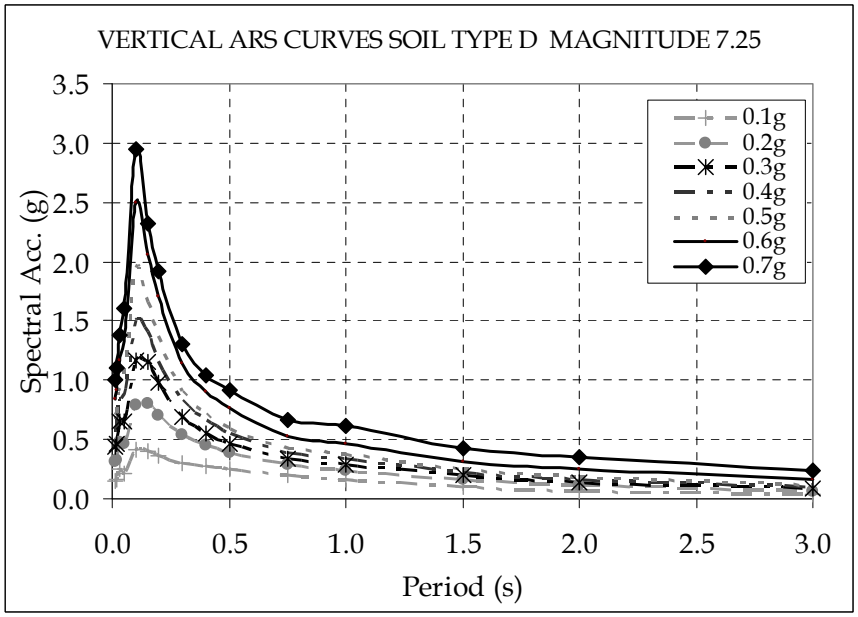

Figure A-8-8 - Proposed Vertical ARS Curves for Soil Type D Magnitude 7.25

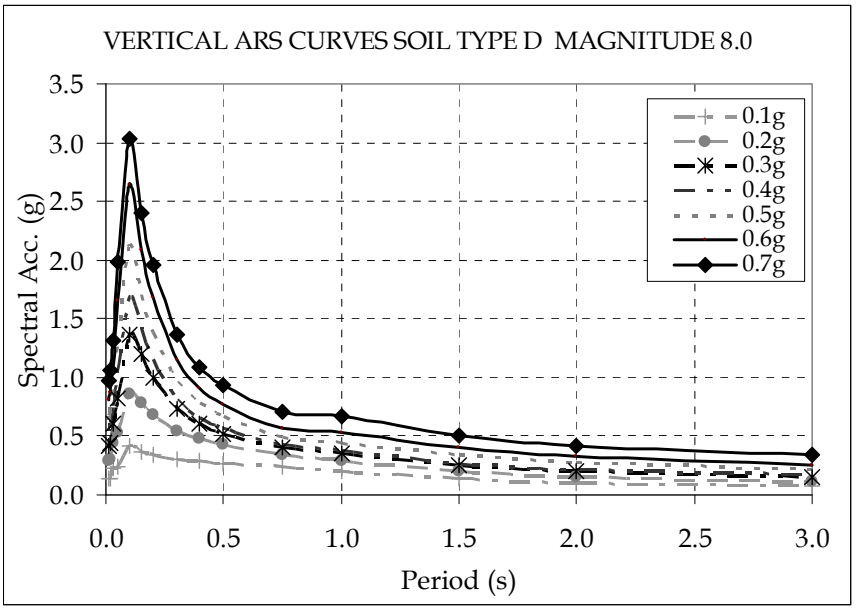

Figure A-8-9 - Proposed Vertical ARS Curves for Soil Type D Magnitude 8.0

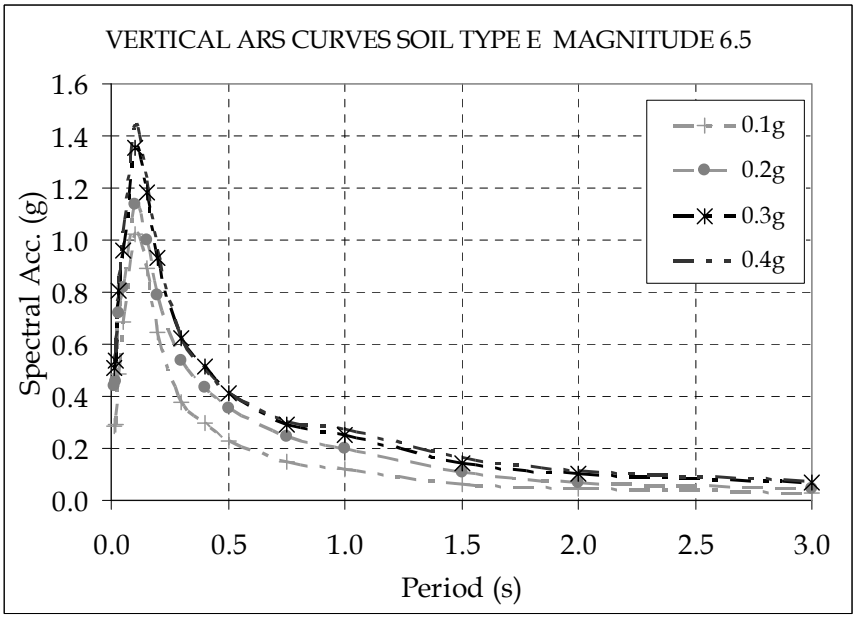

Figure A-8-10 - Proposed Vertical ARS Curves for Soil Type E Magnitude 6.5

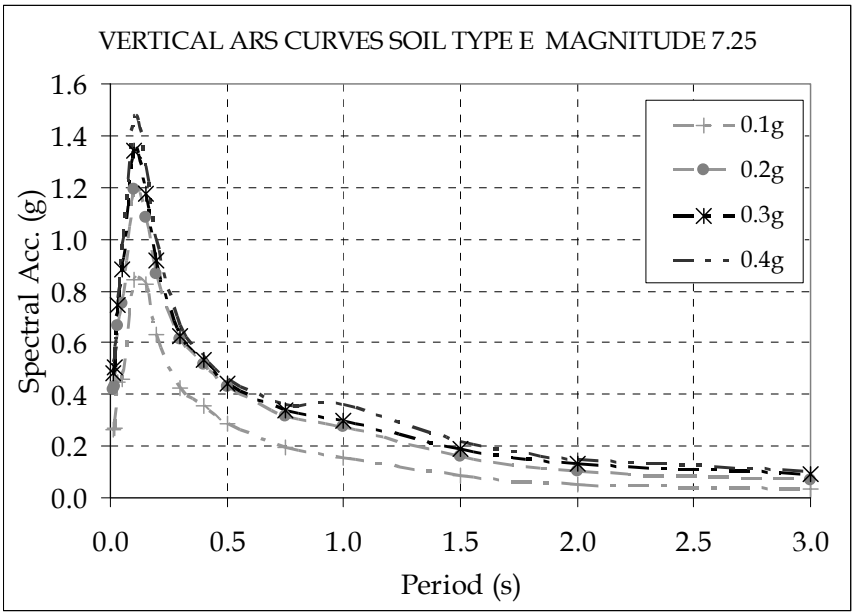

Figure A-8-11 - Proposed Vertical ARS Curves for Soil Type E Magnitude 7.25

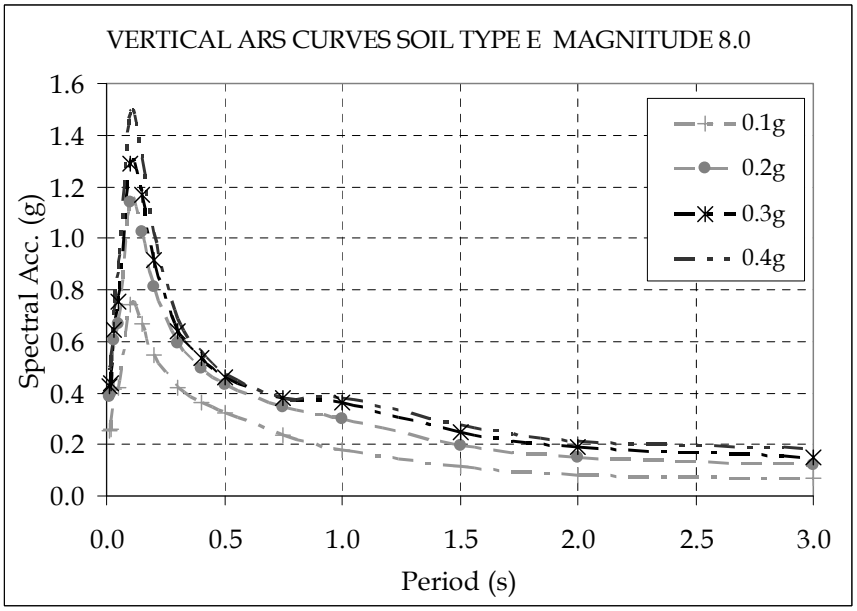

Figure A-8-12 - Proposed Vertical ARS Curves for Soil Type E Magnitude 8.0